

Aus dem Zentrum für Klinische Tiermedizin der Tierärztlichen Fakultät
der Ludwig-Maximilians-Universität München

Arbeit angefertigt unter der Leitung von
Univ.-Prof. Dr. R. Wanke

**Pathomorphologic analysis and therapeutic *in vivo* assay on two
murine models of uromodulin-associated kidney disease**

Inaugural-Dissertation zur Erlangung der tiermedizinischen Doktorwürde
der Tierärztlichen Fakultät
der Ludwig-Maximilians-Universität München

von Stefanie Sklenák

aus Freilassing

München, 2013

Gedruckt mit Genehmigung der Tierärztlichen Fakultät

der Universität München

Dekan: Univ.-Prof. Dr. Joachim Braun

Berichterstatter: Univ.-Prof. Dr. Rüdiger Wanke

Korreferent: Univ.-Prof. Dr. Bernhard Aigner

Tag der Promotion: 09. Februar 2013

Meiner Familie

Table of contents.....	I
Figures and Tables.....	II
Abbreviations.....	III
1 Introduction.....	1
2 Literature.....	3
2.1 Structure and function of the mammalian nephron.....	3
2.2 Structure and function of uromodulin.....	5
2.2.1 Discovery and structure.....	5
2.2.2 Function of uromodulin.....	8
2.3 Uromodulin-associated kidney disease (UAKD).....	11
2.3.1 Pathophysiology of UAKD.....	11
2.3.2 Genetic causes.....	11
2.3.3 Abnormalities at the molecular level.....	12
2.3.4 Effects at the cellular level <i>in vitro</i>	12
2.3.5 Phenotypes of UAKD.....	13
2.3.6 Clinical features of UAKD.....	13
2.3.7 Histopathology.....	14
2.3.8 Ultrastructural alterations.....	16
2.3.9 UAKD therapy.....	17
2.4 Murine models for functional analysis of uromodulin and of UAKD.....	17
2.4.1 Knockout mouse lines.....	17

2.4.2	Mutant human <i>UMOD</i> ^{C148W} transgenic mouse line	19
2.4.3	Tg ^{<i>Umod</i>C147W} transgenic mouse line	20
2.4.4	ENU-induced <i>Umod</i> mutant mice	22
2.4.4.1	<i>Umod</i> ^{A227T} mutant mice	22
2.4.4.2	<i>Umod</i> ^{C93F} mutant mice	25
2.5	ER stress and the unfolded protein response.....	27
2.5.1	Molecular chaperones	28
2.5.2	Chemical chaperones.....	29
2.6	Oxidative stress in chronic kidney disease.....	31
3	Materials and methods	33
3.1	Research design.....	33
3.2	Animals	35
3.3	Genotype analysis	35
3.3.1	Tissue samples.....	35
3.3.2	DNA isolation	36
3.3.3	DNA concentration assessment.....	36
3.3.4	PCR for mouse genotyping	36
3.3.5	Gel electrophoresis	39
3.4	Morphological analysis of age-related renal alterations in <i>Umod</i> mutant mice.....	39
3.4.1	Necropsy and kidney preparation.....	39
3.4.2	Qualitative histological analysis by light microscopic investigations	40

3.4.2.1	Haematoxylin and eosin (H&E) staining	40
3.4.2.2	Giemsa staining	41
3.4.2.3	Masson's trichrome (MT) staining (modified according to Goldner and Weigert)	41
3.4.2.4	PAS-silver staining	43
3.4.2.5	Uromodulin immunostaining of kidney sections	45
3.4.3	Quantitative stereological analysis	46
3.4.3.1	Quantification of the renal volume fractions	46
3.4.3.2	Quantification of the total volumes	47
3.5	<i>In vivo</i> testing of two putative causative therapeutics for UAKD	47
3.5.1	Experimental schedule	47
3.5.2	4-PBA and tempol administration	47
3.5.3	Blood sampling and analysis	48
3.5.4	Metabolic cage experiment	48
3.5.5	Urine sampling and analysis	49
3.5.5.1	Analysis of clinical chemical parameters in urine	49
3.5.5.2	Analysis of urinary osmolality	50
3.5.5.3	Analysis of uromodulin excretion	50
3.5.6	Necropsy and tissue preparation	53
3.5.7	Histological kidney analysis after treatment application	54
3.5.7.1	Light microscopic investigations	54

3.5.7.2	Transmission electron microscopic investigations	54
3.6	Statistical analysis	58
4	Results	59
4.1	Allelic differentiation of <i>Umod</i> mutant mice	59
4.1.1	Genotyping of <i>Umod</i> ^{A227T} mutants.....	59
4.1.2	Genotyping of <i>Umod</i> ^{C93F} mutants	60
4.2	Analysis of disease progression	61
4.2.1	Qualitative analysis of renal histopathology	62
4.2.1.1	Interstitial fibrosis and tubular atrophy (IFTA)	63
4.2.1.2	Inflammatory cell infiltrates.....	64
4.2.1.3	TALH cells.....	64
4.2.1.4	Sporadic kidney alterations	66
4.2.2	Quantitative stereological kidney findings.....	67
4.2.2.1	Interstitial fibrosis and tubular atrophy (IFTA)	67
4.2.2.2	Inflammatory cell infiltrates.....	72
4.2.2.3	TALH cells.....	76
4.3	<i>In vivo</i> testing of two putative causative therapeutics for UAKD.....	81
4.3.1	Body weight	81
4.3.2	Clinical chemical analysis	83
4.3.3	Metabolic cage analysis	92
4.3.4	Urine analysis	95

4.3.4.1	Western blot analysis of 24h-urine	95
4.3.4.2	Clinical chemistry of 24h-urine	96
4.3.4.3	Fractional excretion of urinary solutes.....	101
4.3.5	Histopathology	104
4.3.5.1	Light microscopic analysis	104
4.3.5.2	TEM analysis	105
5	Discussion	106
5.1	Uromodulin-associated kidney disease	106
5.2	<i>Umod</i> mutant mouse lines as a murine model for UAKD	106
5.3	Tubulointerstitial lesions in <i>Umod</i> mutant mice	107
5.4	Renal TALH cell volumes and tubular atrophy	109
5.5	Age-related lesions in <i>Umod</i> mutant mice	110
5.6	Sporadic renal histopathology in <i>Umod</i> mutant mice	111
5.7	UAKD therapy approach.....	111
5.8	Treatment of <i>Umod</i> mutant mice with 4-PBA and tempol	112
5.9	Metabolic pathways and efficacy of 4-PBA as a chemical chaperone.....	116
5.10	Metabolization of tempol	117
5.11	Conclusion and outlook.....	117
6	Summary	119
7	Zusammenfassung	121
8	Acknowledgements	144

Index of figures

Figure 2.1: Primary amino acid structure of uromodulin..... 6

Figure 2.2: Uromodulin maturation, excretion and polymerization in the TAHL. GPI anchoring, disulphide bond formation and N-glycosylation occur in the endoplasmic reticulum..... 8

Figure 2.3: Genomic and protein structure of uromodulin and positions of published *UMOD* mutations causing UAKD.. 11

Figure 2.4: Immunohistochemical staining for uromodulin in human kidney biopsies..... 14

Figure 2.5: Masson Trichrome staining of a representative renal biopsy specimen of a human patient with a *UMOD* mutation. 15

Figure 2.6: Transmission electron microscopy (TEM) of a distal tubular cell.. 16

Figure 2.7: Uromodulin protein structure and sequence alignment of murine uromodulin.... 23

Figure 2.8: Uromodulin protein structure and sequence comparison of AA 6–106 (EGF-like domain II) between different species.. 26

Figure 2.9: Unfolded protein response scheme..... 28

Figure 4.1: Electrophoresis of allele-specific PCR samples of *Umod*^{A227T} mutant mice..... 60

Figure 4.2: Electrophoresis of allele-specific PCR samples of *Umod*^{C93F} mutant mice.. 61

Figure 4.3: IFTA in *Umod* mutant mice..... 63

Figure 4.4: Pattern of inflammatory cell infiltrates in the kidneys of *Umod* mutant mice. 64

Figure 4.5: Distribution of uromodulin within TALH cells in the kidneys of *Umod* mutant and wild-type mice..... 65

Figure 4.6: Tubular and glomerular dilative alterations..... 66

Figure 4.7: Volume fractions of IFTA in kidneys ($V_{V(\text{IFTA}/\text{kid})}$) of 14-month-old *Umod*^{C93F} mutant mice..... 68

Figure 4.8: Total volumes of IFTA in kidneys ($V_{(\text{IFTA},\text{kid})}$) of 14-month-old *Umod*^{C93F} mutant mice..... 68

Figure 4.9: Volume fractions of IFTA in kidneys ($V_{V(\text{IFTA}/\text{kid})}$) of 20-22-month-old *Umod*^{A227T} and *Umod*^{C93F} mice..... 69

Figure 4.10: Total volumes of IFTA in kidneys ($V_{(\text{IFTA},\text{kid})}$) in 20-22-month-old *Umod*^{A227T} and *Umod*^{C93F} mice..... 70

Figure 4.11: Volume fractions of IFTA in kidneys ($V_{V(\text{IFTA}/\text{kid})}$) of *Umod*^{C93F} mice at different ages..... 71

Figure 4.12: Total renal volumes of IFTA ($V_{(\text{IFTA},\text{kid})}$) in *Umod*^{C93F} kidneys at different ages.. 71

Figure 4.13: Volume fractions of inflammatory cell infiltrates in kidneys ($V_{V(\text{IC}/\text{kid})}$) of 14-month-old *Umod*^{C93F} mice..... 72

Figure 4.14: Total volumes of inflammatory cell infiltrates in kidneys ($V_{(\text{IC},\text{kid})}$) of 14-month-old *Umod*^{C93F} mice.. 73

Figure 4.15: Volume fractions of inflammatory cell infiltrates in kidneys ($V_{V(\text{IC}/\text{kid})}$) of 20-22-month-old *Umod*^{A227T} and *Umod*^{C93F} mice..... 74

Figure 4.16: Total volumes of inflammatory cell infiltrates in kidneys ($V_{(\text{IC},\text{kid})}$) of 20-22-month-old *Umod*^{A227T} and *Umod*^{C93F} mice..... 74

Figure 4.17: Volume fractions of inflammatory cell infiltrates in kidneys ($V_{V(\text{IC}/\text{kid})}$) of *Umod*^{C93F} mice at different ages..... 75

Figure 4.18: Total volumes of inflammatory cell infiltrates in kidneys ($V_{(\text{IC},\text{kid})}$) of *Umod*^{C93F} mice at different ages.. 76

Figure 4.19: Volume fractions of TALH cells in kidneys ($V_{V(\text{TALH}/\text{kid})}$) of 14-month-old *Umod*^{C93F} mice. 77

Figure 4.20: Total volumes of TALH cells in kidneys ($V_{(TALH,kid)}$) of 14-month-old *Umod*^{C93F} mice..... 77

Figure 4.21: Volume fractions of TALH cells in the kidneys ($V_{V(TALH/kid)}$) of 20-22-month-old *Umod*^{A227T} and *Umod*^{C93F} mice..... 78

Figure 4.22: Total volumes of TALH cells ($V_{(TALH,kid)}$) in 20-22-month-old *Umod*^{A227T} and *Umod*^{C93F} mice..... 79

Figure 4.23: Volume fractions of TALH cells in kidneys ($V_{V(TALH/kid)}$) of *Umod*^{C93F} mice at different ages..... 80

Figure 4.24: Total volumes of TALH cells in kidneys ($V_{(TALH,kid)}$) of *Umod*^{C93F} mice at different ages..... 80

Figure 4.25: Body weights of homozygous *Umod*^{A227T} mutant and homozygous *Umod*^{C93F} mutant mice compared to wild-type controls between day 0 and day 56 of (A) 4-PBA, (B) tempol and (C) placebo treatment..... 82

Figure 4.26: Plasma urea levels of homozygous *Umod*^{A227T} and *Umod*^{C93F} mutant mice as well as of wild-type controls of the different treatment groups at the ages of (A) 2 months, (B) 3 months and (C) 4 months..... 84

Figure 4.27: Plasma cholesterol levels of homozygous *Umod*^{A227T} mutant and homozygous *Umod*^{C93F} mutant mice as well as of wild-type controls of the different treatment groups at the ages of (A) 2 months, (B) 3 months and (C) 4 months..... 86

Figure 4.28: Plasma triglyceride levels of homozygous *Umod*^{A227T} and *Umod*^{C93F} mutant mice as well as of wild-type controls of the different treatment groups at the ages of (A) 2 months, (B) 3 months and (C) 4 months..... 87

Figure 4.29: Urine volume and urine osmolality of 24h-urine of 4-month-old *Umod*^{A227T} and *Umod*^{C93F} mice..... 93

Figure 4.30: Western blot analysis of urinary uromodulin content in homozygous *Umod*^{C93F} mutant and homozygous *Umod*^{A227T} mutant mice compared to wild-type controls. 95

Figure 4.31: Fractional excretion (FE) of (A) urea, (B) uric acid, (C) sodium, and (D) calcium in the urine of homozygous *Umod*^{A227T} mutant and homozygous *Umod*^{C93F} mutant mice as well as of wild-type controls of different treatment groups. 102

Figure 4.32: TALH cells of wild-type, homozygous *Umod*^{A227T} mutant and homozygous *Umod*^{C93F} mutant mice of the 4-PBA and of the tempol treatment group. 104

Figure 4.33: TALH cells of wild-type, homozygous *Umod*^{A227T} mutant and homozygous *Umod*^{C93F} mutant mice of the 4-PBA and the tempol treatment group..... 105

Figure 5.1: Scheme of the hypothesized impairment of ion exchange in TALH cells expressing mutant uromodulin..... 114

Tables

Table 3.1: Number and age of mice for histological kidney analysis.. 34

Table 3.2: Number of mice in different types of analyses during the treatment assay. 34

Table 4.1: Qualitative assesement of the occurrence of renal alterations in *Umod* mutant and wild-type mice..... 62

Table 4.2: Plasma clinical chemistry of homozygous *Umod*^{A227T} and *Umod*^{C93F} mutant mice and wild-type controls at the age of 2 months.. 89

Table 4.3: Plasma clinical chemistry of homozygous *Umod*^{A227T} and *Umod*^{C93F} mutant mice and wild-type controls at the age of 3 months.. 90

Table 4.4: Plasma clinical chemistry of homozygous *Umod*^{A227T} and *Umod*^{C93F} mutant mice and wild-type controls at the age of 4 months. 91

Table 4.5: 24h-metabolic cage data of 4 month-old homozygous *Umod*^{A227T} and *Umod*^{C93F} mutant mice and wild-type controls.. 94

Table 4.6: Clinical chemistry of 24h-urine from 4 month-old homozygous *Umod*^{A227T} mutant and homozygous *Umod*^{C93F} mutant mice and wild-type controls, day 1. 99

Table 4.7: Clinical chemistry of 24h-urine from 4 month-old homozygous *Umod*^{A227T} mutant and homozygous *Umod*^{C93F} mutant mice and wild-type controls, day 2.. 100

Table 4.8: Fractional excretion of urine parameters of 24h-urine from 4-month-old A227T and C93F homozygotes and wild-type controls, day 2..... 103

Abbreviations

A	arginine
ABC	avidin biotin complex
aa	amino acid
ALT	alanine aminotransferase
APS	ammonium persulfate
AST	aspartate aminotransferase
bidest.	bidestillata
bp	base pairs
BSA	bovine serum albumin
C	cysteine
C3H	C3HeB/FeJ inbred mouse strain
C57BL/6	C57BL/6Jlco inbred mouse strain
cDNA	complementary deoxyribonucleic acid
CFTR	cystic fibrosis transmembrane conductance regulator
CKD	chronic kidney disease
ClC-Kb	kidney-specific chloride channel Kb
CoA	coenzyme A
creatinine-E	creatinine measured by the enzymatic method
creatinine-J	creatinine measured by the Jaffé method
C-terminus	carboxyl-terminus of a polypeptide or protein
D8C	domain of eight cysteine residues
DCT	distal convoluted tubule
dest.	destillata
DNA	deoxyribonucleic acid
DTT	1,4- dithiothreitol
<i>E. coli</i>	<i>Escherichia coli</i>
EDTA	ethylenediaminetetraacetic acid
EGF	epidermal growth factor
ENaC	epithelial sodium channel
ENU	N-ethyl-N-nitrosourea
ER	endoplasmic reticulum

ERAD	endoplasmic-reticulum-associated protein degradation
ES cells	embryonic stem cells
ESRD	end stage renal disease
et al.	et alii
f	female
F	phenylalanine
FE _x	fractional excretion of substance x
FELASA	Federation of European Laboratory Animal Science Associations
FJHN1	familial juvenile hyperuricaemic nephropathy type 1
for	forward (primer)
FVB	FVB/N inbred mouse strain
G1 –G4	generation one to four
GPI	glykosylphosphatidylinositol
GCKD	glomerulocystic kidney disease
h	hour
HA	haemagglutinin
H&E	haematoxylin and eosin
HEK293 cells	human embryonic kidney cell line
het	heterozygous
hom	homozygous
HPLC	high-performance liquid chromatography
HRP	horseradish peroxidase
Hsp	heat shock protein
IFTA	interstitial fibrosis and tubular atrophy
IgG	immunoglobulin G
IC	inflammatory cells
INT	intron
IRI	ischemia reperfusion injury
IU	international units
kDa	kilo Dalton
kid	kidney
M	marker
m	male

MCKD2	medullary cystic kidney disease type 2
mOsm	milliosmole
MT	Masson's trichrome
n	number
Na ⁺ /K ⁺ -ATPase	sodium/potassium-transporting enzyme that catalyses the degradation of adenosine triphosphate to adenosine diphosphate
N-glycosylation	attachment of a sugar to a nitrogen atom in an amino acid residue of a protein
NHE ₃	sodium/hydrogen exchanger 3
NCC	sodium-chloride-symporter
NKCC2	Na ⁺ -K ⁺ -2Cl ⁻ cotransporter
N-terminus	amino terminus of a polypeptide or protein
OD	optic density
PAA	phenylacetic acid
PAS	periodic acid Schiff reaction
PBA	phenylbutyric acid
PCR	polymerase chain reaction
PDI	protein disulphide isomerase
p	p-value, chance of obtaining the same (or more extreme) results if no effect exists (null-hypothesis)
P-PVDF	polyvinylidene difluoride
rev	reverse (primer)
ROMK	renal outer medullary potassium channel
ROS	reactive oxygen species
rpm	rounds per minute
RT-PCR	reverse transcription polymerase chain reaction
SDS-PAGE	sodium dodecyl sulphate polyacrylamide gel electrophoresis
SEM	standard error of the mean
SD	standard deviation
SOD	superoxide dismutase
T	threonine
Taq	Thermus aquaticus
TALH	thick ascending limb of the loop of Henle

TEM	transmission electron microscope
Temed	N,N,N',N'-tetramethylethylenediamine
TG	triglycerides
Tg ^{<i>Umod</i>C147W}	transgenic mouse line harbouring the C147W mutant <i>Umod</i> gene
Tg ^{<i>Umod</i>wt}	transgenic mouse line harbouring the wild-type <i>Umod</i> gene
THP	Tamm-Horsfall protein
TLR4	Toll-like receptor 4
TP	total protein
Tris	trishydroxymethylaminomethane
UAKD	uromodulin-associated kidney disease
<i>UMOD</i>	human uromodulin gene
<i>Umod</i>	murine uromodulin gene
UPR	unfolded protein response
UTI	urinary tract infection
UV	ultraviolet
V	volt
V _(x)	total volume of parameter x
V _{v(x/y)}	volume fraction of x in y
wt	wild-type
ZP	zona pellucida

1 Introduction

The human *UMOD* gene encodes uromodulin, also referred to as Tamm Horsfall protein, and is specifically expressed in cells of the thick ascending limb of the loop of Henle and the early distal convoluted tubule of the nephron. Since its discovery by Igor Tamm and Frank Horsfall in 1950, uromodulin and its function in the organism have been subject to more than 1000 scientific studies. However, its exact physiologic role remains unexplained (Serafini-Cessi *et al.*, 2003; Vyletal *et al.*, 2010). In recent years, there has been a renewed interest in uromodulin due to the detection of a strong association of the *UMOD* gene with chronic kidney diseases (CKD) in humans in several genome wide association studies (Kottgen *et al.*, 2012). Besides the association to the common disease CKD, mutations within the *UMOD* gene causes the orphan renal disease uromodulin-associated kidney disease (UAKD). Associated with *UMOD* mutations are three autosomal dominant disorders: Familial juvenile hyperuricaemic nephropathy (FJHN1), medullary cystic kidney disease type 2 (MCKD) and glomerular cystic kidney disease, all of which have in common hyperuricaemia, tubulointerstitial nephritis and progressive renal failure (Hart *et al.*, 2002; Serafini-Cessi *et al.*, 2003). In recent years the term uromodulin-associated kidney disease (UAKD) has been introduced to summarize these clinical variants based on their underlying genetic cause. Therapy is hitherto confined to allopurinol as a symptomatic treatment of gout caused by hyperuricaemia in UAKD patients (Schaffer *et al.*, 2010).

The pathophysiology of UAKD has been studied *in vitro* and *in vivo* on both transgenic and ENU-mutant mouse models (Bernascone *et al.*, 2010). The autosomal dominant mutant mouse lines *Umod*^{A227T} (= UREHR4) and *Umod*^{C93F} (= UREHD1) were established in the Munich ENU mouse mutagenesis project (Hrabe de Angelis *et al.*, 2000). Both harbour a missense point mutation in the murine *Umod* gene and exhibit increased plasma urea levels as a cardinal symptom (Kemter *et al.*, 2009; Prueckl, 2011).

The larger aim of this study was to assess the suitability of the *Umod*^{A227T} and *Umod*^{C93F} mouse lines as a model for UAKD. For this purpose, the renal histomorphology of *Umod*^{A227T} and *Umod*^{C93F} mutant mice was compared with regard to their allelic status and type of the *Umod* mutation and a potential correlation between their histological and clinical phenotypes

was investigated. In addition, the development of kidney alterations between the ages of 14 and 20-22 months was to be assessed. For this purpose, qualitative and quantitative-morphological analysis was performed on kidneys of mice of both lines and age groups.

Furthermore, a therapeutic approach with the molecular chaperone 4-phenylbutyric acid (4-PBA) and the superoxide dismutase mimetic tempol was conducted to test a potential ameliorating effect of these drugs on the clinical phenotype of *Umod* mutant mice. To this end, both chemicals were administered as a drinking solution to male homozygous mutant mice of both lines and to wild-type littermates (controls) over a period of two months. Urine and blood plasma parameters as well as renal histology of mice in the two treatment groups were compared to those receiving pure drinking water (placebo).

2 Literature

2.1 Structure and function of the mammalian nephron

Each nephron constitutes a structural and functional unit of the kidney. The nephron is essential for blood filtration, followed by solute and water absorption and excretion thereof. Thus, the nephron regulates electrolyte homeostasis as well as blood pressure and volume. Each nephron comprises a glomerulus and a Bowman's capsule, a proximal convoluted tubule, the loop of Henle and a distal convoluted tubule (Hees & Sinowatz, 2000; McGavin & Zachary, 2009).

The renal corpuscle, consisting of glomerulus and Bowman's capsule, lies in the renal cortex. It is the glomerulus where the initial blood filtering occurs. In humans, within 24 hours, 1000-2000 l of blood is pumped through the glomerular capillaries where water, ions and molecules smaller than 69 kDa penetrate the glomerular filter (Hees & Sinowatz, 2000; König *et al.*, 2002). The resulting filtrate is isosmotic with the blood plasma and is called primary urine: It passes on to the proximal convoluted tubule via the urinary pole of the renal capsule. About 99% of the primary urine is reabsorbed while passing through the tubular system of the nephron (Hees & Sinowatz, 2000).

The proximal tubule can be divided into a pars convoluta and a pars recta. Its most characteristic feature is a luminal brush border formed by microvilli to optimize the resorptive function of this nephron compartment. Its cuboidal epithelial cells are rich in mitochondria that provide energy for active transport mechanisms (Hees & Sinowatz, 2000). Na^+/K^+ -ATPase in the basolateral membrane of the epithelial cells is the most significant antiporter in the reabsorption of sodium and water, with the latter flowing out of the lumen along a concentration gradient. The resulting sodium gradient in turn drives co-transport channels for the reabsorption of inorganic phosphate, glucose and amino acids. Both potassium and urea leave the lumen via paracellular solvent drag and simple diffusion. On the other hand, the proximal tubule is an important location for secretion of substances like creatinine and ammonium (Schmidt *et al.*, 2010; von Engelhardt, 2012).

Connecting proximal and distal tubules, the loop of Henle lies mainly in the renal medulla and can be divided into three segments: a descending, a thin ascending and a thick ascending limb (Hees & Sinowatz, 2000). While the descending limb has a low permeability to ions and urea, its high water permeability together with a high solute concentration in the renal medulla allows for osmosis and thus for a substantial increase in urine concentration to occur in this part of the nephron. In the thin ascending limb which is not permeable to water but permeable to ions, the resulting highly osmotic urine then causes ions to pass from the urinary lumen into the medullary interstitium along a concentration gradient. Since this segment is impermeable to water, a hypoosmotic urine and a hyperosmotic interstitium are the result near the renal papilla (McGavin & Zachary, 2009; Schmidt *et al.*, 2010; von Engelhardt, 2012).

This countercurrent multiplier system is completed by the distal straight tubule, or thick ascending limb (TALH) of Henle (Hees & Sinowatz, 2000). Also impermeable to water, TALH cells actively reabsorb sodium, potassium and chloride ions by means of the $\text{Na}^+\text{-K}^+\text{-2Cl}^-$ -cotransporter NKCC2 which is a TALH-specific ion transporter. As potassium ions passively flow back into the lumen via K^+ -channels such as ROMK, a positive electron potential is created in the tubular lumen. Consequently, paracellular absorption of divalent cations such as Ca^{2+} and Mg^{2+} sets in (Kuhlmann *et al.*, 2008; Schmidt *et al.*, 2010). The correct function of the TALH is essential for creation and maintenance of a hypertonic interstitium of the renal medulla and thus for the urine concentration capability of the kidney. Beyond its contribution to a hypotonic urine, the TALH, together with early distal convoluted tubule parts, is the location where uromodulin, formerly called Tamm-Horsfall protein, is expressed and excreted into the urine (Pollak & Arbel, 1969).

Finally, the filtrate reaches the distal convoluted tubule (DCT) which connects the loop of Henle with the collecting duct system (Hees & Sinowatz, 2000). Like its proximal counterpart, the distal convoluted tubule controls urinary pH through bicarbonate and proton exchange. Furthermore, the basolateral $\text{Na}^+\text{-K}^+\text{-ATPase}$ creates a Na^+ concentration gradient which causes sodium to leave the lumen via a $\text{Na}^+\text{-Cl}^-$ -symport, simple diffusion as well as a luminal $\text{Na}^+\text{-H}^+$ -antiport. This creates a net negative electric potential along the DCT, which in turn inhibits a passive Na^+ resorption and active transport remains the only option for sodium absorption. The $\text{Na}^+\text{-H}^+$ -antiport increases H^+ secretion which creates an intracellular

alkalosis and a consequent K^+ -accumulation in the lumen. The hormone aldosterone is the major extrarenal regulator in DCT electrolyte resorption (Reilly & Ellison, 2000; Kuhlmann *et al.*, 2008; Schmidt *et al.*, 2010).

2.2 Structure and function of uromodulin

2.2.1 Discovery and structure

The protein uromodulin was discovered at the Rockefeller Institute in New York City in 1950 by Estonia-born Igor Tamm and his American mentor Frank Lippin Horsfall (Hirst, 1979; Choppin, 2007). Hence uromodulin derived its original name: Tamm Horsfall Protein (THP). Having isolated and purified uromodulin from normal human urine by means of salt precipitation, Tamm and Horsfall investigated its biochemical properties and found that the protein interacted with influenza, mumps and Newcastle disease viral hemagglutination (Tamm & Horsfall, 1950, 1952).

Further investigations showed that THP is the most abundantly expressed protein in mammalian urine, with its urinary excretion in humans ranging from 20 to 200 mg per day, the mean lying between 30 and 50 mg / 24 h under physiological conditions (Kumar & Muchmore, 1990; Kreft *et al.*, 2002). Due to eight glycosylation sites, uromodulin is rich in carbohydrates which can account for up to 30% of its molecular weight of around 90 kDa in SDS-PAGE (Gottschalk, 1952; Grant & Neuberger, 1973). THP expression is confined to the cells of the thick ascending limb of Henle (TALH) and early distal convoluted tubule cells, excluding macula densa (Schenk *et al.*, 1971; Hoyer *et al.*, 1979; Bachmann *et al.*, 1990).

In 1985 Muchmore and Decker examined the urine of pregnant women for its immunosuppressive compounds and, in the process, purified an 85-kDa glycoprotein that was able to withhold antigen-specific T-cell proliferation as well as monocyte cytotoxicity. Due to these immunomodulating properties and its source, namely urine, Muchmore and Decker suggested for the protein to be called “uromodulin”. They also concluded from their experiments that uromodulin was a monomeric protein with several intrachain disulphide bridges, an approximate carbohydrate content of 30% and that it showed a tendency to form aggregates (Muchmore & Decker, 1985). Apart from the above characteristics, uromodulin

was found to resemble THP in that it is synthesized in the kidney and in that it is ubiquitous in non-pregnant female as well as in male urine. Sequence analysis finally revealed that uromodulin and THP are the same glycoprotein and henceforth both terms have been used interchangeably (Pennica *et al.*, 1987).

As for its primary structure, the uromodulin precursor molecule contains 640 amino acids (aa). The first 24 aa at the N-terminus serve as a signal peptide for the protein to be transported to the endoplasmic reticulum (ER) which is also where this signal-residue is removed enzymatically. Although the resulting 616 aa-protein provides 8 sites for N-glycosylation, only 7 of them bind glycan moieties. Glycosylation of uromodulin starts in the ER is continued in the Golgi apparatus (Rindler *et al.*, 1990; van Rooijen *et al.*, 1999; Vyletal *et al.*, 2010) (Figure 2.1).

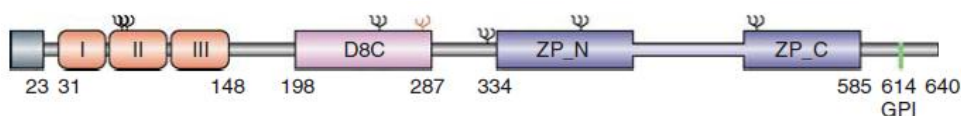


Figure 2.1: Primary amino acid structure of uromodulin. From left to right: leader peptide, (cleavage site at amino acid 23), epidermal growth factor (EGF)-like domains I-III, domain of 8 conserved cysteines (D8C), zona pellucida (ZP) domain and a glycosylphosphatidylinositol (GPI) glycosylation site at amino acid 614. Ψ: N-glycosylation site. Number of amino acids refers to the human uromodulin aa sequence. (Rampoldi *et al.*, 2011) License for the reuse of this figure was obtained in agreement with the Nature Publishing Group.

Further subunits of uromodulin include three epidermal growth-factor-like domains (EGF I-III) which are formed by aa residues 31-64, 65-107 and 108-149, respectively. EGF II and III were found to not only bind calcium but also to be rich in cysteine residues forming stable intramolecular disulphide bridges (Fletcher *et al.*, 1970; Hamlin & Fish, 1977). While the function of EGF-like domains remain incompletely understood, the relevance of their cysteine residues C1-C6 for a correct tertiary protein structure is indisputable (Rampoldi *et al.*, 2003) The existence of a fourth EGF-like domain between EGF III and the zona pellucida domain has hitherto been subject to debate. The peptide in question (aa 281-336) connects the zona

pellucida domain (aa 334-585) to D8C. D8C is the most recently identified subunit of uromodulin, stretching from aa residues 199 to 287. D8C stands for “domain with eight conserved cysteine residues” and has the potential to form four disulphide bridges (Yang *et al.*, 2004; Lens *et al.*, 2005). Zona pellucida and, presumably, EGF-like domains participate in the extracellular polymerization of uromodulin into superhelices (Rampoldi *et al.*, 2003). In total, uromodulin disposes of 24 putative disulphide bridges to link the 48 cysteine residues. ER chaperones facilitate this process (Malagolini *et al.*, 1997) (Figure 2.1).

At the C-terminus, a hydrophobic 16 aa- peptide signals to ER-transpeptidase to link a glycosylphosphatidylinositol (GPI) anchor to the C-terminus that results from the cleavage of the aforesaid 16 aa-signal stretch. (Pennica *et al.*, 1987; Ferguson & Williams, 1988; Rindler *et al.*, 1990). The GPI-addition, together with the Golgi-perfected glycans, is essential for the glycoprotein to reach and integrate into the apical plasma membrane of TALH cells (Brown & Rose, 1992; Benting *et al.*, 1999).

Fixed to the outer layer of the plasma membrane by its GPI fragment, the mature uromodulin molecule protrudes into the lumen where proteolytic cleavage at residue phenylalanine 587 releases a 563-aa glycoprotein into the urine (Rindler *et al.*, 1990; Santambrogio *et al.*, 2008; Vyletal *et al.*, 2010). Urinary uromodulin is made up of double-helix filaments that polymerize to 1500-4000 nm long supramolecular strands with a tendency to assemble in gelatinous matrices (Bayer, 1964; Hoyer *et al.*, 1979; Jovine *et al.*, 2002) (Figure 2.2).

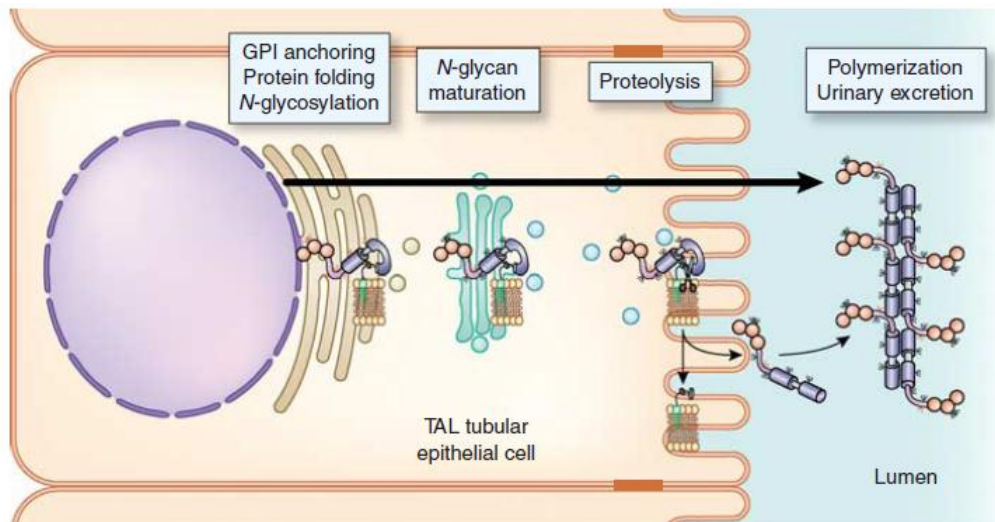


Figure 2.2: Uromodulin maturation, excretion and polymerization in the TAHL. GPI anchoring, disulphide bond formation and N-glycosylation occur in the endoplasmic reticulum. Glycan chains are modified in the Golgi apparatus. Release of an intramolecular hydrophobic interaction by a not yet identified protease (scissors) creates a polymerization-competent monomer that polymerizes in filaments. (Rampoldi *et al.*, 2011) License for the reuse of this figure was obtained in agreement with the Nature Publishing Group.

2.2.2 Function of uromodulin

Uromodulin can polymerize to gel-like matrices. Notably, uromodulin polymers take on various forms, and reversibly so, depending on cation concentrations: 100 mmol/l NaCl and 1 mmol/L CaCl₂ each trigger uromodulin gelation and both concentrations typically occur in normal urine (Stevenson *et al.*, 1971; Wiggins, 1987). These gel-like interconnections are hypothesized to form a water-proof layer on top of the luminal surface of TALH cells, thereby contributing to the upkeep of the medullary countercurrent gradient (Hoyer & Seiler, 1979; Hoyer *et al.*, 1979). Because of interactions with uromodulin molecules that are still cell-anchored, the gel is likely to move forward at a slow pace and thus to prolong the passage of sodium and potassium in the TALH so as to augment their reabsorption there (Vyletal *et al.*, 2010).

Type 1 fimbriated *E.coli*, a major pathogen in urinary tract infections (UTIs), carry another lectin-type adhesin with an affinity for high-mannose sequences which are found in both

urinary uromodulin and the urothelial membrane glycoproteins uroplakin Ia and Ib (Sharon, 1987; Wu *et al.*, 1996; Barnett & Stephens, 1997; Martinez *et al.*, 2000). The competitive binding of THP to *E.coli* fimbria shown *in vitro* validly suggests how uromodulin could obviate bacterial colonization of the urinary tract *in vivo* (Pak *et al.*, 2001). Transurethral introduction of *Klebsiella pneumoniae* and *Staphylococcus saprophyticus* into the bladder of wild-type and uromodulin-knockout mice revealed a decreased clearance of these bacteria from the urinary tract in knockout mice. This finding suggests that the protective function of uromodulin against bacterial cystitis is not confined to infections with *E.coli* (Raffi *et al.*, 2005)

Mo *et al.* (2004a) for the first time delivered *in vivo* results from uromodulin knockout mice indicating that uromodulin has a protective potential against calcium oxalate crystal formation.

Numerous investigations have been undertaken concerning the affinity of uromodulin for other urinary proteins. Rhodes *et al.* (1993) demonstrated that urinary uromodulin binds immunoglobulin G. Evidence was provided for enhanced uromodulin-IgG interaction in both glomerulo- and interstitial nephritis patients. This appeared not to be true for children with malignancies of lymphoid cells (Olczak *et al.*, 1999b; Olczak *et al.*, 1999a).

In vitro experiments regarding the binding of uromodulin glycomoiety to plant lectins, cytokines or albumin indicated for the resulting bonds to repress lymphocyte proliferation (Serafini-Cessi *et al.*, 1979; Cummings & Kornfeld, 1982; Hammarstrom *et al.*, 1982). Beyond that, polymorphonuclear neutrophils, lymphocytes and monocytes can bind to, and be activated by, uromodulin (Horton *et al.*, 1990; Thomas *et al.*, 1993; Yu *et al.*, 1993).

El-Achkar *et al.* (2008) showed that uromodulin-knockout (*Umod*^{-/-}) mice are more susceptible to acute ischemic damage. Thus, after renal ischemia reperfusion injury, proximal tubular cells were more damaged and Toll-like receptor 4 (TLR4) was expressed to a greater extent in the proximal tubular cells of *Umod*^{-/-} than in *Umod*^{+/+} mice. From their results the authors concluded that uromodulin can act as an indirect anti-inflammatory agent on neighbouring tubular segments as well. Therefore the authors suggested that the absence of uromodulin led to an increased inflammatory response and renal injury in THP^{-/-} mice.

The presence of uromodulin in the primary cilia of TALH cells points to a potential ciliary function of the protein. Ciliary expression of uromodulin was found to be reduced in MCKD2 patients harbouring an *UMOD* mutation (Zaucke *et al.*, 2010).

Since uromodulin and its regulatory mechanisms have, for the most part, been studied under *in vitro* or standardized *in vivo* conditions, there is controversy as to whether the above observations are applicable to physiological or pathological processes in the body. (Moonen & Williamson; Vyletal *et al.*, 2010). Comprehension of uromodulin in its full biological context remains therefore insufficient. However, the interest of the scientific community in uromodulin has risen in recent years, as a strong association of the uromodulin gene with chronic kidney diseases in humans has been identified in several genome wide association studies (Boger & Heid, 2011; Kottgen *et al.*, 2012). The results of two studies also suggest a connection of single nucleotide polymorphisms close to the *UMOD* gene to hypertension and cardiovascular disease (Iwai *et al.*, 2006; Padmanabhan *et al.*, 2010). Padmanabhan *et al.* (2010) consider an impaired renal function as an influence on their findings .

More than 50 *UMOD* mutations have hitherto been detected in humans (Figure 2.3). The majority of them clusters in exons 4, 5 and 8 of the gene which is located on chromosome 16p12.3 (http://www.genenames.org/data/hgnc_data.php?hgnc_id=12559; Vyletal *et al.*, 2010; Bollee *et al.*, 2011; Smith *et al.*, 2011). More than 90% of them constitute missense mutations and 62% of all *UMOD* mutations affect a cysteine residue and thus potentially alter the tertiary protein structure (Williams *et al.*, 2009). In-frame deletions occur to a small extent as well and can reduce the protein by up to 33 aa (Hart *et al.*, 2002; Vyletal *et al.*, 2010). Thus, the most frequent consequence of *UMOD* mutations is an aa exchange, oftentimes in the form of one more or less cysteine residue. So far, mutations leading to a complete loss of uromodulin expression could not be related to UAKD (Bleyer *et al.*, 2011).

2.3.3 Abnormalities at the molecular level

While the known mutations in the *UMOD* gene lead neither to a complete loss of expression nor to the expression of a shortened protein, they may alter the aa sequence of uromodulin, with cysteine being the most frequently substituted residue (Dahan *et al.*, 2003). The majority of such mutations was found in exon 4 which encodes the EGF-like domains (Hart *et al.*, 2002). Since all 24 cysteine residues are assumed to be part of intramolecular disulphide bridges, mutations affecting cysteine will lead to severe abnormalities in tertiary structure and protein stability. Similarly, a mutation-induced decrease in calcium affinity of EGF-like domains is likely to result in comparable structural alterations (Werner *et al.*, 2000; Rampoldi *et al.*, 2003).

2.3.4 Effects at the cellular level *in vitro*

Transient transfections of various cell lines with both mutant and wild-type *UMOD* constructs showed that plasma membrane expression of mutant uromodulin was significantly decreased when compared to wild-type controls. Immunofluorescence revealed that this impairment of protein trafficking was due to the conglomeration of immature mutant uromodulin in the enlarged endoplasmic reticulum. Wild-type uromodulin was still secreted in transfected cells but to a significantly lesser extent (Choi *et al.*, 2005b). Western blot analysis on the other hand resulted in equal transcription/translation efficiencies for both wild-type and mutant uromodulin. The dominant negative effect of the mutation is evident in the fact that the

amount of wild-type uromodulin still generated falls to substantially less than fifty per cent (Bleyer *et al.*, 2011). Of the intracellular uromodulin found in wild-type transfected cells, the greater fraction was localized in the Golgi apparatus (Bernascone *et al.*, 2006)

In 2005 Choi *et al.* observed a stronger early apoptosis signal in cells transfected with mutant uromodulin constructs. They also found, however, that colchicine, a mitosis inhibitor used to treat gout, and sodium 4-phenylbutyrate, a chemical chaperone, both enhanced uromodulin trafficking and excretion and led to a decrease in cell death. On the other hand, allopurinol, therapeutically used to control hyperuricaemia, had no effect on cell viability (Choi *et al.*, 2005b). Since *in vitro* experiments can only provide for cellular-level research, more coherent investigations of UAKD pathophysiology have to be conducted *in vivo*.

2.3.5 Phenotypes of UAKD

For a long time familiar juvenile hyperuricaemic kidney disease (FJHN) and medullary cystic kidney disease type 2 (MCKD2) were regarded as two distinct diseases with overlapping symptoms. The key phenotypic differentiator was the occurrence of corticomedullary cysts in MCKD2 versus a lack thereof in FJHN (Scolari *et al.*, 2004). It turned out that the largely common phenotype was no coincidence: both FJHN and MCKD2 were genetically mapped to the same chromosomal region (16p11 – 16p13) and were caused by mutations in the *UMOD* gene. (Kamatani *et al.*, 2000; Dahan *et al.*, 2001; Hart *et al.*, 2002; Wolf *et al.*, 2007). An artificial separation between these two diseases has since given way to the widely-used term MCKD2/FJHN complex (Dahan *et al.*, 2001; Bleyer *et al.*, 2003).

An Italian family displays yet a third phenotype due to a missense mutation in *UMOD* (C315R): glomerulocystic kidney disease (GCKD) (Gusmano *et al.*, 2002; Rampoldi *et al.*, 2003).

2.3.6 Clinical features of UAKD

Hyperuricaemia is the first clinical sign of UAKD and usually starts during childhood due to insufficient renal excretion of uric acid. Most patients, especially males, develop gout and gouty arthritis in their teen years (Bleyer *et al.*, 2003; Vylet'al *et al.*, 2006). Over time, urinary uromodulin excretion diminishes to the point of complete absence. Urine concentration ability

may be impaired, leading to polyuria and paediatric enuresis (Bleyer *et al.*, 2011). Further clinical signs of UAKD in humans frequently include a reduced fractional excretion of uric acid (men: < 5%; women: < 6%) or a creatinine clearance below 80 ml/min. Serum creatinine levels may rise above norm anytime between five and forty years of age. (Hart *et al.*, 2002; Bleyer & Hart, 2007). It is not until later in life (between the third and seventh decade) that patients develop chronic renal failure and end stage renal disease and require renal replacement therapy. As UAKD progresses, ultrasound imaging may reveal macroscopic alterations of the kidney such as reduced renal volume or medullary cysts. However, those are inconsistent findings and cannot be regarded as pathognomonic for UAKD. (Dahan *et al.*, 2003; Bleyer *et al.*, 2011).

2.3.7 Histopathology

Immunohistochemical staining of kidney biopsies of affected patients illustrates how mutant uromodulin forms clusters within the cytoplasm of TALH, thus contrasting the picture of control biopsies where anti-THP staining revealed a more even distribution of the protein throughout the cell, with a slight emphasis along the apical cell membrane (Dahan *et al.*, 2003; Rampoldi *et al.*, 2003) (Figure 2.4).

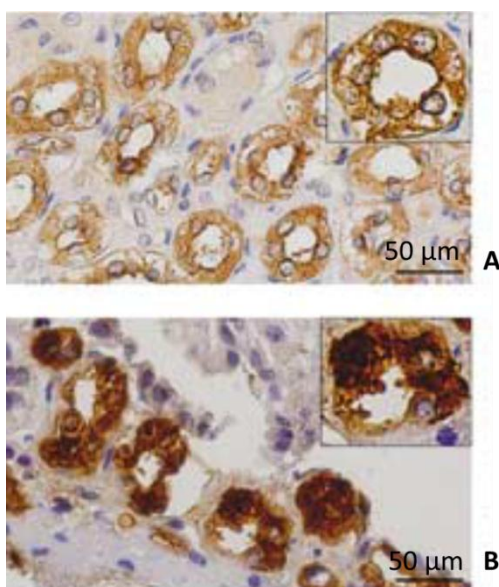


Figure 2.4: Immunohistochemical staining for uromodulin in human kidney biopsies. (A) Homogenous intracellular distribution and apical reinforcement of the uromodulin signal in the TALH cells of a control kidney biopsy. (B) Kidney biopsy of human with *UMOD* mutation showing condensed perinuclear clusters of the protein. (Vylet'al *et al.*, 2006) License for the reuse of this figure was obtained in agreement with the Nature Publishing Group.

Another common finding in both MCKD2/FJHN and GCKD is progressive interstitial fibrosis and tubular atrophy accompanied by thickened, lamellated basal membranes (Rampoldi *et al.*, 2003; Nasr *et al.*, 2008; Smith *et al.*, 2011) (Figure 2.5). Interstitial fibrosis and tubular atrophy are also referred to as IFTA (Bröcker *et al.*, 2010). Typically, the renal interstitium of UAKD patients is focally infiltrated with inflammatory cells (Dahan *et al.*, 2003). Occasionally, dilated or cystic tubules are part of the histopathology in MCKD2/FJHN patients but to a significantly lesser extent than the features described above (Scolari *et al.*, 2004). If at all, they are mostly diagnosed comparatively late (Bleyer *et al.*, 2005). GCKD is distinguished by cystic dilations of the glomerular tuft while tubular cysts occur rather sparsely (Sharp *et al.*, 1997; Scolari *et al.*, 2004). Whether the sporadic occurrence of glomerulosclerosis is a consequence of tubular atrophy or not is subject to debate (Bleyer *et al.*, 2005; Bleyer *et al.*, 2011).



Figure 2.5: Masson Trichrome staining of a representative renal biopsy specimen of a human patient with a *UMOD* mutation. Interstitial fibrosis appears as blue staining and surrounds tubules and glomeruli. Some of the tubules are dilated and show a flattened, at times wrinkled, epithelium. Original magnification x10. (Adam *et al.*, 2012) License for the reuse of this figure was obtained in agreement with Elsevier.

2.3.8 Ultrastructural alterations

In UAKD patients, the histopathological findings coincide with abnormalities on the ultrastructural level. Electron microscopy of renal biopsy tissue of UAKD patients revealed lamellar perinuclear stacks in TALH and distal tubule cells. What appeared to be hyperplastic membranes of the endoplasmic reticulum (ER) contained electron-dense accumulations of granules. The latter could be proven to be uromodulin by means of immunohistochemistry. No such abnormalities were observed in other cell compartments, nor were they found in proximal tubular cells. Cortical patches of tubular atrophy and interstitial fibrosis as well as interstitial infiltrates of mononuclear leukocytes were further findings which, in their context, all hinted to a storage disease that caused chronic tubulointerstitial nephropathy (Scolari *et al.*, 2004; Nasr *et al.*, 2008). As for the assumption that the impairment of protein processing be confined to the ER, immunofluorescence staining revealed a colocalization of ER- and UMOD-markers in individuals suffering from UAKD (Vyletal *et al.*, 2010) (Figure 2.6).

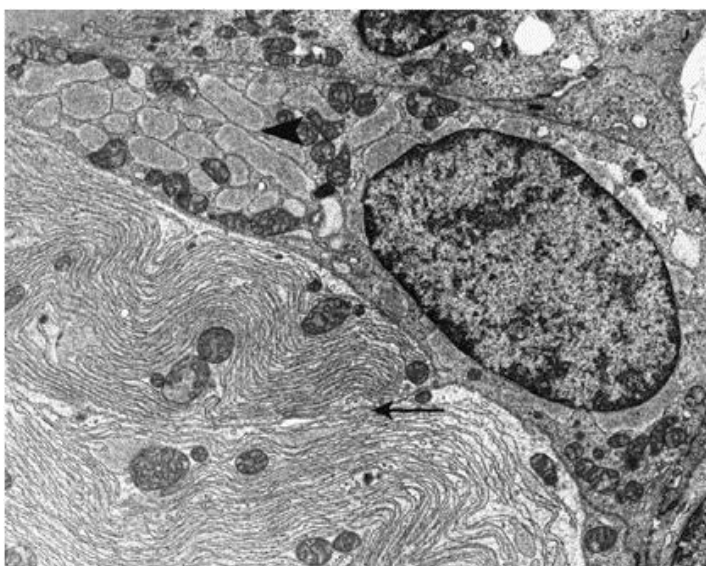


Figure 2.6: Transmission electron microscopy (TEM) of a distal tubular cell. The cell contains hyperplastic ER bundles (arrow) where few mitochondria alternate with areas of dilated ER containing storage material (arrowhead). Electron micrograph, original magnification x6000. (Nasr *et al.*, 2008). License for the reuse of this figure was obtained in agreement with the Nature Publishing Group.

2.3.9 UAKD therapy

To date, UAKD has been treated only symptomatically, meaning that patients receive allopurinol or, in case of intolerance, the uricosuric benzbromarone so as to ameliorate hyperuricaemia and gout (Fairbanks *et al.*, 2002; Schaffer *et al.*, 2010). Allopurinol inhibits xanthine oxidase, an enzyme that is necessary to form uric acid from xanthine and hypoxanthine (Pacher *et al.*, 2006). While opinions diverge on the effect of allopurinol on the progression of renal disease, *in vitro* studies revealed that it did not help the intracellular trafficking of mutant uromodulin, nor did it improve cell viability (Moro *et al.*, 1991; Fairbanks *et al.*, 2002; Bleyer *et al.*, 2003; Choi *et al.*, 2005b)

2.4 Murine models for functional analysis of uromodulin and of UAKD

In vivo research of the function of uromodulin and of UAKD has been performed on knockout, transgenic and ENU-mutant mouse lines. In 2004, two knockout mouse lines were generated: *Umod*^{tm1Kuma} (Bates *et al.*, 2004) and *Umod*^{tm1Xrw} (Mo *et al.*, 2004b). To elucidate the pathomechanism of UAKD, a transgenic mouse line expressing the human C148W *UMOD* mutation was established by a Japanese group (Takiue *et al.*, 2008b) while the murine mutation (C147W) corresponding thereto is represented by the Italian Tg^{*Umod*C147W} mouse line (Bernascone *et al.*, 2010). *Umod*^{A227T} and *Umod*^{C93F} are both UAKD mouse lines derived from the Munich ENU-mouse mutagenesis project and harbour a point mutation in the *Umod* gene (Kemter *et al.*, 2009; Prueckl, 2011).

2.4.1 Knockout mouse lines

The two knockout lines *Umod*^{tm1Kuma} and *Umod*^{tm1Xrw} were produced by means of gene targeting: A targeting vector disrupting the *Umod* gene was constructed, linearized, and electroporated into murine embryonic stem (ES) cells. ES cells showing the correct gene targeting were microinjected into blastocysts of C57BL/6J mice to obtain chimeras that were crossed with Black Swiss mice. Their offspring was screened for heterozygous (*Umod*^{+/-}) mutant animals which were interbred to create wild-type (*Umod*^{+/+}) and homozygous (*Umod*^{-/-}) mutant knockout mice. In line *Umod*^{tm1Xrw}, exons 1-4 and a proximal promoter region of the *Umod* gene were deleted. In line *Umod*^{tm1Kuma}, exon 2 of *Umod* was disrupted.

Both knockout lines were independently used to examine the role of uromodulin in ascending urinary tract infections. For this purpose, bladders of wild-type and knockout mice were inoculated with Type 1-fimbriated *E.coli*. *Umod*^{tm1Kuma} mice were also infected with Type P-fimbriated *E.coli*. Despite the ability of the urothelium to chip bacteria-infested, apoptotic cells, bacterial colonization remained significantly higher in experimentally infected bladders of knockout mice. Since lectin adhesins of Type 1 fimbriae have been shown to bind to mannosylated glycoproteins of urothelial plaques, the results of the *Umod* knockout experiments gave rise to the assumption that uromodulin, being itself rich in mannose moieties, competitively binds to Type 1 fimbriae and thus acts as defence mechanism against urinary tract infection with this strain of *E.coli* (Bates *et al.*, 2004; Mo *et al.*, 2004b). In addition, Mo *et al.* (2004a) observed that their uromodulin-deficient mice (*Umod*^{tm1Xrw}/*Umod*^{tm1Xrw}) were more prone to developing renal calcium oxalate crystals than wild-type controls. In their experiment drinking water had been supplemented with the oxalate precursor ethylene glycol (1%) and 4 IU/ml vitamin D₃ to augment calcium absorption. The authors listed calcium-binding EGF-like domains of uromodulin as a potential explanation for its direct interference with renal stone formation. *Umod*^{tm1Xrw} knockout mice did not show features of UAKD, i.e. they exhibited neither renal cysts nor fibrosis up to 24 months of age (Bates *et al.*, 2004). The blood chemistry and kidney function of *Umod*-knockout mice was inconspicuous under steady-state conditions. *Umod*^{-/-} mice of the *Umod*^{tm1Xrw} strain showed only significantly higher urinary sodium and chloride excretions than wild-type controls. Other ions and urinary creatinine excretion remained unchanged. It was therefore suggested that renal NaCl reabsorption might be impaired due to a uromodulin deficiency (Mo *et al.*, 2007).

Like the *Umod*^{tm1Xrw} knockout strain, *Umod*^{tm1Kuma} knockout mice did not exhibit alterations in kidney morphology, serum electrolytes, water intake, or urine excretion of potassium and uric acid. In contrast to *Umod*^{tm1Xrw} knockout mice, *Umod*^{tm1Kuma} knockout mice had no alterations in urinary sodium excretion compared to wild-type littermate controls. Augmenting fluid consumption of *Umod*^{tm1Kuma} mice by sucrose administration had no effect on blood and urine parameters of knockout mice. However, there were three significant differences between *Umod*^{-/-} (*Umod*^{tm1Kuma} / *Umod*^{tm1Kuma}) mice and their wild-type littermate controls: creatinine clearance in knockout mice was lowered by 63% compared to wild-type

controls. Secondly, wild-type mice counterbalanced water deprivation by reducing their urinary flow to 47%. *Umod*^{-/-} mice still excreted 72% of the original urine volume under these circumstances. No significant electrolyte losses were observed, though. Thirdly, a mild upregulation of various distal nephron transporters (α -subunit of Na⁺-K⁺-ATPase, NKCC2, NHE3, barttin, ClC-K2, ROMK, NCC, α -subunit of ENaC) was detected in *Umod*^{-/-} mice under steady state conditions while juxtaglomerular mRNA expression of both COX-2 and renin were downregulated by 51% and 32%, respectively (Bachmann, Mutig et al. 2005).

The *Umod*^{tm1Xrw} knockout strain was used to investigate the role of uromodulin in ischemia reperfusion injury (IRI). After reperfusion ischemia uromodulin expression rose in TAL cells and the interstitium of the outer medulla in *Umod*^{+/+} mice. Tubular dilation, necrosis and epithelial detachment were detected in both *Umod*^{-/-} and *Umod*^{+/+} kidneys after IRI, particularly in the outer medulla. In knockout mice necrotic tubules were visible after 15 minutes clamp time while it took 30 minutes of IRI for wild-type kidneys to develop diffuse tubular necrosis. Overall renal injury was more severe in *Umod*^{-/-} mice at all times of IRI (15, and 30 minutes). As for tubular cast formation, it was found to correlate to the degree of renal injury rather than to the presence of absence of uromodulin (El-Achkar *et al.*, 2008).

2.4.2 Mutant human *UMOD*^{C148W} transgenic mouse line

In 2008 Takiue et al. published a transgenic mouse line harbouring the human *UMOD* mutation C148W which had been found in FJHN/MCKD2 patients (Rampoldi *et al.*, 2003). For the construction of the transgene, murine *Umod* promoter sequences were fused to the human *UMOD* cDNA sequence after incorporation of the T444G mutation. The 5587 bp murine *Umod* promoter-augmented T444G human *UMOD* chimeric gene construct was injected into fertilized oocytes of C57BL/6 inbred mice. 32% of the F0 offspring were found to harbour the transgene. Hemizygous mice were compared to non-transgenic littermates which served as wild-type controls (Rezende-Lima *et al.*, 2004; Takiue *et al.*, 2008b). RT-PCR revealed murine *Umod* gene expression in both transgenic and wild-type kidneys whereas human *UMOD* mRNA detection was confined to transgenic kidneys. Both Western blot and immunofluorescence results showed the presence of human and murine uromodulin protein in microsomes of TALH cells. Murine uromodulin was expressed in the form of a 103

kDa and a 117 kDa protein in both strains. A comparison of the renal uromodulin levels of wild-type and transgenic mice revealed a significant increase of the 103 kDa protein in transgenic kidneys. Interstrain comparison of urine uromodulin excretion showed no difference at any age. However, transgenic mice excreted endogenous uromodulin only. Both forms of murine uromodulin (103 kDa and 117 kDa) as well as the 93 kDa human uromodulin appeared in the soluble and insoluble fraction of the Triton X-100 extraction, indicating that they all reached the plasma membrane (Takiue *et al.*, 2008a). *UMOD*^{C148W} transgenic mice did not exhibit impaired kidney function (Takiue *et al.*, 2008b). The authors suggest mice hemizygous for the *UMOD*^{C148W} mutation could serve as a model for the initial stages of UAKD granted that mutant uromodulin causes the accumulation of wild-type uromodulin in the plasma membrane and only later leads to decline in urinary excretion, followed by intracellular retention, cell death and extensive renal pathology (Takiue *et al.*, 2008a)

2.4.3 Tg^{UmodC147W} transgenic mouse line

The second transgenic mouse model for UAKD was published by Bernascone *et al.* in 2010 to mirror the human *UMOD* mutation C148W by integrating the equivalent murine mutation C147W into an *Umod* minigene. The transgene comprised a 2.9 kb promoter, exons 1-11, the 3' sequence and, in front of EGF-like domain I, an HA-tag to mark the transgenic uromodulin. Two strains were produced: one with the wild-type *Umod* sequence and the other one harbouring the *Umod* mutation C147W. FVB mouse eggs were fertilized and injected with wild-type or C147W *Umod* transgene copies and produced 8 wild-type and 5 C147W transgenic founder mice. Both lines showed stable transmission of a fully inserted transgene and were inconspicuous compared to their non-transgenic littermates in terms of viability and general condition. Wild-type transgenic *Umod* mRNA expression was found to be 50% of the endogenous gene while C147W *Umod* transcription approximated the endogenous level to 80%. Western blot analysis showed that both Tg^{Umodwt} and Tg^{UmodC147W} mice expressed two isoforms of transgenic uromodulin: the mature 120 kDa protein and its immature ER precursor protein of about 100 kDa. Compared to Tg^{Umodwt} kidneys, those of Tg^{UmodC147W} mice showed a markedly increased amount of both proteins, particularly of the precursor protein. Regarding the exact localization of uromodulin expression, immunofluorescence co-staining with nephron segment-specific markers confined it to the TALH and the distal convoluted

tubule. Western blot analysis of the urine revealed a clear reduction of both transgenic and endogenous uromodulin in $Tg^{UmodC147W}$ mice. Immunohistochemistry for transgenic uromodulin depicted a protein accumulation in a granular pattern within the tubular cells of $Tg^{UmodC147W}$ kidneys rather than on the apical cell membrane. Kidney sections of 3-month-old $Tg^{UmodC147W}$ mice compared to those at 6 months of age showed that intracellular aggregation intensified with age. Tg^{Umodwt} kidney cells contained homogeneously spread uromodulin with an increased localization along the apical membrane. In some $Tg^{UmodC147W}$ kidney sections, the authors detected an increased amount of uromodulin along the basolateral membrane of tubular cells as well as interstitial uromodulin deposits and referred to an interstitial protein release as a potential explanation. Regarding the difference between wild-type and mutant uromodulin distribution within TALH cells, immunofluorescence results were concordant with immunohistochemistry. A co-localization of mutant uromodulin and ER chaperone markers specified the endoplasmic reticulum as the organelle of protein retention. In addition, the presence of intraluminal casts was a frequent observation in $Tg^{UmodC147W}$ mice. In a comparison of baseline plasma and urine parameters between $Tg^{UmodC147W}$ and Tg^{Umodwt} mice $Tg^{UmodC147W}$ plasma showed significantly increased urea and creatinine concentrations. Plasma vasopressin activity was higher in mutant mice as well. Both water intake and urine excretion in mutant mice were higher than in Tg^{Umodwt} mice. Furthermore, $Tg^{UmodC147W}$ strain had hypercalciurea as well as lowered urinary pH and osmolality. The urine concentrating ability of $Tg^{UmodC147W}$ mice remained low after water deprivation. Since the expression of vasopressin and its target genes was elevated after water deprivation, the authors suspected this hypoosmolality to be based on kidney malfunction. Progressive histopathological lesions in $Tg^{UmodC147W}$ kidneys were found by light and electron microscopy: Findings at 12 weeks of age included tubular dilation and casts, tubular atrophy, and foci of interstitial fibrosis and inflammatory infiltrates. At 24 weeks of age, tubulointerstitial damage had progressed and intensified. At this age, some of the dilated tubules had become cystic and were HA-positive, indicating a selective damage of TALH cells expressing mutant uromodulin. The renal medullary interstitium was infiltrated with a higher number of macrophages than at 12 weeks of age. Tubular basement membrane disintegration and epithelial detachment thereof were further observations. On ultrastructural analysis of TALH epithelium, intracellular membrane stacks appeared hyperplastic but ribosome-less and were filled with droplets of high electron

density. Other cellular compartments (organelles, membrane) were frequently defective as well. Tg^{Umod^{wt}} mice exhibited no pathological findings between 3 and 6 months of age. An downregulation of both mRNA and protein expression of TALH-specific transporters (NKCC2, ROMK, CIC-Kb) but not of transporters characteristic for other nephron segments was regarded as further evidence for selective TALH damage (Bernascone *et al.*, 2010).

2.4.4 **ENU-induced *Umod* mutant mice**

Two mutant mouse lines are subject to this study: *Umod*^{A227T} (UREHR4) and *Umod*^{C93F} (UREHD1). Both are derived from the Munich ENU mouse mutagenesis project in which intraperitoneal injection of ENU 10-week-old male C3H mice produced random point mutations in spermatogonial stem cells. After mating them to C3H females, offspring occurred with mutant phenotypes interfering with various organ and metabolism functions (Aigner *et al.*, 2007). For the generation of novel mouse models showing kidney disease, clinical chemical analysis was carried out at an interval of 3 weeks in 3-month-old animals. G1 mice with elevated plasma urea levels (>70 mg/dl) in both tests were selected for further breeding with wild-type CH3 females. Inheritance of abnormal phenotypes was tested in G2 offspring from the mating of the affected G1 mouse and wild-type C3H mice. The screen for recessive mutations was carried out on G3 mice produced in a two-step breeding scheme from G1 mice which did not harbour dominant mutations. Inheritance of phenotypes in the inbred C3H genetic background was tested on G4 intercross or G4 x G3 backcross offspring (Rathkolb *et al.*, 2000b; Rathkolb *et al.*, 2000a; Aigner *et al.*, 2007). Thus, the ENU mouse mutagenesis project resulted in the development of five mouse lines exhibiting increased plasma urea levels: The two mouse lines which are subject to this study are line UREHD1 and line UREHR4. Both mutant mouse lines harbour a dominant mutation, with mutant mice of line UREHD1 exhibiting a stronger phenotype than line UREHR4 (Aigner *et al.*, 2007; Kemter *et al.*, 2009; Prueckl, 2011).

2.4.4.1 ***Umod*^{A227T} mutant mice**

The mutant mouse line UREHR4 was phenotypically grouped as an autosomal recessive mutant mouse line exhibiting increased plasma urea levels. In 2009, Kemter *et al.* identified the causative mutation of this mutant mouse line within the uromodulin cDNA nucleotide

position 971 leading to an aa exchange from alanine to threonine at position 227. Henceforth, the mouse line has been referred to as *Umod*^{A227T}. The mutation is of interest in that it occurs in a region of the gene which is well conserved between species and where numerous human *UMOD* mutations causing UAKD are known (W202, R204, C217, R222, C223, T225, P236, and C248) (Figure 2.7) (Bleyer *et al.*, 2003; Dahan *et al.*, 2003; Wolf *et al.*, 2003; Kudo *et al.*, 2004).

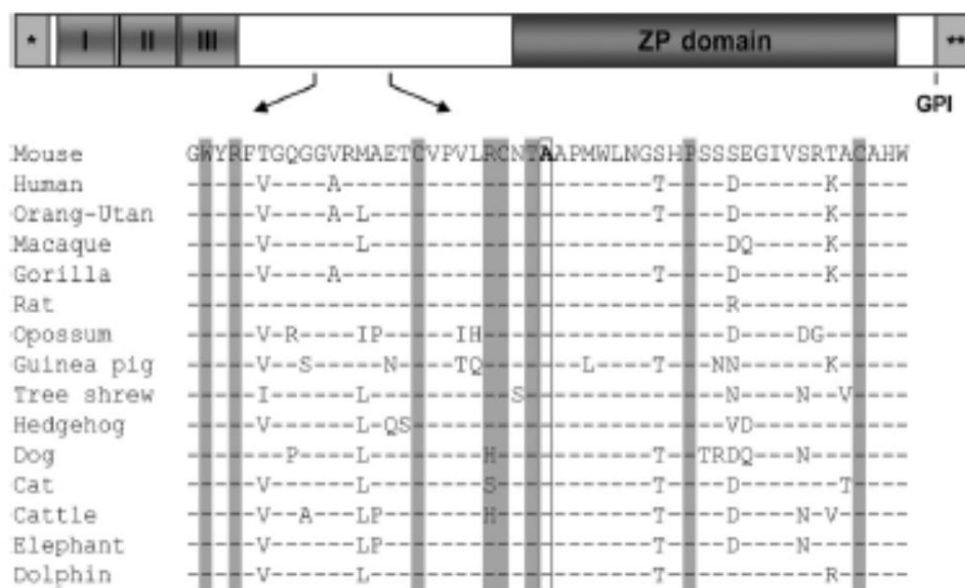


Figure 2.7: Uromodulin protein structure and sequence alignment of murine uromodulin. AA 202–252 correspond to aa 201–251 of the human sequence. I-III: EGF-like domains; ZP domain: zona pellucida domain; *, N-terminal signal peptide; **, sequence contained in propeptide which is cleaved during protein processing and linked to a GPI anchor. Bold A: alanine at position 227. The positions of the different mutations reported in humans are highlighted (W202, R204, C217, R222, C223, T225, P236, C248) (6, 10, 21, 36). (Kemter *et al.*, 2009)

Clinical chemistry data of plasma and urine were collected for wild-type, heterozygous and homozygous *Umod*^{A227T} mutant mice of both genders. Wild-type littermates served as controls for all analyses performed. As adult heterozygous mutants mice also exhibited a mild phenotype significantly different from wild-type littermate controls, the *Umod*^{A227T} mutation were reclassified as a dominant mutation.

At 2 weeks of age, neither urea nor creatinine levels in the plasma of mutant mice were increased. While a trend towards higher plasma cholesterol and triglyceride levels was observed for two-week-old heterozygous mutant females, this did not apply to homozygous mutant females or mutant males. Four-month-old homozygous and heterozygous mutant mice of both genders exhibited plasma urea and creatinine levels that were significantly raised above those of sex-matched wild-type littermates. At this age, the plasma of both male and female mutant mice contained lower amounts of cholesterol, triglycerides and non-esterified fatty acids than that of gender-matched wild-type mice. Between ages 3 and 4 months, homozygous mutants excreted urine of comparatively low osmolality, its volume being 1.5 fold higher than that of wild-type controls. Homozygous mutant mice of both genders also showed a marked decrease in urine-to-plasma ratios of sodium, potassium, urea and uric acid. Regarding fractional excretion values, however, only those for urea and uric acid were significantly lower in homozygous mutant mice. Hyperuricaemia did not occur presumably due to preserved uricase activity in mice which is absent in humans. Moreover, hypercalciuria, hypermagnesiuria and a decreased excretion of uromodulin were observed in both male and female homozygous mutant mice. Although mature, fully glycosylated uromodulin was detected in the urine of homozygous mutant mice, urinary uromodulin excretion was considerably decreased in homozygous mutant mice compared to wild-type mice. Only a mild increase of water consumption was detected in homozygous mutants. Water deprivation revealed impaired urine concentrating abilities of homozygous mice. Body weight, fat mass and fat content were reduced in *Umod*^{A227T} mutants of both genders whereas their lean content was higher than that of wild-types. Also, homozygous mutant mice exhibited a significant reduction in metabolic rate. Osteopenia due to increased urinary calcium excretion was evident in four-month-old homozygous mutant mice where dual-energy X-ray absorptiometry revealed a decline in bone mineral density and content. Upon light microscopy, kidneys sections of 3-6 month-old heterozygous and homozygous mutant mice did not differ from those of wild-type controls. Immunohistochemistry analysis on the other hand revealed that uromodulin distribution in mutant TALH cells compared to that of UAKD patients: protein clusters assembled around the nucleus and differed therefore from the homogenous, apically reinforced staining visible in wild-type kidney sections. Electron microscopy of mutant TALH cells bore further resemblance with UAKD histopathology: piles

of what appeared to be hyperplastic ER membranes with sporadically visible granules surrounded the nucleus. Mice heterozygous for the *Umod*^{A227T} mutation exhibited a milder phenotype than homozygous mutant mice of this line. Also, elevated plasma urea levels were detected at a higher age in heterozygous than in homozygous *Umod*^{A227T} mutant mice (Kemter *et al.*, 2009). The authors suggest that mutant *Umod*^{A227T} uromodulin exerts a gain-of-toxic function by interfering with the ER homeostasis due to highly impaired uromodulin maturation and retention within the hyperplastic ER. The coordinated interaction of the numerous ion transporters expressed in TALH cells is important for the TALH function of reabsorbing up to 20% of the glomerular filtrate and for the ability of the kidney to concentrate and dilute urine (Gamba & Friedman, 2009). Therefore, structural alterations and disturbance of ER homeostasis due to maturation retardation of mutant uromodulin might cause TALH dysfunction in *Umod*^{A227T} mutant mice through which the impaired renal function like impaired urinary concentration ability, hypercalciuria and hypermagnesiuria can be explained (Greger, 1985; Gamba, 2005). Due to the afore-discussed parallels to UAKD pathology, the *Umod*^{A227T} line is regarded as a suitable murine model for this disease (Kemter *et al.*, 2009).

2.4.4.2 *Umod*^{C93F} mutant mice

The founder of this mouse line was male No. 20003171 of the Munich ENU mouse mutagenesis project. This G1 mouse exhibited high plasma urea levels in the clinical chemical screen and was subsequently identified as carrier of a dominant mutation. The mutant line UREHD1 was bred by mating phenotypically heterozygous mutant mice to C3H wild-type littermates (Aigner *et al.*, 2007). The exact point mutation was later identified as the base pair exchange G→T of nucleotide 278 of the *Umod* gene. Causing a substitution of cysteine (C) by phenylalanine (F) at position 93 of uromodulin, this mutation affects disulphide bond C93-C105 in the EGF-like domain II of uromodulin (<http://www.uniprot.org/uniprot/Q91X17>; Prueckl, 2011). An analogue disulphide bond exists in human uromodulin between C94 and C106 and can be disrupted by UMOD mutation C106Y (Figure 2.8) (<http://www.uniprot.org/uniprot/P07911>); Zaucke *et al.*, 2010).

haemoglobin and red blood cell distribution width. On the whole, a phenotypic analogy could be drawn between of heterozygous *Umod*^{C93F} mutant and homozygous *Umod*^{A227T} mutant mice (Prueckl, 2011).

2.5 ER stress and the unfolded protein response

Secretory proteins such as uromodulin undergo a series of folding, intra- and intermolecular disulphide bond formation and glycosylation that is initialized in the ER (Hubbard & Ivatt, 1981; Kornfeld & Kornfeld, 1985; Fewell *et al.*, 2001; Schroder & Kaufman, 2005). Only properly processed polypeptides leave the ER for further intracellular trafficking and modification in the Golgi apparatus (Ellgaard *et al.*, 1999). A cellular mechanism referred to as “quality control” leads to the retention of misfolded or incomplete molecules in the ER where they become subject to further modification or degradation (Hurtley & Helenius, 1989; Klausner & Sitia, 1990). To a certain degree, abnormal polypeptides are physiological by-products of protein synthesis which the cell is capable of coping with. If, however, an extensive accumulation of mutant, misfolded protein results in ER stress which in turn initiates the unfolded protein response (UPR) (Gething *et al.*, 1986; Kozutsumi *et al.*, 1988). The UPR tackles an ER-overload in two ways: ER hyperplasia and activation of ER-associated chaperones and foldases are countermeasures to deal with already assembled protein (Schroder & Kaufman, 2005). This mechanism has been well conserved in the cellular evolution of yeast, worms, flies and vertebrates (Ishikawa *et al.*, 2011). In addition, increased ER associated degradation (ERAD) disburdens the organelle from unfolded protein (Friedlander *et al.*, 2000; Travers *et al.*, 2000). To prevent further protein influx to the ER, DNA transcription and mRNA translation are reduced to a minimum (Harding *et al.*, 1999; Martinez & Chrispeels, 2003; Pakula *et al.*, 2003). If ER stress cannot be alleviated through the UPR, the affected cells will become apoptotic (Ma & Hendershot, 2002; Rutkowski & Kaufman, 2004). It has been suggested that reactive oxygen species are of relevance as triggers for ER stress (Yokouchi *et al.*, 2008). On the other hand, reactive oxygen species are a side-product of increased protein oxidation during ER stress and may bring the UPR into action (Malhotra & Kaufman, 2007) (Figure 2.9).

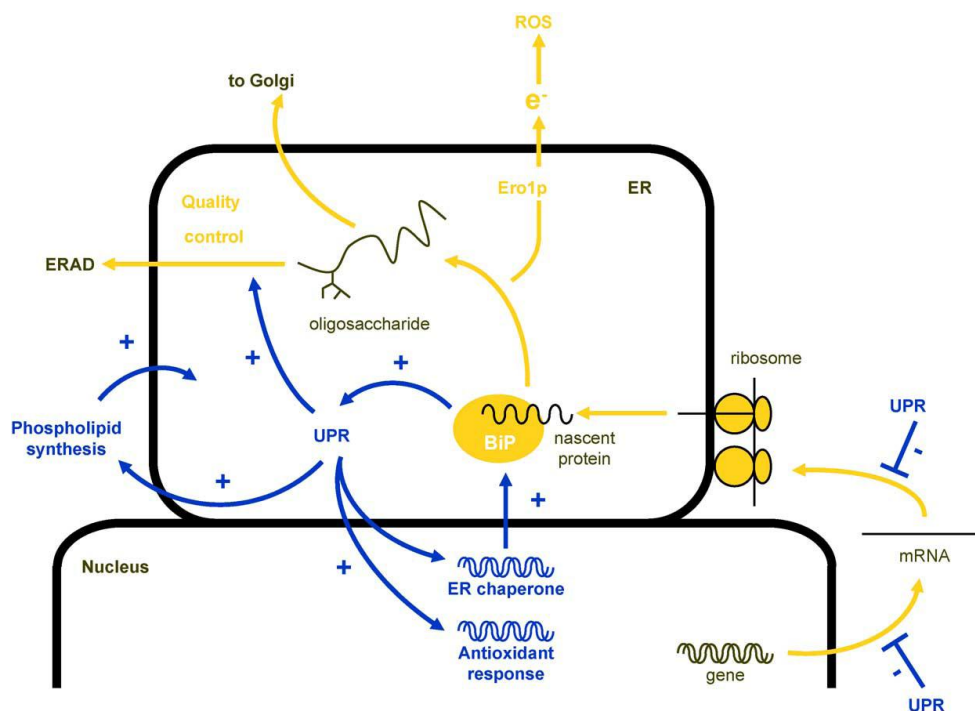


Figure 2.9: Unfolded protein response scheme. Protein passage through the ER (orange) and main mechanisms of the unfolded protein response (blue) to accommodate the ER protein folding capacity to the protein influx into the ER. ER: endoplasmic reticulum, ROS: reactive oxygen species (Schroder & Kaufman, 2005). License for the reuse of this figure was obtained in agreement with Elsevier.

2.5.1 Molecular chaperones

Although the primary structure of a protein encodes its three-dimensional arrangement and suffices for correct protein folding *in vitro*, conditions *in vivo* are more complex and require a quality control mechanism (refer to 2.5) to assure biosynthesis of intact proteins (Anfinsen, 1973; Dobson & Karplus, 1999; Lee & Tsai, 2005). Chaperones play an essential part in protein quality control: they are proteins of various sizes and structures that catalyse protein biosynthesis without integrating into the final protein structure (Ellis, 2006). They do not only assist in correct polypeptide folding, oligomerisation, glycosylation or disulphide bond formation but also prevent protein aggregation (Fewell *et al.*, 2001; Hartl & Hayer-Hartl, 2002; Ellgaard & Helenius, 2003; Young *et al.*, 2004). While chaperones are continuously expressed in the cell, their synthesis rate rises under cellular stress (Gething & Sambrook, 1992). This was first discovered in cells exposed to heat and has given some chaperones the

name heat shock protein (Hsp). In the meantime, it has been found to apply to a myriad of cellular stress conditions leading to an accumulation of immature protein (Ananthan *et al.*, 1986; Craig & Gross, 1991). ER-associated chaperones and enzymes constitute three major groups: heat shock proteins (e.g. Hsp70) and their respective co-chaperones (e.g. Hsp40), lectins (e.g. calnexin, calreticulin) and protein disulphide isomerases (PDIs) (Nishikawa *et al.*, 2005). Typically, ER chaperones recognize and bind regions of nascent proteins that would not be exposed in the native state. Hsp70, for instance, binds and releases hydrophobic polypeptide regions in an ATP-dependent cycle (Bukau & Horwich, 1998). The ER membrane chaperone calnexin and its luminal analogue calreticulin, on the other hand, recognize monoglucosylated oligosaccharides of glycoproteins as their substrate (Trombetta & Parodi, 2003). While these lectins stabilize the polypeptide, enzymes such as PDIs catalyse intramolecular bond formation (Schrag *et al.*, 2003). Proteins that fail to achieve their final structure remain bound to chaperones and thus eventually become a target for degradation (Hammond & Helenius, 1995).

2.5.2 Chemical chaperones

The term “chemical chaperones” was given to a group of exogenous, low molecular weight compounds which were found to assist and correct protein folding (Welch & Brown, 1996). This was first observed in the treatment of cells expressing mutant cystic fibrosis transmembrane conductance regulator protein (CFTR) with substances like glycerol and trimethylamine N-oxide (Brown *et al.*, 1996). Hence, an ever increasing number of chemicals, including 4-PBA, have been discovered to improve protein homeostasis in ER storage diseases (Qi *et al.*, 2004; Ozcan *et al.*, 2006; Basseri *et al.*, 2009; Malo *et al.*, 2012).

Sodium 4-phenylbutyrate:

Sodium 4-phenylbutyrate (4-PBA) is the salt of 4-phenylbutyric acid, an aromatic fatty acid of low molecular weight (186.18 g/mol) that acts as a non-competitive inhibitor of histone deacetylase. In humans 4-PBA functions as a pro-drug, meaning that, after oral administration, mitochondrial β -oxidation in liver and kidney cells converts 4-PBA to 4-phenylacetic acid (4-PAA) which is equally able to inhibit histone deacetylase and to penetrate the blood-brain barrier (Spira & Carducci, 2003; Scandinavian Formulas, 2011). 4-

PAA is conjugated to coenzyme A (CoA) and the resulting compound, 4-phenylacetyl-coenzyme A (4-PAA-CoA) binds to glutamine. This results in the formation of 4-phenylacetyl which is excreted with the urine (Yu *et al.*, 2001). In other mammals 4-PAA binds glycine rather than glutamine so that the compound excreted is phenylacetylglycine (Moldave & Meister, 1957). 4-PBA is licensed in Europe and by the FDA as a treatment for urea cycle disorders where its metabolites serve as ammonia scavengers (Brusilow, 1991; Iannitti & Palmieri, 2011). 4-PBA has furthermore been found to promote foetal haemoglobin production in sickle cell anaemia and β thalassemia (Dover *et al.*; Dover *et al.*, 1994; Collins *et al.*, 1995). Clinical and *in vitro* trials indicate that 4-PBA could ameliorate spinal muscular atrophy and cancer (Carducci *et al.*, 2001; Mercuri *et al.*, 2004). More recent investigations attend to the chaperone-like qualities of PBA, beginning with Rubenstein *et al.* who observed that 4-PBA interfered *in vitro* with the binding of Hsp70 to $\Delta F508$ mutant CFTR protein in cystic fibrosis epithelial cells, thus “smuggling” mutant protein past degradation and allowing for it to be translocated to the plasma membrane (Rubenstein & Zeitlin, 2000). Since then, chaperone-like qualities of 4-PBA were observed *in vivo* and *in vitro* for a number of ER storage diseases (Chamcheu *et al.*, 2011; Malo *et al.*, 2012; Misawa *et al.*, 2012). Regarding the effect of 4-PBA on intracellular trafficking of mutant uromodulin, two separate *in vitro* experiments have delivered concordant results: two sets of HEK293 and TALH cells were stably transfected with a vector coding for an in-frame *UMOD* bp deletion (H177_185del) and with another vector carrying a *UMOD* missense mutation (C148Y). For both types of cell and mutation, incubation with 4-PBA increased the amount of wild-type and mutant protein excreted from the ER and released into the culture medium. Moreover, it shifted the primarily cytosolic accumulation of mutant protein to an increased appearance along the plasma membrane. Viability of 4-PBA-treated mutant cells equalled that of untreated wild-type cells. In contrast, apoptosis occurred later and to a smaller extent in 4-PBA-incubated cells (Choi *et al.*, 2005b). The chaperone-like effect of 4-PBA on MCKD cells expressing wild-type and C126R or C217G mutant uromodulin was strikingly similar (Ma *et al.*, 2012). In addition to the results explicated above, Ma *et al.* were able to show that there was not only less of the molecular chaperone Hsp70 in C126R and C217G mutant cells but that 4-PBA incubation of these cells also boosted Hsp70 expression near wild-type levels. *In vivo* experiments concerning the interaction of 4-PBA and mutant uromodulin have not been published so far.

2.6 Oxidative stress in chronic kidney disease

Chronic renal failure creates a disequilibrium between pro-oxidant metabolites and antioxidant systems in a way that reactive oxygen species (ROS) such as superoxide anions and peroxides cannot be sufficiently coped with by endogenous antioxidants like glutathione or superoxide dismutase (Hasselwander & Young, 1998; Martin-Mateo *et al.*, 1999; Hambali *et al.*, 2011). There is evidence that ROS play a role in the signalling pathways of cellular apoptosis and renal fibrosis which are common features of chronic kidney disease (Sarkar *et al.*, 2011; Nie & Hou, 2012).

4-Hydroxy-TEMPO: a superoxide dismutase mimetic:

4-Hydroxy-TEMPO (4-hydroxy-2,2,6,6-tetramethylpiperidin-1-oxyl), also referred to as tempol, is a heterocyclic nitroxide antioxidant (molecular weight 172.24 g/mol) (Wilcox, 2010; Sigma-Aldrich, 2011). Tempol can penetrate the plasma membrane and mimics superoxide dismutase (SOD) by catalysing the conversion of superoxide anions and other ROS to H₂O₂ and O₂ (Krishna *et al.*, 1992; Krishna *et al.*, 1996; Wilcox & Pearlman, 2008). The stable organic free radical tempol can be reduced to hydroxylamine by NADPH and cytochrome c in liver microsomes as well as by the sulfhydryl residues of proteins (Couet *et al.*, 1985; Iannone *et al.*, 1989). *In vitro* and *in vivo* comparisons of liver and kidney cells showed a shorter half-time reduction for tempol in kidney cells, which was attributed to renal mitochondria-richness (Kamataria *et al.*, 2002; Ueda *et al.*, 2003). Furthermore, renal injury was found to impair reducing conditions (Ueda *et al.*, 2002; Oteki *et al.*, 2005). Both acute and long-term administration of tempol to male spontaneously hypertensive rats (SHR) resulted in a blood pressure fall in more than 85% of all rats in the experiments (Okamoto & Aoki, 1963; Patel *et al.*, 2006; Wilcox & Pearlman, 2008). Intravenously injected tempol induced a rapid response which, besides a blood pressure decline, included a lower heart rate and sympathetic tone but was reversed after 15 minutes (Xu *et al.*, 2002, 2004; Patel *et al.*, 2006). The result of long-term oral and subcutaneous tempol administration was confined to a gradual decrease of blood pressure which then remained low for several weeks (Welch *et al.*, 2005). Systemic tempol administration reduced blood pressure in hypertensive mouse models as well (Dikalova *et al.*, 2005). The blood pressure-reducing properties of tempol were also

observed in animal models where hypertension had been caused by renal artery clipping (Welch *et al.*, 2003; Guron *et al.*, 2006; Christensen *et al.*, 2007), angiotensin II-infusion (Cai *et al.*, 2003; Wang *et al.*, 2003), deoxycorticosterone acetate and/or aldosterone salt (Ghosh *et al.*, 2004; Hirono *et al.*, 2007), or lead and zinc administration (Vaziri *et al.*, 2001). Renal effects of prolonged tempol administration entail an increase in renal blood flow through medullary vasodilatation as well as enhanced natriuresis (Feng *et al.*, 2001; Zou *et al.*, 2001). Contradictive suggestions have been made as to whether tempol promotes or hinders proximal tubular reabsorption (Wu & Johns, 2004; Banday *et al.*, 2005). In contrast, experiments performed on perfused TALH segments unanimously indicated an interaction of tempol with superoxide, the levels of which rise due to increased luminal flow, tubular transport or stretch. Inhibition of superoxide in turn reduced Na⁺ reabsorption in the TALH-segment (Ortiz & Garvin, 2002; Garvin & Hong, 2008).

3 Materials and methods

3.1 Research design

This study was performed on the *Umod*^{A227} and *Umod*^{C93F} mutant mouse lines and pursued two objectives.

First, the development and progression of renal alterations was compared between homozygous mutant, heterozygous mutant and wild-type mice of each mouse line. To this end, the occurrence of alterations was assessed qualitatively in both mouse lines. IFTA as well as inflammatory cell infiltrates, being the most consistent findings in *Umod* mutant mice, were quantified with stereological methods. Whether tubular atrophy affected TALH cells in particular was investigated by assessing the renal TALH cell content of these mice. The morphologic analysis of kidneys was performed in mice of two age groups (14-month-old and 20-22-month-old mice) to obtain information about disease progression and putative correlation of morphologic parameters and clinical phenotype.

The second part of the study investigated the potential of the chemical chaperone 4-PBA and of the radical scavenger tempol as causative therapy for UAKD. Therefore, 4-PBA and tempol were administered orally to homozygous mutant and wild-type males of both mouse lines over a period of two months. A placebo group obtaining no drug served as control group. Evaluations of blood and urine parameters as well as morphological kidney analyses were performed to evaluate the putative therapeutic effect of drug administration.

Morphological kidney analysis	Number of animals examined											
	<i>Umod</i> ^{A227T}			<i>Umod</i> ^{C93F}								
	wt		het	hom		wt		het	hom			
m		f		m		f		m		f		
Qualitative histological kidney												
14 months of age							10 5		9 11		7 4	
20-22 months of age	18 13		18 7		20 10		15 19		28 19		4 3	
Quantitative evaluation of histologic kidney alterations												
14 months of age							6		7		7	
20-22 months of age	6		6		6		6		6		6	

Table 3.1: Number and age of mice for histological kidney analysis. wt: wild-type mice, het: heterozygous mutant mice, hom: homozygous mutant mice. m: male, f: female.

Type of analysis	Number of animals (male) examined in each treatment group								
	4-PBA			tempol			placebo		
	wt	A227T	C93F	wt	A227T	C93F	wt	A227T	C93F
Determination of body weight (every 7 days)	19	19	11	13	17	11	14	3	8
Spot urine samples (every 14 days)	19	19	11	13	17	11	14	3	8
Clinical chemical analysis of blood plasma									
2 months of age	19	19	11	13	17	11	14	3	8
3 months of age	19	19	11	13	17	11	14	3	8
4 months of age	19	19	11	13	17	11	15	6	13
Clinical chemical analysis of urine (at 4 months of age)	19	19	11	13	17	11	15	6	13
Metabolic cage analysis	19	19	11	13	17	11	15	6	13
Necropsy (at 4 months of age)									
perfusion fixation of kidneys	9	9	6	5	5	5	1	1	2
kidney preparation for molecular analysis	9	10	5	8	12	6	14	5	11
Western blot analysis (urinary uromodulin)	19	19	11	13	17	11	15	6	13
Immunohistochemical analysis (kidney)	9	9	6	5	5	5	1	1	2
Ultrastructural analysis (kidney)	3	4	3	3	4	4	2	2	2

Table 3.2: Number of mice in different types of analyses during the treatment assay. wt: wild-type mice, A227T: homozygous *Umod*^{A227T} mutant mice, C93F: homozygous *Umod*^{C93F} mutant mice.

3.2 Animals

The two mouse lines, *Umod*^{C93F} and *Umod*^{A227T}, which were established in the Munich ENU mouse mutagenesis project, were analysed in this study. Both mutant mouse lines harbour a mutation within the *Umod* gene leading to an aa exchange. Major characteristics of the phenotype of *Umod*^{C93F} and *Umod*^{A227T} mutant mice include increased plasma urea levels and impaired urine concentrating ability (Kemter *et al.*, 2009; Prueckl, 2011).

The mutant lines were maintained in the mouse facility at the Chair for Molecular Animal Breeding and Biotechnology, Moorversuchsgut, Oberschleißheim under a controlled specific-pathogen-free (SPF) hygiene standard according to the Federation of European Laboratory Animals Science Associations (FELASA) protocols (Nicklas *et al.* 2002; <http://www.felasa.eu/>). Mouse husbandry was performed under standard environmental conditions (22 ± 2°C, 40-50% relative humidity, 12 h light: 12 h dark cycle) and mice were provided with a standard rodent diet (V1124-3; Ssniff, Soest, Germany) and water *ad libitum*. Cages and drinking bottles were exchanged weekly. Depending on age and weight, groups of two to four animals per cage were kept in polycarbonate cages (Makrolon type II and II long). All animal experiments were conducted under the approval of the responsible animal welfare authority (Regierung von Oberbayern).

Both mutant lines *Umod*^{A227T} and *Umod*^{C93F} were bred by crossing heterozygous mutant animals as well as by mating homozygous mutant males to heterozygous mutant females.

Offspring were weaned three weeks post-partum and marked by ear punching. A small tissue sample was taken for DNA isolation and genotyping.

3.3 Genotype analysis

3.3.1 Tissue samples

Tail tissue samples for DNA isolation were taken from three week old mice and stored at -20°C until further usage.

3.3.2 DNA isolation

For tissue digestion, 3-5 mm of mouse tails were each transferred into 1.5 ml Eppendorf tubes. After the addition of 400 μ l cutting buffer master mix (375 μ l cutting buffer (2.5 ml 1 M Tris/HCl pH 7.5, 5 ml 0.5 M EDTA pH 8.0, 1 ml 5 M NaCl, 250 μ l 1 M DTT, 127 μ l Spermidine, add distilled H₂O to make 50 ml), 20 μ l 20% SDS, 5 μ l proteinase K [20 mg/ml]), tubes were incubated at 60°C overnight. On the following day, enzymatically indigestible tissue (bones, hair) was removed by centrifugation (5 minutes at 13000 rpm). The supernatant was transferred into a new 1.5 ml Eppendorf tube and DNA precipitation was achieved by the addition of 400 μ l isopropanol and centrifugation at 13000 rpm for two minutes. The DNA pellet was washed twice in 70% ethanol. The pellets were air dried at room temperature. Depending on the pellet size, DNA was resuspended in 30–300 μ l 10 mM Tris/HCl buffer (pH 8.0) and incubated at 37°C for 60 minutes. Until further usage the samples were stored at 4°C.

3.3.3 DNA concentration assessment

The concentration and purity of genomic DNA were determined by measuring optic density (OD) at the wavelengths 260 nm and 280 nm using a Gene Quant Pro spectrophotometer (Amersham Biosciences, Freiburg, Germany). 1:20 dilutions of DNA were used for this purpose. The final DNA concentration was adjusted to 100ng/ μ l.

3.3.4 PCR for mouse genotyping

PCR was carried out using the Taq polymerase Kit (Qiagen). The standard concentration of genomic DNA was 100 ng/ μ l. PCR conditions were optimized for the product lengths and the annealing temperature of the primers used. All PCR reactions were performed in 0.2 ml reaction tubes and prepared on ice. The standard composition of the reaction master mix for Taq-Polymerase with a final volume of 20 μ l was as follows:

	1x Preparation (µl)
Aqua bidest.	9.15
O-Solution (Qiagen)	4
10x Coraload PCR Buffer (Qiagen)	2
MgCl ₂ 50 mM (Qiagen)	1.25
dNTPs 2 mM	0.5
Primer 1 (2µM)	1
Primer 2 (2 µM)	1
Taq Polymerase 5 U/µl (Qiagen)	0.1
DNA template	1

The DNA templates were amplified using the Eppendorf PCR Thermocycler Gradient (Eppendorf, Hamburg) and the GeneAmp® PCR System 9700 Thermocycler (Applied Biosystem, California,USA).

PCR conditions for genotyping the mouse lines since annealing temperature and extension time were as follows:

PCR conditions for *Umod*^{A227T}:

	wild-type	mutant	time	} 35x
Initial denaturation	94°C	94°C	5 min	
Denaturation	94°C	94°C	40 sec	
Annealing	66,5°C	65°C	40 sec	
Extension	72°C	72°C	1 min	
Final Extension	72°C	72°C	10 min	
Cool down	4 °C	4°C	15 min	

PCR conditions for *Umod*^{C93F}:

	wild-type	mutant	time] 35x
Initial denaturation	94°C	94°C	5 min	
Denaturation	94°C	94°C	40 sec	
Annealing	63.5°C	65°C	40 sec	
Extension	72°C	72°C	50 sec	
Final Extension	72°C	72°C	8 min	
Cool down	4 °C	4°C	15 min	

Genotyping in both mutant lines was carried out by allele-specific PCR in two separate PCR reactions, one with primers for the amplification of the wild-type (wt) allele, and the other with primers for the amplification of the mutant (mut) allele.

All oligonucleotides were obtained in HPLC-purified form from Thermo Fisher Scientific, Ulm.

Oligonucleotides for genotyping *Umod*^{A227T} mice:

Umod_3_for	5' - TGT GAG CCA GGA CTG GAC TG - 3'	(wt and mut)
Umod_21_rev	5' - ATT GAG CCA CAT GGG TGC AGC - 3'	(wt)
Umod_22_rev	5' - ATT GAG CCA CAT GGG TGC AGT - 3'	(mut)

Oligonucleotides for genotyping *Umod*^{C93F} mice:

Umod_26_for	5' - TCA CAA CGT GCT CCT GCC AGA C - 3'	(wt)
INT1_UMOD_rev	5' - GTC AGA CGA AAA CCA TCC TTA C - 3'	(wt)
INT2_UMOD_for_neu	5' - GGC TCG TTT AAG TGC TCG TT - 3'	(mut)
Umod_2_rev	5' - TAG CCC ACA CCA TAC TCT GTG C - 3'	(mut)

3.3.5 Gel electrophoresis

DNA fragments were separated according to their size via agarose gel electrophoresis. Agarose gels were prepared with 1× TAE buffer, 2% and ethidiumbromide (0.5 µg/ml). The DNA samples and a molecular weight standard were loaded into the gel slots and an electric current was applied. Bands were visualized by UV-light and photographs were taken (BioRad) for documentation. The DNA fragments were characterized by comparison with an appropriate molecular weight standard.

3.4 Morphological analysis of age-related renal alterations in *Umod* mutant mice

3.4.1 Necropsy and kidney preparation

Mice of an age of 14 months and of 20 – 22 months were anaesthetized with ketamine-xylazine (1.0 ml ketamine 10%, 0.25ml xylazine 2%, 5.0 ml NaCl 0.9%) followed by cervical dislocation. The organs were dissected, blotted on tissue paper to remove fluid, and weighed to the nearest 0.1 mg. The organs kidney, liver, spleen, urinary bladder, stomach, lung, and heart were weighed. Carcass weight (excluding head, skin and tail) was weighed to the nearest 0.01 g. Tail samples were collected for genotype analysis and stored at -20°C (refer to section 3.3). Left and right kidneys were separately immersion-fixed in 4% paraformaldehyde in PBS (37°C, pH 7.4).

For stereological analyses, kidneys were cut perpendicular to the longitudinal axis of the kidney into 5-7 slices of equal thickness which were arranged with equal orientation in a tissue capsule, routinely processed and embedded in paraffin (Histomaster, Bavimed, Germany). From the paraffin-embedded kidney slices, approximately 4µm thick sections were cut, using a HM 315 microtome (Microm GmbH, Germany). Sections were mounted on glass slides (Engelbrecht, Germany) and dried in a heating cabinet (Wagner & Munz GmbH, Germany) at 37°C for at least 12 hours. For immunohistochemical analyses and PAS-silver staining, the sections were mounted on 3-aminopropyltriethoxy-silane-treated glass slides (Starfrost® microscope slides, Engelbrecht, Germany).

3.4.2 Qualitative histological analysis by light microscopic investigations

Haematoxylin and eosin (H&E), Giemsa, Masson's trichrome (MT), and PAS silver as well as uromodulin immunostaining were performed on kidney sections of both mouse lines and age groups for qualitative analysis. Blind qualitative evaluation of kidneys from *Umod*^{C93F} and *Umod*^{A227T} mutants as well as of wild-type mice was performed to assess the occurrence and distribution of renal histologic alterations. For each of a total of 220 animals, both the left and right kidney was evaluated. After complete evaluation of all animals, mouse line, genotype, gender and age were assigned to the specimen. Photographs of structural alterations were taken, using a Leica DFC 320 Digital Camera (Leica, Germany) connected to a microscope (Orthoplan, Leitz, Germany). For scale bars, an object micrometre (Zeiss, Germany) was photographed at the corresponding magnifications.

3.4.2.1 Haematoxylin and eosin (H&E) staining

To apply the H&E stain to the paraffin sections, the following solutions were prepared beforehand:

- 1% Eosin solution
10 g Eosin G (Merck, Germany) were dissolved in 1000 ml hot aqua dest. and left to cool down. After the addition of 1.5 ml of 100% glacial acetic acid (Nr. 100063, Merck, Darmstadt) the solution was filtrated and stored at room temperature.
- 1% HCl ethanol stock solution
7000 ml of 96% ethanol were mixed with 2500 ml aqua bidest. and 100 ml of 25% HCl (neoLab, Germany).
- 0.5% HCl ethanol, ready-to-use
100 ml of 1% HCl stock solution was mixed with 100 ml of 70% ethanol.

Following deparaffinization in xylene (Merck, Germany) and rehydration via descending alcohol series (2x 100% → 2x 96%, → 1x 70% ethanol), the slides were left in a glass cuvette containing Mayer's haematoxylin (Merck, Germany) for 5 minutes, followed by a 5-minute rinsing with tab water. After differentiation in 0.5% HCl ethanol the slides were rinsed with tab water for 5 minutes and then dipped into 1% eosin solution 2-7 times. After dehydration in an

ascending alcohol series (1x 70% → 2x 96%, → 2x 100% ethanol), the slides were put in xylene (Merck, Germany) and mounted under coverslip slides (Menzel GmbH & Co KG, Germany) using Roti[®]-Histokitt (Carl Roth, Germany).

3.4.2.2 Giemsa staining

To apply Giemsa's staining to the paraffin sections, the following solutions were prepared beforehand:

- Phosphate buffer
200 ml of dipotassium hydrogen phosphate (Nr.105104, Merck, Germany) at a concentration of 9.12 g/L were mixed with 160 ml of disodium hydrogen phosphate dihydrate (Nr. 106580, Merck, Germany) and the pH was adjusted to 6.7.
- 7% Giemsa solution
200 ml of phosphate buffer (pH 6.7) was added to 14 ml of Giemsa stock solution (Nr. 109204, Merck, Germany). The solution was set to a pH 6.7.
- 0.5% acetic acid
5.0 ml of 100% glacial acetic acid (Nr. 100063, Merck, Germany) was added to 1.0 L of distilled water.

The kidney sections were deparaffinised in xylene (Merck, Germany) and rehydrated in a graded alcohol series (2x 100% → 2x 96%, → 1x 70% ethanol). The sections were then rinsed with aqua dest. for 5 minutes and were immersed in 7% Giemsa solution and kept in a water bath at 65°C. After 60 minutes, the slides were taken out and dipped into phosphate buffer for 2 seconds, into 0.5% acetic acid (2x2 seconds) and into aqua dest. for 2 seconds. The slides were then run through an ascending alcohol series (1x 70% → 2x 96%, → 2x 100% ethanol) in order to dehydrate and were kept in xylene (Merck, Germany) until coverslip slides (Menzel GmbH & Co KG, Germany) were mounted using Roti[®]-Histokitt (Carl Roth, Germany).

3.4.2.3 Masson's trichrome (MT) staining (modified according to Goldner and Weigert)

To apply the MT staining to the paraffin sections, the following solutions were prepared beforehand:

- Weigert's iron haematoxylin

Solution A

10 g of Haematoxylin crystalline (Merck, Germany) were dissolved in 1000 ml 96% ethanol. Solution A was left to maturation for 1 week.

Solution B

11.6 g of Iron (III) chloride (Merck, Germany) was dissolved in 980 ml aqua dest. and 10 ml of 25% HCl (neoLab, Germany). Solution B (prepared as a 1:1 mixture) was stored separately.

- Red colour solution

Solution A

10g of acid fuchsine (Sigma, Germany) was added to 1000 ml boiling aqua dest. 10 ml 100% glacial acetic acid (Applichem, Germany). The mixture was left to cool down in closed glass bottle.

Solution B

10g of xyloidine Ponceau (Waldeck, Germany) was added to 1000 ml boiling aqua dest. 10 ml 100% glacial acetic acid (Applichem, Germany). The mixture was left to cool down in closed glass bottle.

Azophloxine solution

1.25 g Azophloxine (Chroma, Germany) was dissolved in 250 ml aqua dest and 0.5 ml 100% glacial acetic acid (Applichem, Germany) were added.

To create the red colour solution, 20 ml of Solution A, 80 ml of solution B and 20 ml of the Azophloxine solution were mixed.

- Phosphotungstic acid-orange G solution

15 g of tungstophosphoric acid (Merck, Germany) and 10 g of orange G (Merck, Germany) were dissolved in 1000 ml aqua dest..

- Aniline blue

10 g aniline blue (Serva Feinbiochemica, Germany) were dissolved in 1000 ml aqua dest. and 10 ml of 100% glacial acetic acid (Applichem, Germany) were added.

- 0.5% acetic acid

5 ml of glacial acetic acid 100% (Applichem, Germany) were added to 995 ml aqua dest..

Following deparaffinization in xylene (Merck, Germany) and rehydration via descending alcohol series (2x 100% → 2x 96%, → 1x 70% ethanol), the slides were left in a glass cuvette containing Weigert's iron haematoxylin for 5 minutes, followed by a 5-minute rinsing with tap water. After differentiation in 0.5% HCl ethanol the slides were rinsed with warm tap water for 5 minutes. A 5-minute incubation with red colour solution was followed by 5 minutes of rinsing in 0.5% acetic acid, a 3-minute application of phosphotungstic acid-orange G solution and another rinsing in 0.5% acetic acid for 5 minutes. Anilin blue was applied to the sections for 5 minutes after which they were washed in 0.5% acetic acid for 5 minutes, and dehydrated through an ascending alcohol series (1x 70% → 2x 96%, → 2x 100% ethanol). The slides were immersed in xylene (Merck, Germany) and mounted under coverslip slides (Menzel GmbH & Co KG, Germany) using Roti[®]-Histokitt (Carl Roth, Germany).

3.4.2.4 PAS-silver staining

The following solutions were necessary to perform Rambourg's technique (1967) of periodic acid-Schiff Silver staining (modified for paraffin sections):

- 1% periodic acid solution
10 g periodic acid (Sigma, Germany) was added dissolved in 1000 ml aqua dest. 1.6 g sodium acetate (Merck, Germany) was dissolved in 100 ml aqua dest. The separately prepared solutions were mixed and stored at 4°C.
 - Sivler methenamine solution
 - 3 g hexamine (= hexamethyletetramine) were dissolved in 100 ml aqua dest. to create 3% hexamine (methamine) solution
 - 5 g silver nitrate (AppliChem, Germany) were dissolved in 100 ml aqua dest. to create a 5% silver nitrate solution.
 - 2 g disodium tetraborate decahydrate (Borax, Merck, Germany) was dissolved in 100 ml warm aqua dest. to create a 2% borax solution
- 36 ml 3% hexamine solution and 4 ml 5% silver nitrate solution were stirred until the resulting precipitate had redissolved. 4 ml 2% borax solution were then added. The final solution was stirred and then filtered. The silver methenamine solution was warmed up 10 minutes previous to usage.

- 0.1% gold chloride solution
0.1 g gold chloride (Merck, Germany) was added to 100 ml aqua dest..
- 2% sodium thiosulfate solution
2 g sodium thiosulfate (Merck, Germany) were added to 100 ml aqua dest..
- Schiff's reagent (Carl Roth, Germany)

The PAS-silver stain was performed as follows. First the kidney sections were deparaffinised in xylene (VWR, Germany) and rehydrated in a graded alcohol series (2x 100% → 2x 96%, → 1x 70% ethanol). The sections were rinsed with aqua dest. for 5 minutes, followed by an immersion in 1% periodic acid solution for 15 minutes and another 5-minute washing in aqua dest.. The slides were then placed in a standing cuvette and immersed in filtered silver methenamine solution at 60°C for 25 minutes. From that point on, the sections analysed every 2-5 minutes under the light microscope. As soon as the basal membrane was clearly visible the sections were washed with aqua dest. for 5 minutes. By dipping the slides into 0.2% gold chloride solution for 6 seconds, the staining was differentiated. This was followed by 5 minutes of washing with aqua dest., fixation in 2% sodium thiosulfate solution for 1 minute and another 5 minutes of washing in aqua dest. For drying, all slides were laid out on a heating plate at 70°C for 10 minutes and then reimmersed in aqua dest.. After that, the sections were left in Schiff's reagent in complete darkness at room temperature for at least 45 minutes. After a 5-minute rinsing with aqua dest., the reaction intensity was checked on microscopically and Schiff's reagent was reapplied if necessary. Otherwise, the slides were immersed in haematoxylin for 2 minutes and afterwards washed with aqua dest. for 5 minutes. Differentiation was achieved by briefly dipping the slides into 0.5% HCl alcohol (6-10 times) and was stopped by watering with aqua dest. for 5 minutes. The sections were dehydrated in an ascending alcohol series (1x 70% → 2x 96%, → 2x 100% ethanol) and finally immersed in xylene (VWR, Germany). Coverslip slides (Menzel GmbH & Co KG, Germany) were mounted onto the slides and sealed with Roti[®]-Histokitt (Carl Roth, Germany).

3.4.2.5 Uromodulin immunostaining of kidney sections

Immunohistochemical staining using the avidin-biotin-complex (ABC) technique was carried out to detect uromodulin. Besides qualitative evaluation of the uromodulin staining pattern, it also served as a marker for TAHL cells used for quantitative evaluation (refer to section 3.4.3).

1x TBS buffer was required for this procedure and diluted from a 10x TBS stock solution that consisted of:

80 g NaCl

30 g Tris

Ad 10000 ml aqua bidest.

Adjust to pH 7.4 with 37% HCl

Kidney sections were deparaffinised in xylene for 15 minutes, rehydrated in a descending alcohol series (2x 100% → 2x 96%, → 1x 70% ethanol) and washed in distilled water. In order to retrieve antigens the slides were boiled in 10 mM citrate buffer (pH 6.0) containing 0.05% Tween for 46 minutes with the steamer-microwave-method. After a 20-minute cool-down, TBS buffer was used to wash the sections for 10 minutes. Endogenous peroxidase activity was blocked by incubation 0.3% hydrogen peroxide in TBS at room temperature for 15 minutes, followed by a 5 minute-washing in TBS. The Biotin-Blocking Kit (Vector, Peterborough, UK) was used to perform a biotin blocking procedure, consisting of two 15 minute-incubations with avidin and then biotin at room temperature. Slides were washed in TBS for 10 minutes after each incubation. Afterwards, tissue slides were incubated for one hour at room temperature with 2% goat serum (diluted in TBS) for blocking. Rabbit- α -THP antibody (#sc-20631, Santa Cruz, Germany) was then applied to the sections at a dilution of 1:1000 in TBS. After an overnight incubation in the refrigerator, excess primary antibody was removed by 10 minutes of washing in TBS after which the sections could be incubated with the secondary antibody: biotinylated goat- α -rabbit IgG (Vector, UK) which had been diluted in 2% goat serum in TBS (1:200). Incubation duration was one hour, followed by a washing in TBS for 10 minutes. An avidin-biotin complex (1:100 in TBS, Vector, UK) was then administered to the sections for 30 minutes at room temperature. After a final 10 minute-washing with TBS, H₂O₂-activated chromogen 3,3'-diaminobenzidine (DAB, KEM-EN-TEC, Denmark) was pipetted onto the sections and left on

them for several minutes, until immunoreactivity was visible. It was taken care to rinse the slides with running tap water before the stain became too intense. Mayer's haematoxylin (Merck, Germany) was used as a counterstain that was stopped by running tap water. Tissue dehydration was achieved by means of an ascending alcohol series. After clearing in xylene, all sections were mounted under coverslip slides (Menzel GmbH & Co KG, Braunschweig) using Roti[®]-Histokitt (Carl Roth, Germany).

3.4.3 Quantitative stereological analysis

Quantitative stereological investigations of murine kidneys were performed using the unbiased model-independent stereological methods as previously described (Gundersen & Jensen, 1987; Wanke *et al.*, 1994; Herbach *et al.*, 2005). The kidneys of at least six male mice per age group, line and genotype were evaluated. All three parameters were analysed for each kidney. Only right kidneys were used.

3.4.3.1 Quantification of the renal volume fractions

The volume fractions (V_V) of TALH cells, interstitial fibrosis and tubular atrophy (IFTA) and inflammatory cells (IC) in the kidney were determined by the point-counting method (Weibel, 1979). Point-counting was carried out on paraffin sections by means of an image analysing system which consisted of a light microscope (BX41, Olympus, Germany), a colour video camera (DP72, Olympus, Germany) and the software new CASTTM (computer assisted stereological toolbox, Visiopharm®, Denmark).

For all three components (TALH cells, IFTA, inflammatory cells) systematic random sampling was used to evaluate a pre-defined number of analysis samples per section. Counting frames containing a point grid were placed upon the selected samples. The mean number of points counted per kidney was 10000 ± 300 for TALH and inflammatory cells and 8000 ± 300 for IFTA. The volume fractions of TALH, IFTA, and inflammatory cells in the kidney ($V_{V(\text{TALH/kid})}$, $V_{V(\text{IFTA/kid})}$ and $V_{V(\text{IC/kid})}$ respectively) were calculated by dividing the sum of points hitting the TALH cells, IFTA and inflammatory cells, respectively ($\sum P_{(\text{TALH})}$, $\sum P_{(\text{IFTA})}$ and $\sum P_{(\text{IC})}$) by the sum of points hitting renal tissue ($\sum P_{(\text{kid})}$).

3.4.3.2 Quantification of the total volumes

The renal volume was calculated by dividing its weight by its specific weight (1.05 mg/mm^3) (Wanke, 1996). The total volumes of TALH, IFTA and inflammatory cells in the kidney ($V_{(\text{TALH,kid})}$, $V_{(\text{IFTA,kid})}$ and $V_{(\text{IC,kid})}$) were calculated as the products of the respective volume fraction ($V_{V(\text{TALH/kid})}$, $V_{V(\text{IFTA/kid})}$ and $V_{V(\text{IC/kid})}$) and $V_{(\text{kid})}$.

3.5 *In vivo* testing of two putative causative therapeutics for UAKD

For testing a potential therapeutic effect of 4-PBA and tempol in UAKD, male homozygous *Umod*^{A227T} mutant mice, male homozygous *Umod*^{C93F} mutant mice and their respective wild-type littermates were used. There were three treatment groups: 4-PBA in drinking water, tempol in drinking water and placebo (drinking water with no chemicals added).

3.5.1 Experimental schedule

The age of two months (= day 0) marked the beginning of the experiment which lasted for 60 ± 4 days and was therefore performed on two to four-month-old mice. On day 0, the body weight of each mouse was taken and samples of spot urine were collected. 4-PBA and tempol were given continuously from day 0 throughout the experiment by the drinking water (refer to section 3.5.2). From day 0, body weight was measured weekly and spot urine was collected every other week. Sampling of blood plasma was performed at day 0, day 30 ± 4 and at day 60 ± 4 at the end of the experiment (refer to section 3.5.3). On day 56 ± 4 , the mice were individually transferred to metabolic cages (Tecniplast, No. 3600M021, Italy) for the assessment of the 24h-urine excretion as well as of drinking water and food intake. A 2-day conditioning period to the metabolic cage preceded the two days of actual data collection. On day 60 ± 4 the animals were anaesthetized and, after retro-orbital blood collection, formalin perfusion and necropsy were performed (refer to section 3.5.6).

3.5.2 4-PBA and tempol administration

The chemical chaperone 4-PBA acid (Scandinavian Formulas, Pennsylvania, USA, water solubility: 0.62 g/ml) was dissolved in drinking water and administered at a dosage of 1 g/kg body weight. 4-PBA solutions were renewed every third day. As a superoxide dismutase

mimetic, 4-hydroxy-tempo (Sigma Aldrich, St. Louis, Missouri, USA, water solubility: 1.679 g/ml) was given as a 2 mM drinking solution. Due to its sensitivity to light, tempol was administered in black drinking bottles (Tecniplast, Italy) and exchanged every other day. Corresponding amounts of 4-PBA or tempol powder were weighed to the nearest 0.1 mg. The solutions were weighed into drinking bottles and the weight of the full, lid-covered bottles was recorded. On the day of solution exchange, the bottles were weighed again to determine the water intake per cage. Using this result, the average intake per mouse and day was assessed.

3.5.3 Blood sampling and analysis

For blood sampling, mice were anaesthetized (1.0 ml ketamine 10%, 0.25 ml xylazine 2%, 5.0 ml NaCl 0.9%) by intraperitoneal injection (80-100 μ l/10 g body weight) .

The retro-orbital sinus was punctured with Na-heparin treated glass capillaries (Hirschmann Laborgeräte, Germany) and blood was collected in 1 ml lithium-heparin treated tubes (Kabe Labortechnik, Germany). By centrifuging the blood twice at 7000 rpm for 10 minutes, a volume of approximately 120 μ l plasma was obtained, transferred into 1.5 ml tubes and stored at -80°C until further usage. The plasma parameters (sodium, potassium, calcium, chloride, phosphate, total protein, creatinine, uric acid, urea, cholesterol, TG, AST, ALT, lipase, amylase) were measured by Dr. B. Rathkolb, (Chair for Molecular Animal Breeding and Biotechnology, LMU München) within the German Mouse Clinic (Prof. Dr. M. Hrabé de Angelis) of the Helmholtz Zentrum München. An Olympus AU400 autoanalyzer (Olympus, Germany) was used with the respective kits. Plasma creatinine was determined using two different methods, Jaffé's kinetic method (OSR6178, Beckman Coulter, California, USA; creatinine-J) and the enzymatic method (OSR61204, Beckman Coulter, California, USA; creatinine-E).

3.5.4 Metabolic cage experiment

On day 56 \pm 4 of the experiment, homozygous mutant animals and wild-type littermate controls were individually transferred to metabolic cages (Tecniplast, No. 3600M021, Italy) for two consecutive days for habituation. Crushed food (V1124-3; Ssniff, Soest, Germany) and water (containing 4-PBA, tempol, or neither) were provided *ad libitum*. On day 0 of analysis, the metabolic cages were cleaned. Body weight, food weight, and drinking bottle weight were

measured before the mice were put in the cages. Urine was collected every 24 hours and stored at -80°C , and body weight, 24h-water intake, 24h-food intake, 24h-urine volume, and 24h-faeces excretion were measured. The mice were provided with fresh water and food on a daily basis. Both 4-PBA and tempol solutions were renewed daily while the mice were in the metabolic cages. The metabolic cage drinking bottles containing tempol solution were covered in aluminium sheet to prevent light penetration. To avoid urine evaporation, 1 ml paraffin was added in the urine collecting tubes (for urine processing refer to section 3.5.5). On day 2 of the metabolic cage analysis (day 60 ± 4 of treatment application), necropsy of mice for tissue preparation was performed (refer to section 3.5.6).

3.5.5 Urine sampling and analysis

The samples of both spot and 24h-urine of metabolic cage analysis were prepared for storage or further analysis in the same way. Urine was transferred into a labelled 1.5-ml- or 2.0-ml-Eppendorf tube. The samples were centrifuged at 7000 rpm for 10 minutes. The supernatant was then pipetted into new 2.0 ml tubes and two 200- μl -aliquots of the 24h-urine were filled into 1.5-ml-tubes. The urine was kept at -80°C until further usage.

3.5.5.1 Analysis of clinical chemical parameters in urine

A 200 μl aliquot of 24h-urine of day 1 and day 2 of metabolic cage analysis were used for clinical chemical analysis, performed by Dr. B. Rathkolb, (Chair for Molecular Animal Breeding and Biotechnology, LMU München) within the German Mouse Clinic (Prof. Dr. M. Hrabé de Angelis) of the Helmholtz Zentrum München. The following clinical chemical parameters of urine were determined: sodium, potassium, chlorine, calcium, magnesium, inorganic phosphate, creatinine, uric acid, urea, glucose, total protein, and albumin. Daily excretion of solutes was normalized to 25 g of body weight (based on the body weight measured on day 0 of analysis) and calculated as follows:

$$\text{solute excretion}_{24\text{h urine}} = \text{urine volume}_{24\text{h}} \times [\text{solute}]_{24\text{h urine}}$$

$$\text{solute excretion}_{24\text{h urine},25\text{g}} = \text{solute excretion}_{24\text{h}} / \text{body weight}_{\text{day}0} \times 25$$

Daily fractional excretion of solutes was calculated using the creatinine clearance of creatinine measured by the Jaffe method in the following way:

$$\text{creatinine clearance} = \text{urine volume}_{24\text{h}} \times [\text{Crea}]_{24\text{h urine}} / [\text{Crea}]_{\text{plasma}}$$

$$\text{FE}_{\text{solute}} = (\text{urine volume}_{24\text{h}} \times [\text{solute}]_{24\text{h urine}}) / (\text{creatinine clearance} \times [\text{solute}]_{\text{blood}})$$

3.5.5.2 Analysis of urinary osmolality

Osmolality of 24h-urine was measured with the freezing point method using a digital micro osmometer type 5B (Roebing, Germany). As the maximum measurement point of the micro osmometer is 2.000 mOsm/kg H₂O, urine from polyuric mice was measured undiluted, whereas more concentrated urine was diluted in distilled water at a ratio of 1:2 or 1:4 etc. if need be. Each sample was measured twice.

3.5.5.3 Analysis of uromodulin excretion

Uromodulin excretion was determined by sodiumdodecylsulfat-polyacrylamide gel electrophoresis (SDS-PAGE) and Western immunoblot analysis. Therefore, the creatinine concentration of 24h-urine was determined (refer to section 3.5.4) and urine samples were standardized for equal creatinine concentration. For SDS-PAGE analysis, equal amounts of creatinine-standardized urine were boiled for 10 minutes after addition of ¹/₅.th 5xLaemmli (327.5 mM Tris-HCl pH 6.8, 5 mM EDTA, 10% SDS, 50% glycerol, 0.01% bromophenol blue) and 2-mercaptoethanol at a final concentration of 5%.

SDS-PAGE:

SDS-PAGE described by Laemmli in 1970 is a two-step separation of proteins along an electric potential. The anionic detergent SDS binds to the protein and the resulting positive charge of the protein is proportional to the mass of the molecule. Hence, the fractionation visible is mainly due to size. First all samples travel through a macroporous stacking gel of low acrylamide concentration so as to focus all proteins to a small area. The second part consists of a fine pored, more highly concentrated separating acrylamide gel in which smaller proteins will have travelled farther towards the anode after a certain amount of time.

The separating gel (10%, 4 gels) consists of:

8 ml	aqua bidest.
5 ml	1.5 M Tris-HCl (pH8.8)
6.66 ml	30% acrylamide/bis solution (29:1)
200 µl	10% SDS
10 µl	Temed
100 µl	10% APS

The stacking gel (5%, 4 gels) consists of:

7 ml	aqua bidest.
1.25 ml	10,5M Tris-HCl (pH6.8)
1.5 ml	30% acrylamide/bis solution (29:1)
100 µl	10% SDS
5.5 µl	Temed
125 µl	10% APS

The 1x SDS-Page running buffer consists of:

100 ml	10x TBE
Ad 1000 ml	aqua bidest.

The Laemmli SDS-PAGE method was performed using the Miniprotean III-System (Biorad), respectively. The separating gel was poured between to glass plates in a gel caster which were then carefully covered with aqua bidest. The separating gel was left to polymerize for at least 60 minutes. Then, after complete removal of any aqua bidest., the stacking gel was poured on top of the separating gel and combs were stuck into it. It also polymerized for at least 60 minutes at room temperature. 1x SDS-PAGE running buffer was filled into the prepared Miniprotean

system and the combs were removed. The gel pockets were rinsed with buffer in order to remove any acrylamide remnants that had not polymerized. A molecular weight size marker was run in one lane of each gel. The voltage applied to the Miniprotean III-system was 100 V until the separating gel was reached, followed by 140 V.

Semi-dry-blot:

With completion of SDS-PAGE, the proteins were transferred from the gel to a protein-binding Immobilon PVDF-membrane via electrophoresis. To perform this semi-dry-blot procedure a Trans-Blot SD electroblotter (BioRad) was used. A blot-sandwich was prepared on the lower anode unit in the following way:

- 1 thick gel blotting paper (Biorad), soaked in transfer buffer
- PVDF-membrane (activated with 100% methanol and labelled)
- Gel
- 1 thick of gel blotting paper (Biorad), soaked in transfer buffer

The Ponceau S-solution consisted of:

0.2 g	Ponceau S
3 ml	Glacial acetic acid

The cathode was then applied with mild pressure. Protein transfer occurred from cathode towards anode under 50 V for 45 minutes blotting time. After that, the proteins bound to the PVDF-membrane were reversibly stained with Ponceau S-solution for 2-5 minutes and the background was discoloured with aqua dest. The membrane was dried and the molecular weight size markers were labelled with a biro. Until further usage the membrane was stored at 4°C.

Western-immunoblot:

The PVDF-membrane was put in a 50ml plastic tube and blocked by covering it in TBS-T BSA (5%) in a hybridization oven (room temperature) for 60 minutes. This causes saturation of potential protein binding sites on the membrane. Afterwards the membrane was washed three times in TBS-T (0.1% Tween in TBS) at room temperature (1x 15 minutes, 2x 5 minutes). The primary antibody (rabbit-anti-THP, #sc-20631, Santa Cruz) was diluted 1:1,800 in TBS-T-BSA (5%) and the membrane was incubated with it overnight at 4°C. After three more TBS-T washings of the membrane at room temperature (1x 15 minutes, 2x 5 minutes), the secondary antibody [HRP-conjugated goat-anti-rabbit IgG, Cell Signaling, diluted 1:2,000 in TBS-T-BSA (5%)] was added for 60 minutes at room temperature. Again, the membrane was washed three times in TBS-T at room temperature (1x 15 minutes, 2x 5 minutes). Signals were detected by means of an enhanced chemiluminescence detection solution and hyperfilm ECL (GE Healthcare).

3.5.6 Necropsy and tissue preparation

At the age of 4 months (experimental days 60±4), after the final measurements for the metabolic cage experiment (day 2), necropsy of mice was performed. Beforehand, they were anaesthetized with ketamine-xylazin solution, weighed and punctured retroorbitally for collecting blood samples (refer to section 3.5.3).

For necropsy, mice were divided in two groups: in the first group of mice, kidneys were fixed via orthograde vascular perfusion. For this purpose, after euthanasia, the abdominal and thoracic cavity were opened by incision so that the perfusion needle could be injected into the left ventricle and, with the start of perfusion, the inferior vena cava was cut cranial to the diaphragm to provide outflow of the perfusate. Perfusion started with PBS (pH 7.4, 37°C) until the blood was washed out of the circulation. After about 20 seconds, perfusion was continued with 4% buffered paraformaldehyde solution and perfusion fixation occurred for 5 minutes. Afterwards, the organs were dissected, blotted on tissue paper to remove fluid, and weighed to the nearest 0.1 mg. Kidney (without capsule), liver, spleen, and heart were weighed. Kidneys were lamellated perpendicular to the longitudinal kidney axis into 5-7 slices of equal thickness. Small 1 mm³ kidney cortex samples were selected by systematic random sampling and immersion fixed in

6.25% glutaraldehyde (Serva, Germany) in PBS (pH 7.4) which was further processed for transmission electron microscopic analyses (refer to section 3.5.7.2). The residual kidneys slices were postfixed in 4% paraformaldehyde for further 24 hours by immersion and processed for paraffin histology.

For the second group of mice, necropsy was performed as described in section 3.4.1. Both kidneys were immediately frozen on dry ice and stored at -80°C for future molecular analyses.

3.5.7 Histological kidney analysis after treatment application

3.5.7.1 Light microscopic investigations

For qualitative analysis of kidney sections by light microscopy, H&E and PAS-silver staining were performed (refer to sections 3.4.2.1 and 3.4.2.4.).

3.5.7.2 Transmission electron microscopic investigations

Transmission electron microscopic investigations were performed using using a Zeiss EM 10 electron microscope (Zeiss, Germany).

In advance, 1 mm³ kidney cortex samples were prepared in the following way. After fixation by immersion in 6.25% glutaraldehyde (Serva, Germany) in PBS (pH 7.4) at 8°C for 48 hours, 1 mm³ kidney samples were postfixed in 1% osmiumtetroxide (OsO₄, Merck, Germany), on a tumbling shaker, dehydrated and embedded in Epon (Epon is a trademark of the Shell Company (USA), but Serva (Germany) distributes the identical chemical substance under the designation “glycid ether 100” containing 2% osmium tetroxide (Serva, Germany)). Postfixed samples were washed in washing solution for 3 x 2 min at room temperature, dehydrated through a series of ascending acetone solutions (Carl Roth, Germany) at 4°C and incubated in a solution containing equal amounts of 100% acetone and Epon for 1 h at room temperature, followed by incubation in pure glycid ether 100 two times for 30 min at room temperature. Samples were embedded in a glycid ether embedding mixture in dried gelatine capsules (Plano, Germany). Polymerization took place at 60°C for approximately 48 h.

Epon blocks were trimmed, using a Reichert-Jung TM60 milling machine (Leica, Germany). Semi-thin sections (0.5 µm) were produced with a Reichert-Jung Ultracut E microtome (Leica,

Germany), and stained with Toluidine blue O and Safranin O. The regions of interest within the semi-thin sections were identified by light microscopy and their positions were marked in a drawing. Then, these areas of the Epon blocks were trimmed further, and ultra-thin sections (70-80 nm) were prepared (Reichert-Jung Ultracut E, Leica, Germany). The sections were mounted on coated copper rings, contrasted with 2% uranyl acetate and lead citrate, and examined under the electron microscope.

Materials:

- Sörensen's phosphate buffer (Mulisch & Welsch, 2010)

Solution A	192 ml
Solution B	808 ml

<i><u>Solution A</u></i>	
Potassium dihydrogen phosphate (neoLab, Germany)	9.078 mg
Aqua dest.	ad 1000 ml
<i><u>Solution B</u></i>	
Sodium phosphate dibasic dihydrate (neoLab, Germany)	11.876 mg
Aqua dest.	ad 1000 ml

- Washing solution

D(+) Saccharose (neoLab, Germany)	6.84 g
Sörensen's phosphate buffer	ad 100 ml

- Fixative solution for Epon embedding

D(+) Saccharose (neoLab, Germany)	0.45 g
0.1 M HCl (Merck, Germany)	2 ml
Veronal-acetate buffer	2 ml
Osmium tetroxide solution 2%	5 ml
Aqua dest.	1 ml

<i><u>Veronal-acetate buffer</u></i>	
5.5-Diethylbarbituric acid Na-salt (Merck, Germany)	1.47 g

Sodium acetate (Merck, Germany) 0.97 g

Aqua dest. 50 ml

Adjust pH to 10.3

Osmium tetroxide solution 2%

Osmium tetroxide (Chempur, Germany) 1 mg

Aqua dest. 50 ml

- Ascending acetone series (Roth, Germany):

Acetone 50%: 3 x 2 min, 4°C

Acetone 70%: 2 x 10 min, 4°C

Acetone 90%: 2 x 10 min, 4°C

Acetone 100%: 2 x 20 min, 4°C

Acetone 100%: 1 x 20 min, room temperature

- Glycid ether embedding mixture

Solution A 70ml

Solution B 130 ml

Solution A

Glycid ether 100 (Serva, Germany) 62 ml

2-Dodecenyl succinic acid anhydride (Serva, Germany) 100 ml

Solution B

Glycid ether 100 (Serva, Germany) 100 ml

Methylnadic anhydride (Serva, Germany) 89 ml

Staining procedures:

- Staining protocol for semi-thin sections (Toluidine blue & Safranin O)

Toluidine blue

Di-sodium tetraborate (Merck, Germany) 1 g

Toluidine blue (Roth, Germany) 0.8 g

Aqua dest. 100 ml

Dissolve di-sodiumtetraborate in distilled water, add Toluidine blue and stir for approximately 2 h. Filter before use. Stain sections for 45-60 sec on a heating plate (Meditel, Germany) at 55°C, rinse with aqua dest. and let dry.

Safranin O

Di-sodiumtetraborate (Merck, Germany)	1 g
Safranin O (Chroma, Germany)	1 g
D(+) Saccharose (Merck, Germany)	40 g
Formaldehyde 37% (Roth, Germany)	2-3 drops
Aqua dest.	ad 100ml

Dissolve di-sodiumtetraborate in aqua dest., add Safranin O and saccharose and stir for approximately 2 h. Add formaldehyde after 24 h. Filter before use. Stain sections for 15 sec on a heating plate (Meditel, Germany) at 55°C, rinse with aqua dest. and let dry. Cover the sections with coverslips (Menzel, Germany) using Histofluid (Superior, Germany).

- Contrasting ultra-thin sections with uranyl acetate and lead citrate

Uranyl acetate

Uranyl acetate (Merck, Germany)	1 g
Aqua bidest.	50 ml

Swing carefully without stirring. Filter before use. Stain sections for 30 min at room temperature.

Lead acetate

Sodium citrate (Merck, Germany)	6 ml
Lead nitrate solution (Merck, Germany)	4 ml
Sodium hydrate solution (Merck, Germany)	8 ml
Aqua bidest.	32 ml

Mix sodium citrate with aqua bidest. and stir gently. Add lead nitrate solution drop by drop until the solution becomes milky (precipitation). Use sodium hydrate to clear the solution. Filter before use. Stain sections for 10 min at room temperature.

3.6 Statistical analysis

Data were evaluated statistically using the Microsoft Excel 2003 software program. Data are presented as means \pm standard deviation (SD). Data charts were created with GraphPad Prism 5.0 (GraphPad Software, California USA). The significance of values was determined using the Student's t-test. The Bonferroni method was applied to control the familywise error rate in multiple pair comparisons. p values $< (0.05 / \text{number of groups})$ were considered to be significant.

4 Results

4.1 Allelic differentiation of *Umod* mutant mice

Genotyping of *Umod*^{A227T} and *Umod*^{C93F} mice was conducted by allele-specific PCR-amplification of the wild-type and the mutant allele, which enabled the distinction between wild-type, homozygous mutant or heterozygous mutant animals, respectively (refer to section 3.3).

4.1.1 Genotyping of *Umod*^{A227T} mutants

In order to genotype the mice of the *Umod*^{A227T} line, the wild-type allele was specifically amplified using the allele-specific reverse primer Umod_21_rev (5' attgagccacatgggtgcagc 3') and the forward primer Umod_3_for (5' tgtgagccaggactggactg 3'), which yielded a 205 bp PCR product. Usage of allele-specific reverse primer Umod_22_rev (5' attgagccacatgggtgcagt 3') and forward primer Umod_3_for (5' tgtgagccaggactggactg 3') resulted in the amplification of the mutant allele (PCR product length of 205 bp) (Figure 4.1).

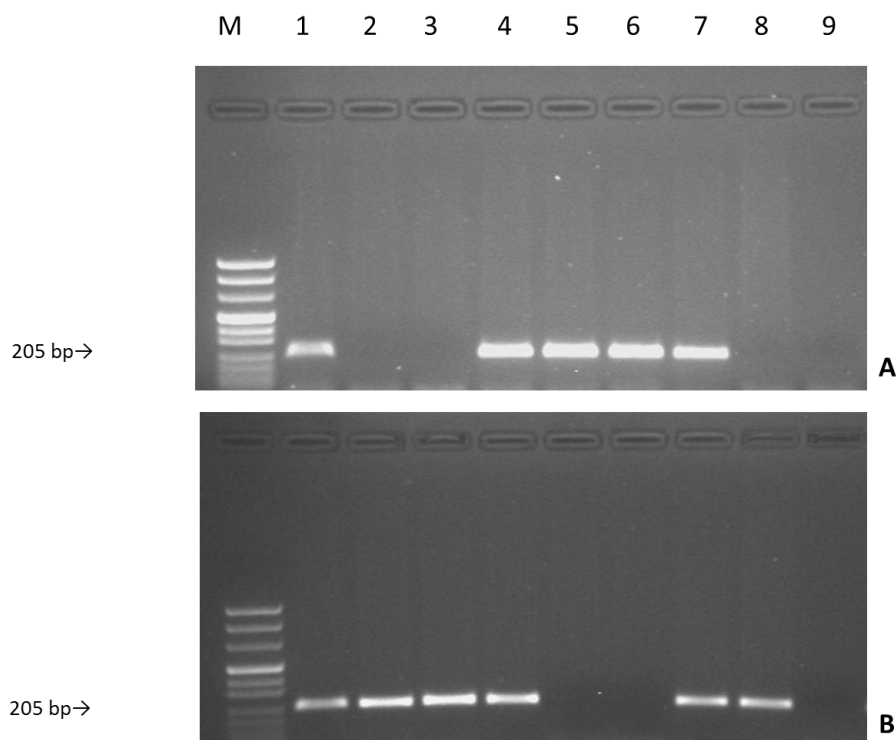


Figure 4.1: Electrophoresis of allele-specific PCR samples of *Umod*^{A227T} mutant mice. (A) Mutant allele; (B) Wild-type allele; lane M: pUC 8 marker, lanes 2, 3 and 8: wild-type; lanes 1, 4, and 7: heterozygous mutant; lanes 5 and 6: homozygous mutant; lane 9: negative control (aqua bidest.).

4.1.2 Genotyping of *Umod*^{C93F} mutants

For the *Umod*^{C93F} mutant mouse line, PCR-amplification of the wild-type allele was performed by means of the allele-specific reverse primer INT1_UMOD_rev (5' gtcagacgaaaaccatccttac 3') and the forward primer Umod_26_forward (5' tcacaacgtgctcctgccagac 3') and yielded a 171 bp PCR product. The allele-specific forward primer INT2_UMOD_for_neu (5' ggctcgtttaagtgcctgtt 3') and the reverse primer Umod_2_rev (5' tagccacaccatactctgtgc 3') produced the corresponding mutant 321 bp DNA segment (Figure 4.2).

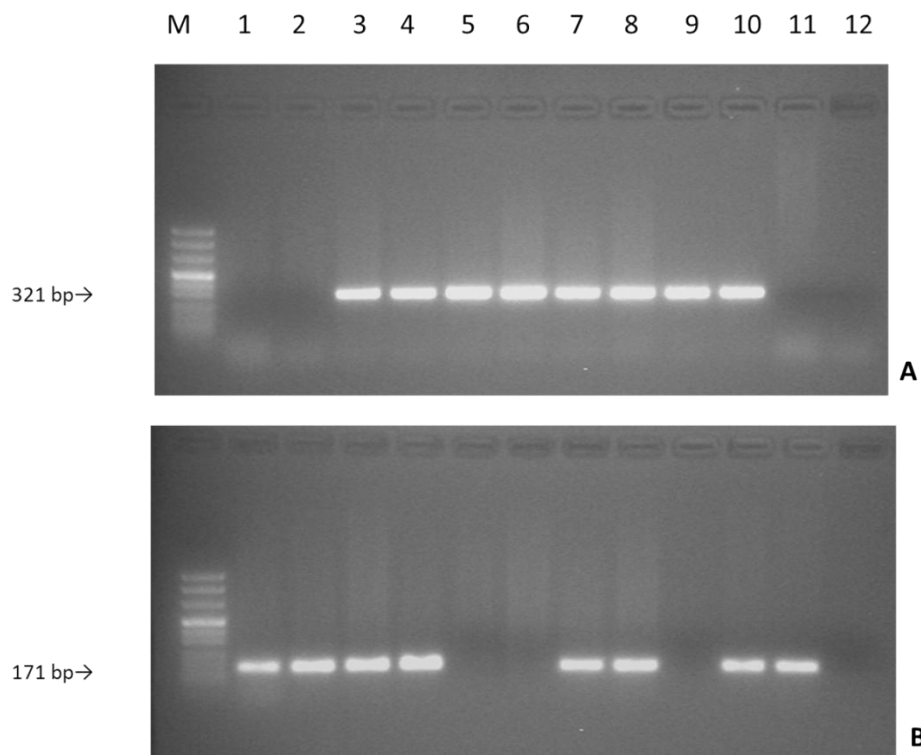


Figure 4.2: Electrophoresis of allele-specific PCR samples of *Umod*^{C93F} mutant mice. (A) Mutant allele; (B) Wild-type allele; lane M: pUC 8 marker, lanes 1, 2 and 11: wild-type; lanes 3, 4, 7, 8 and 10: heterozygous mutant; lanes 5, 6 and 9: homozygous mutant; lane 12: negative control (aqua bidest.).

4.2 Analysis of disease progression

Compared to wild-type kidneys, renal histology of *Umod*^{A227T} and *Umod*^{C93F} mutant mice showed alterations in heterozygous mutant and homozygous mutant animals of both lines and age groups (14 months and 20-22 months). IFTA as well as inflammatory cell infiltrates were consistent pathologic findings in *Umod*^{A227T} and *Umod*^{C93F} mutant mice. Therefore, these two parameters were quantified by means of an unbiased, model-independent stereological approach in wild-type and mutant animals of each mouse line and age group. Morphometric analysis of renal TALH cell fractions was performed in order to investigate whether the development of kidney malfunction, together with a significant increase in IFTA in *Umod*^{A227T} and *Umod*^{C93F} mutant mice, was caused by TALH cell atrophy.

4.2.1 Qualitative analysis of renal histopathology

Qualitative evaluation of kidneys of *Umod*^{A227T} and *Umod*^{C93F} mutant mice at 20-22 months of age as well as of *Umod*^{C93F} mutant mice at 14 months of age revealed an increased occurrence of histologic alterations in heterozygous mutant and homozygous mutant mice of both lines and age groups when compared to wild-type controls (Table 4.1).

Line		<i>Umod</i> ^{A227T}						<i>Umod</i> ^{C93F}											
Age		20-22 months						14 months			20-22 months								
		wt		het		hom		wt		het		hom							
		m	f	m	f	m	f	m	f	m	f	m	f						
		Number of animals																	
		18	13	18	7	20	10	10	5	9	11	7	4	15	19	28	19	4	3
		Number of animals with renal alterations																	
Tubular cysts		0	0	0	0	2	1	0	0	0	0	1	1	0	0	9	4	2	2
Glomerulocystic changes		0	0	0	0	0	1	0	0	0	0	1	0	0	0	2	3	1	0
Dilation	tubular	4	1	8	2	17	7	1	0	1	2	3	1	3	3	25	17	4	3
	Bowman's capsule	2	0	6	1	12	1	0	0	1	0	0	1	2	1	13	7	2	3
Hydronephrosis		0	0	3	2	5	3	0	0	0	0	2	2	0	1	5	6	3	1
Glomerulosclerosis		0	1	3	0	13	7	0	0	0	0	3	2	4	3	21	12	4	3
Interstitial fibrosis	mild	8	5	6	4	0	0	2	1	7	8	3	0	6	5	1	2	0	0
	moderate	0	0	8	3	8	5	0	0	2	3	2	3	1	0	19	12	0	0
	severe	0	0	0	0	12	5	0	0	0	0	2	1	0	0	8	5	4	3
Inflammation	mild	4	4	6	2	0	0	2	1	6	5	1	0	7	6	5	5	0	0
	moderate	0	0	3	5	14	8	0	0	2	1	5	4	0	2	13	7	1	0
	severe	0	0	1	0	6	2	0	0	0	1	1	0	0	0	10	7	3	3

Table 4.1: Qualitative assessment of the occurrence of renal alterations in *Umod* mutant and wild-type mice.

m: male, f: female, wt: wild-type mouse, het: heterozygous mutant mice, hom: homozygous mutant mice. Criteria for interstitial fibrosis (approximations): >5% to 25% $\hat{=}$ mild, >25% to 50% $\hat{=}$ moderate, >50% $\hat{=}$ severe. Criteria for interstitial inflammation (approximations): >10% to 25% of parenchyma inflamed $\hat{=}$ mild, >25% to 50% of parenchyma inflamed $\hat{=}$ moderate, >50% of parenchyma inflamed $\hat{=}$ severe (classifications based on Racusen *et al.*, 1999).

4.2.1.1 Interstitial fibrosis and tubular atrophy (IFTA)

At 14 months of age, wild-type kidneys showed no pathological alterations while all heterozygous and homozygous *Umod*^{C93F} mutant mice exhibited IFTA. IFTA was predominantly apparent in the renal medulla with streaky extensions into the cortex. In some homozygous *Umod*^{C93F} mutant kidneys, the cortex was segmentally retracted due to focal interstitial fibrosis.

At 20-22 months of age, sparse foci of IFTA appeared in some but not all wild-type kidneys. IFTA was further spread and appeared more intensely in age-matched mutants of both mouse lines. Although fields of IFTA were still primarily located in the corticomedullary region, 20-22-month-old mutant mice also exhibited more cortical IFTA than those at 14 months of age. IFTA in the renal cortex was sometimes accompanied by segmental retraction thereof (Figure 4.3).

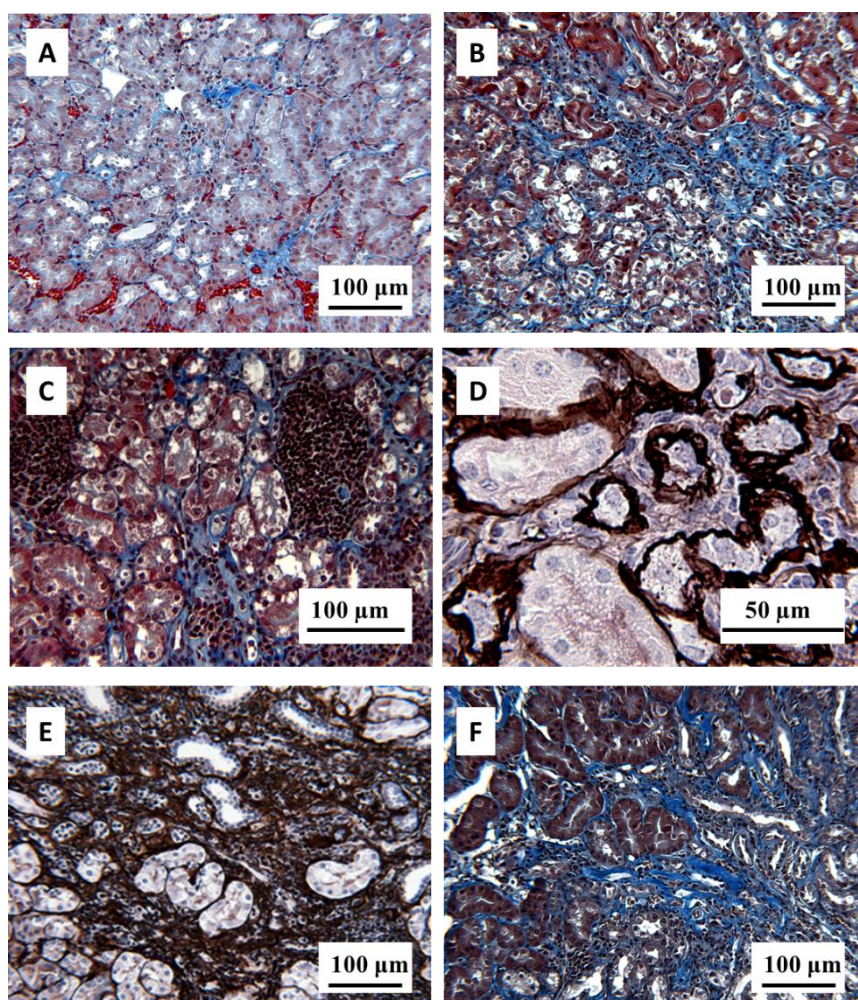


Figure 4.3: IFTA in *Umod* mutant mice. (A) Mild interstitial fibrosis in the kidney of a heterozygous *Umod*^{A227T} mutant mouse at 20 months of age. (B) Moderate interstitial fibrosis ramifying between tubules and (C) interstitial fibrosis accompanied by inflammatory cell infiltrates in the kidneys of homozygous *Umod*^{C93F} mutant mice at 14 months of age. (D) Interstitial fibrosis surrounding atrophic tubules in the kidney of a 14-month-old homozygous *Umod*^{C93F} mutant mouse. Severe interstitial fibrosis in the kidneys of heterozygous *Umod*^{C93F} mutant mice at (E) 14 months of age and (F) 22 months of age. (A), (B), (C), (F): MT staining. (D), (E): PAS silver staining.

4.2.1.2 Inflammatory cell infiltrates

Upon light microscopy, more and larger inflammatory cell infiltrates were detected in kidneys of 14-month-old *Umod*^{C93F} mutant mice when compared to wild-type controls. The infiltrates found consisted mainly of lymphocytes and plasma cells and tended to be localized near the corticomedullary border.

At an age of 20-22 months, the majority of larger inflammatory infiltrates found in the kidneys of *Umod*^{A227T} and *Umod*^{C93F} mutant mice was localized in the renal medulla and around vessels at the corticomedullary junction. Further, multiple smaller foci of inflammation were spread within the renal interstitium, also mainly in the corticomedullary region. In contrast, sparse and more scattered infiltrates were found in the kidneys of some wild-type mice (Figure 4.4).

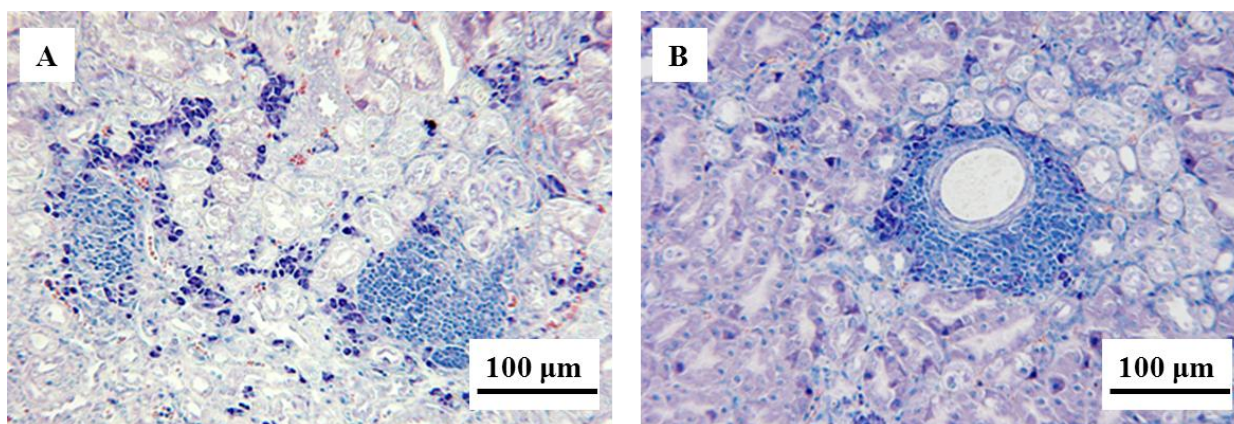


Figure 4.4: Pattern of inflammatory cell infiltrates in the kidneys of *Umod* mutant mice. (A) Larger infiltrates as well as disseminated inflammatory cells in the renal interstitium of a 14-month-old heterozygous *Umod*^{C93F} mutant mouse. (B) Perivascular inflammation in the kidney of a homozygous *Umod*^{A227T} mutant mouse at 20 months of age. Giemsa staining.

4.2.1.3 TALH cells

At 14 months of age, immunohistochemistry for uromodulin revealed a homogenous distribution of the protein in wild-type TALH epithelial cells with distinct apical membrane reactivity of the signal. In contrast, TALH cells of *Umod*^{C93F} mutant mice showed a strong uromodulin signal in coarse clots around the nucleus. Looking at the distribution pattern of the TALH segments of the

kidney, section profiles of wild-type mice showed radial streaks of TALH in medulla and cortex. TALH segments found in kidneys of *Umod*^{C93F} mutant mice, on the other hand, were primarily located in the medulla with scarce and irregular scatters in the cortex.

At the age of 20-22 months, the immunohistochemical staining pattern in TALH cells of both *Umod*^{A227T} and *Umod*^{C93F} mutant mice showed coarse, perinuclear dense aggregates. In contrast, a homogenously distributed and apically reinforced uromodulin signal was visible in TALH cells of wild-type mice. TALH cells of heterozygous and homozygous *Umod*^{A227T} mutant as well as of heterozygous *Umod*^{C93F} mutant mice contained both cytosolic and clustered uromodulin. TALH cells of homozygous *Umod*^{C93F} mutant mice contained almost exclusively aggregated uromodulin (Figure 4.5).

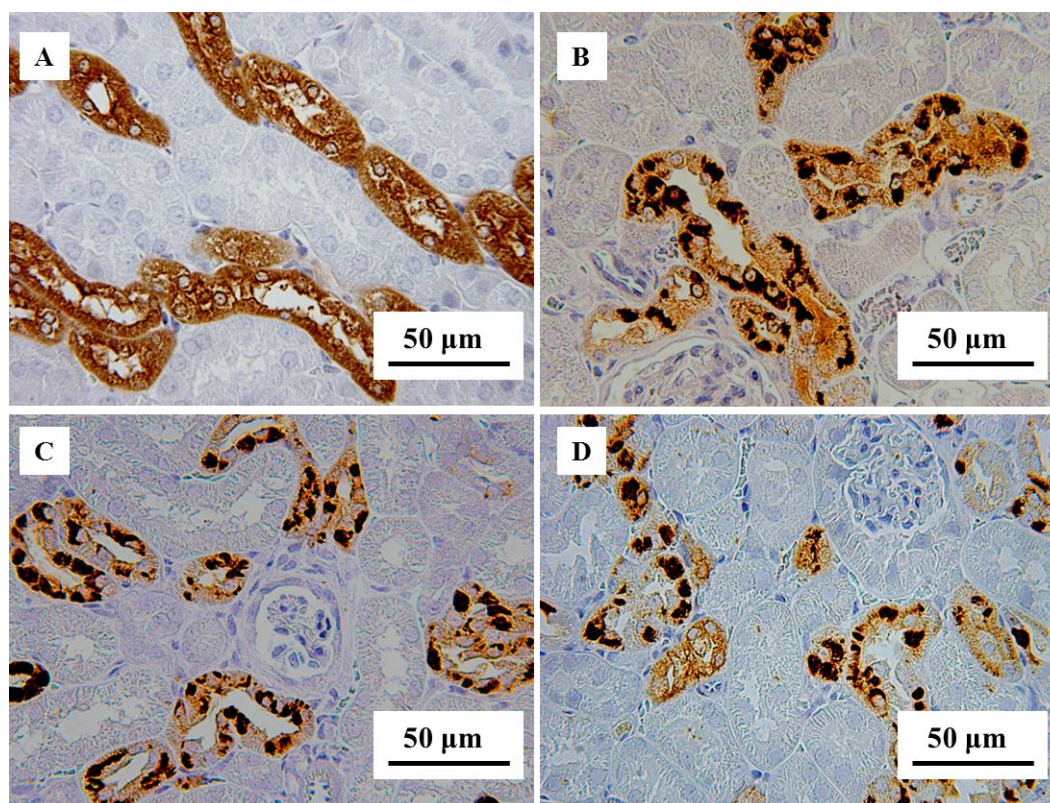


Figure 4.5: Distribution of uromodulin within TALH cells in the kidneys of *Umod* mutant and wild-type mice.

(A) TALH cells in the kidney of a 20-month-old wild-type mouse containing evenly distributed uromodulin with an enhanced presence along the luminal cell membrane. (B) TALH cells of a homozygous *Umod*^{A227T} mutant mouse at 20 months of age, containing both clustered and homogenous cytosolic uromodulin. TALH cells of (C) a 14-month-old heterozygous *Umod*^{C93F} mutant and (D) a 20-month-old homozygous *Umod*^{C93F} mutant mouse where uromodulin is primarily present in the form of coarse perinuclear aggregates in the TALH cells.

4.2.1.4 Sporadic kidney alterations

Besides larger aggregates of inflammatory cell infiltrates and farther spread IFTA, some kidneys of 14-month-old *Umod*^{C93F} mutant mice exhibited mild to moderate tubular dilation which was partially accompanied by epithelial disintegration. Renal cysts were a rare finding. In addition, periglomerular fibrosis and mildly to moderately dilated Bowman's capsules were occasionally found in mutant and some wild-type mice of this age group. Mild to moderate dilation of the renal pelvis was inconsistently found in both heterozygous and homozygous *Umod*^{C93F} mutant mice at 14 months of age.

At 20-22 months, some but not all wild-type kidneys occasionally showed mild dilation of tubules and Bowman's capsules. Further sporadic abnormalities included glomerulosclerosis.

Tubular dilation ranging from mild to high-degree was a frequent finding in 20-22-month-old *Umod*^{A227T} and *Umod*^{C93F} mutant mice and occurred mostly in the outer medulla. Some glomeruli were sclerotic and / or surrounded by a mildly to moderately dilated Bowman's space. The above described abnormalities were found to a higher degree in heterozygous *Umod*^{C93F} mutant than in heterozygous *Umod*^{A227T} mutant mice. Mild to moderate dilation of the renal pelvis occurred in homozygous mutant mice of both lines as well as in heterozygous *Umod*^{C93F} mutant mice at 20-22 months of age (Figure 4.6).

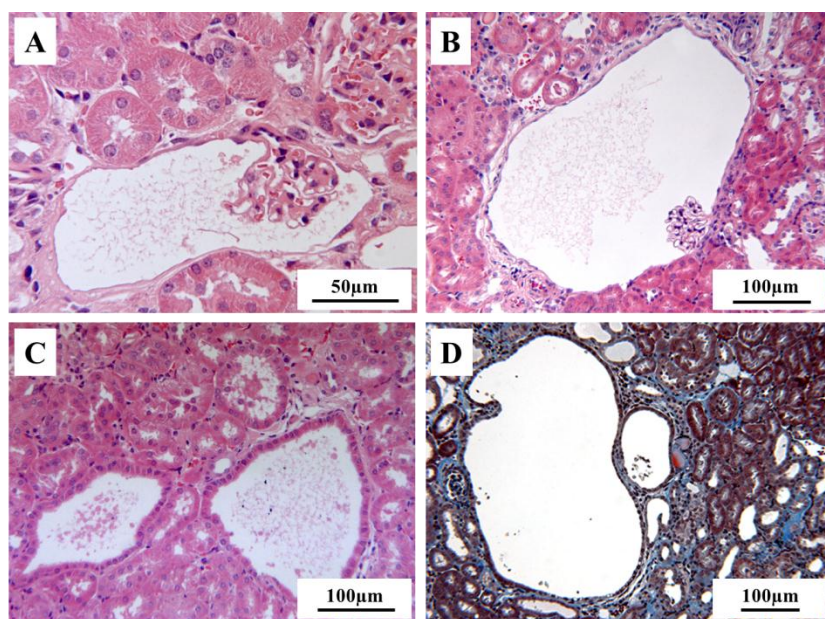


Figure 4.6: Tubular and glomerular dilative alterations. (A) Dilated and (B) cystic Bowman's capsule and (C) tubular dilation/cyst in the kidneys of 20-month-old heterozygous *Umod*^{C93F} mutant mice. (D) Cystic and dilated tubules, surrounded by interstitial fibrosis and tubular atrophy in the kidney of a 20-month-old homozygous *Umod*^{A227T} mutant mouse. (A), (B), (C): H&E staining. (D): MT staining.

4.2.2 Quantitative stereological kidney findings

20-22-month-old heterozygous and homozygous mutant males of both lines (*Umod*^{A227T} and *Umod*^{C93F}) were compared to age- and gender-matched wild-type controls with regard to volume fractions and total volumes of IFTA, inflammatory cell infiltrates and TALH cells (refer to section 3.4). In order to assess age-related progressions of pathological alterations, 14-month-old male *Umod*^{C93F} mutant male mice were evaluated for the aforementioned parameters and compared to age- and gender-matched wild-type controls as well as to the 20-22-month-old *Umod*^{C93F} mice. For each genotype of each mouse line and age group, the right kidneys of 6-7 mutant mice and 6-12 wild-type mice were evaluated.

4.2.2.1 Interstitial fibrosis and tubular atrophy (IFTA)

PAS-silver staining of paraffin kidney sections was used to quantify the volume fraction and total renal volume of IFTA.

4.2.2.1.1 *Umod*^{C93F} mutant mice at 14 months of age

Both heterozygous and homozygous *Umod*^{C93F} mutant mice at 14-months of age exhibited significantly higher fractional volumes of IFTA ($V_{V(\text{IFTA}/\text{kid})}$) than age-matched wild-type mice. $V_{V(\text{IFTA}/\text{kid})}$ was also significantly higher in homozygous than in heterozygous *Umod*^{C93F} mutant mice (Figure 4.7).

Analogous to volume fractions of IFTA ($V_{V(\text{IFTA}/\text{kid})}$), total volumes of IFTA ($V_{(\text{IFTA},\text{kid})}$) were significantly increased in both heterozygous and homozygous *Umod*^{C93F} mutant mice when compared to wild-type controls (Figure 4.8).

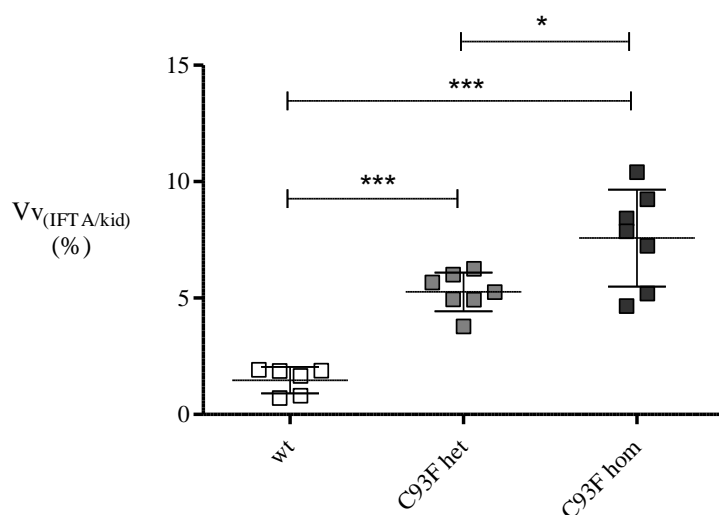


Figure 4.7: Volume fractions of IFTA in kidneys ($Vv_{(IFTA/kid)}$) of 14-month-old $Umod^{C93F}$ mutant mice. Compared to wild-type littermates, mutants showed a significant increase in renal volume fractions of IFTA. Scatter dot plot lines represent mean \pm SD; n=6-7 per genotype. wt: wild-type mice, het: heterozygous mutant mice, hom: homozygous mutant mice. Student's t-test with Bonferroni adjustment: *, $p < 0.016$, **, $p < 0.01$, ***, $p < 0.001$.

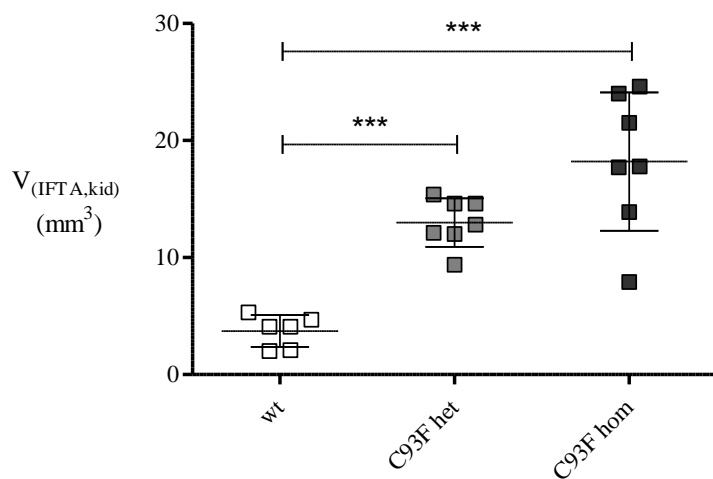


Figure 4.8: Total volumes of IFTA in kidneys ($V_{(IFTA,kid)}$) of 14-month-old $Umod^{C93F}$ mutant mice. Compared to wild-type littermates, mutant mice showed a significant increase in $V_{(IFTA,kid)}$. Scatter dot plot lines represent mean \pm SD; n=6-7 per genotype. wt: wild-type mice, het: heterozygous mutant mice, hom: homozygous mutant mice. Student's t-test with Bonferroni adjustment: *, $p < 0.016$, **, $p < 0.01$, ***, $p < 0.001$.

4.2.2.1.2 *Umod*^{C93F} and *Umod*^{A227T} mutant mice at 20-22 months of age

While volume fractions of IFTA in the kidneys ($V_{V(\text{IFTA}/\text{kid})}$) of heterozygous *Umod*^{A227T} mutant mice were comparable to the volume fractions measured in age-matched wild-type kidneys, $V_{V(\text{IFTA}/\text{kid})}$ of homozygous *Umod*^{A227T} mutant as well as of heterozygous and homozygous *Umod*^{C93F} mutant mice surpassed the wild-type level to a significant degree. Moreover, homozygous *Umod*^{C93F} mutant $V_{V(\text{IFTA}/\text{kid})}$ values were distinctly higher than those of homozygous *Umod*^{A227T} mutant mice and heterozygous *Umod*^{C93F} mutant mice (Figure 4.9). Assessment of the total renal volumes of IFTA ($V_{(\text{IFTA},\text{kid})}$) revealed analogous alterations (Figure 4.10).

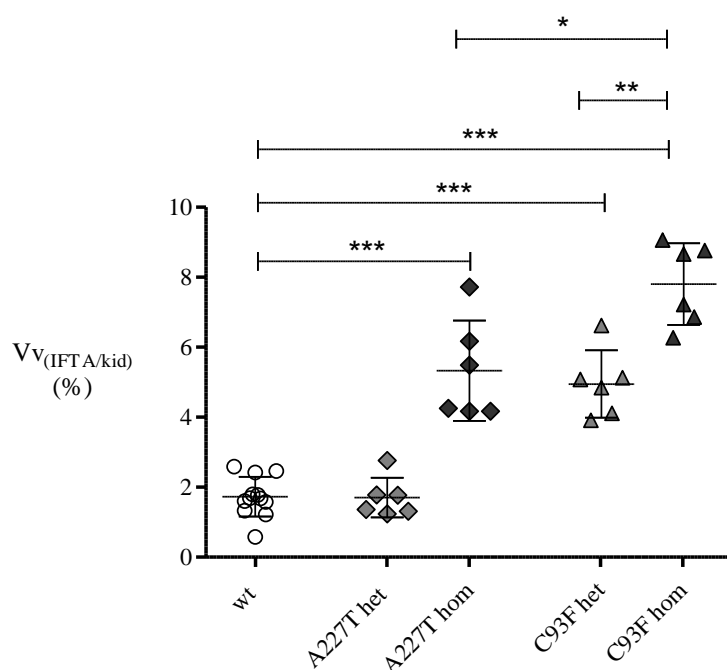


Figure 4.9: Volume fractions of IFTA in kidneys ($V_{V(\text{IFTA}/\text{kid})}$) of 20-22-month-old *Umod*^{A227T} and *Umod*^{C93F} mice. Homozygous mutant mice of both lines as well as heterozygous *Umod*^{C93F} mutant mice exhibited significantly higher volume fractions of IFTA than wild-type littermates. Maximum $V_{V(\text{IFTA}/\text{kid})}$ values were measured in homozygous *Umod*^{C93F} mutant kidneys while $V_{V(\text{IFTA}/\text{kid})}$ values of heterozygous *Umod*^{C93F} mutant mice were similar to those of homozygous *Umod*^{A227T} mutant mice. Scatter dot plot lines represent mean \pm SD; number of animals analysed: n=12 wild-type mice, n=6 mutant mice per genotype and mouse line. wt: wild-type mice, het: heterozygous mutant mice, hom: homozygous mutant mice. Student's t-test with Bonferroni adjustment: *, p<0.01, **, p<0.001, ***, p<0.0001.

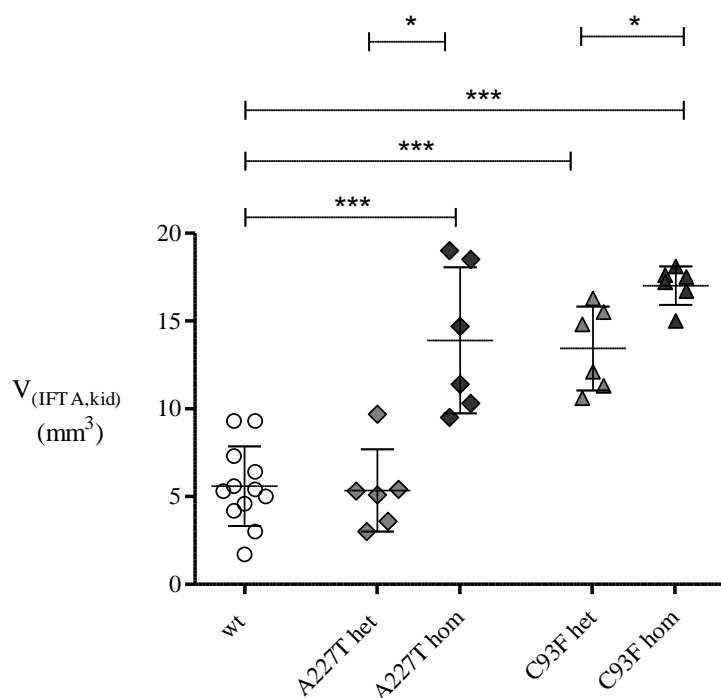


Figure 4.10: Total volumes of IFTA in kidneys ($V_{(IFTA,kid)}$) in 20-22-month-old $Umod^{A227T}$ and $Umod^{C93F}$ mice. Compared to wild-type littermates, heterozygous $Umod^{C93F}$ mutant and homozygous mutant mice of both lines showed a significant increase in $V_{(IFTA,kid)}$. Within each mutant mouse line, $V_{(IFTA,kid)}$ levels of homozygous mutant mice lay also above those of heterozygous mutant mice. Scatter dot plot lines represent mean \pm SD; number of animals analysed: n=12 wild-type mice, n=6 mutant mice per genotype and mouse line. wt: wild-type mice, het: heterozygous mutant mice, hom: homozygous mutant mice. Student's t-test with Bonferroni adjustment: *, p<0.01, **, p<0.001, ***, p<0.0001.

4.2.2.1.3 $V_{(IFTA/kid)}$ and $V_{(IFTA,kid)}$ in $Umod^{C93F}$ mutant mice at different ages

Although the values of both renal volume fractions ($V_{(IFTA/kid)}$) and total volumes ($V_{(IFTA,kid)}$) of IFTA were distinctly increased in $Umod^{C93F}$ mutant mice within each age group (refer to sections 4.2.2.1.1 and 4.2.2.1.2), neither parameter progressed notably between the age of 14 months and 20-22 months within the respective genotype groups (Figure 4.11 and Figure 4.12).

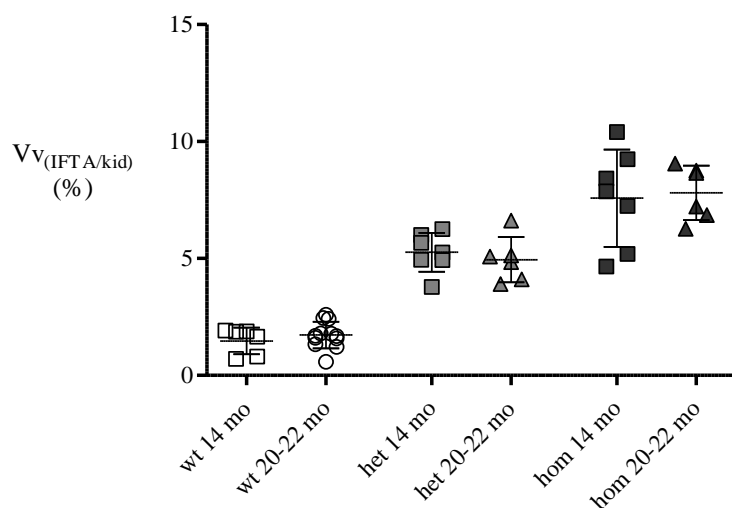


Figure 4.11: Volume fractions of IFTA in kidneys ($V_{v(\text{IFTA}/\text{kid})}$) of $Umod^{C93F}$ mice at different ages. Within each genotype group, $V_{v(\text{IFTA}/\text{kid})}$ did not change significantly with age. Scatter dot plot lines represent mean \pm SD; number of animals analysed: n=6-12 wild-type mice, n=6-7 mutants per genotype and mouse line. wt: wild-type mice, het: heterozygous mutant mice, hom: homozygous mutant mice. Student's t-test vs. genotype-matched mice: *, $p < 0.05$, **, $p < 0.01$, ***, $p < 0.001$.

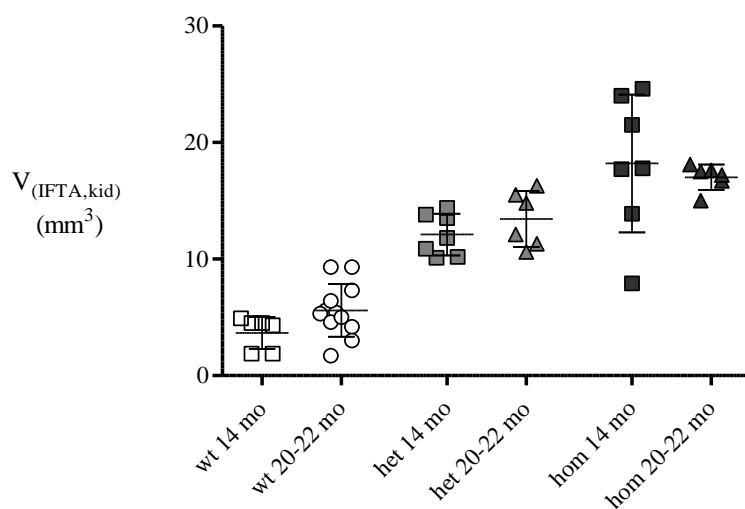


Figure 4.12: Total renal volumes of IFTA ($V_{(\text{IFTA},\text{kid})}$) in $Umod^{C93F}$ kidneys at different ages. Within the respective genotype groups, $V_{(\text{IFTA},\text{kid})}$ did not change significantly between 14 and 20-22 months. Scatter dot plot lines represent mean \pm SD; number of animals analysed: n=6-12 wild-type mice, n=6-7 mutants per genotype and mouse line. wt: wild-type mice, het: heterozygous mutant mice, hom: homozygous mutant mice. Student's t-test vs. genotype-matched mouse: *, $p < 0.05$, **, $p < 0.01$, ***, $p < 0.001$.

4.2.2.2 Inflammatory cell infiltrates

Giemsa-stained kidney sections of *Umod*^{A227T} and *Umod*^{C93F} mutant mice were compared to those of age-matched wild-type mice (14 and 20-22 months) with regard to the fractional and total volumes of inflammatory cell infiltrates.

4.2.2.2.1 *Umod*^{C93F} mutant mice at 14 months of age

Both volume fractions ($V_{V(IC/kid)}$) and total renal volume ($V_{(IC,kid)}$) of inflammatory cell infiltrates were significantly higher in *Umod*^{C93F} mutant mice than in wild-type controls. $V_{V(IC/kid)}$ measured for homozygous *Umod*^{C93F} mutant mice was also significantly higher than $V_{V(IC/kid)}$ in heterozygous *Umod*^{C93F} mutant mice (Figure 4.13 and Figure 4.14).

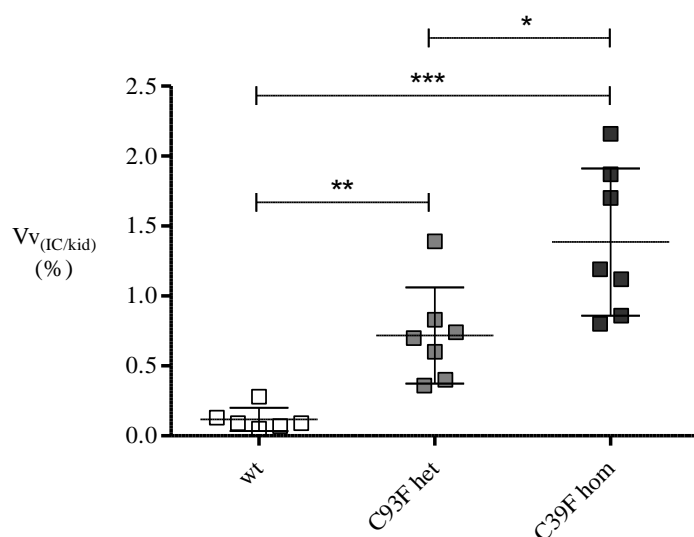


Figure 4.13: Volume fractions of inflammatory cell infiltrates in kidneys ($V_{V(IC/kid)}$) of 14-month-old *Umod*^{C93F} mice. Volume fractions of inflammatory cell infiltrates in the kidneys were significantly higher in both heterozygous *Umod*^{C93F} mutant and homozygous *Umod*^{C93F} mutant mice versus wild-type littermates. Scatter dot plot lines represent mean \pm SD; n=6-7 per genotype. wt: wild-type mouse, het: heterozygous mutant mouse, hom: homozygous mutant mouse. Student's t-test with Bonferroni adjustment: *, p<0.016, **, p<0.01, ***, p<0.001.

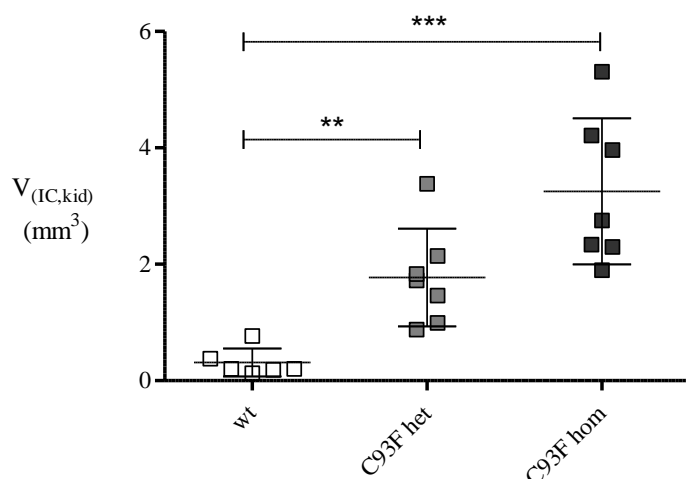


Figure 4.14: Total volumes of inflammatory cell infiltrates in kidneys ($V_{(IC,kid)}$) of 14-month-old $Umod^{C93F}$ mice. Compared to wild-type littermates, mutants showed a significant increase in $V_{(IC,kid)}$. Scatter dot plot lines represent mean \pm SD; n=6-7 per genotype. wt: wild-type mice, het: heterozygous mutant mice, hom: homozygous mutant mice. Student's t-test with Bonferroni adjustment: *, $p < 0.016$, **, $p < 0.01$, ***, $p < 0.001$.

4.2.2.2.2 $Umod^{C93F}$ and $Umod^{A227T}$ mutant mice at 20-22 months of age

Regarding volume fractions of inflammatory cell infiltrates ($V_{V(IC/kid)}$), heterozygous $Umod^{A227T}$ mutant mice had similar values as wild-type mice. In contrast, $V_{V(IC/kid)}$ of homozygous $Umod^{A227T}$ mutant mice as well as of heterozygous and homozygous $Umod^{C93F}$ mutant mice were significantly higher compared to wild-type controls (Figure 4.15).

Total volumes of inflammatory cell infiltrates ($V_{(IC,kid)}$) were lowest in wild-type and heterozygous $Umod^{A227T}$ mutant kidneys. $V_{(IC,kid)}$ in homozygous $Umod^{A227T}$ mutant mice was higher than $V_{(IC,kid)}$ of both wild-type and heterozygous $Umod^{A227T}$ mutant kidneys. $V_{(IC,kid)}$ in heterozygous and homozygous $Umod^{C93F}$ mutant mice surpassed wild-type levels significantly (Figure 4.16).

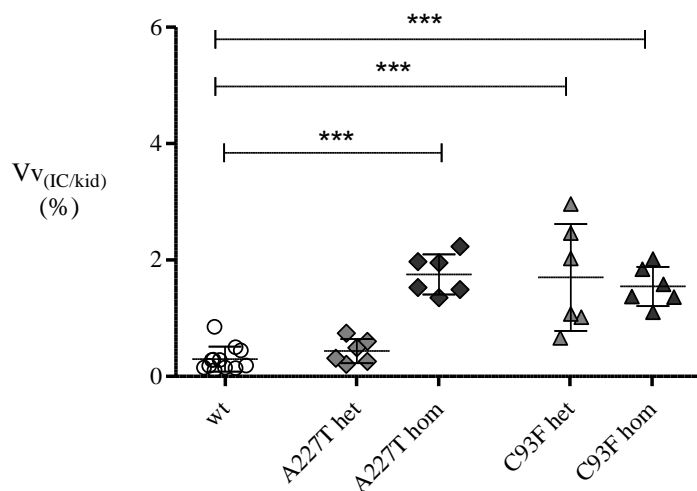


Figure 4.15: Volume fractions of inflammatory cell infiltrates in kidneys ($V_{v(IC/kid)}$) of 20-22-month-old $Umod^{A227T}$ and $Umod^{C93F}$ mice. Homozygous mutant mice of both lines as well as heterozygous $Umod^{C93F}$ mutant mice exhibited significantly higher volume fractions than wild-type controls. Scatter dot plot lines represent mean \pm SD; number of animals analysed: n=12 wild-type mice, n=6 mutants per genotype and mouse line. wt: wild-type mice, het: heterozygous mutant mice, hom: homozygous mutant mice. Student's t-test with Bonferroni adjustment: *, p<0.01, **, p<0.001, ***, p<0.0001.

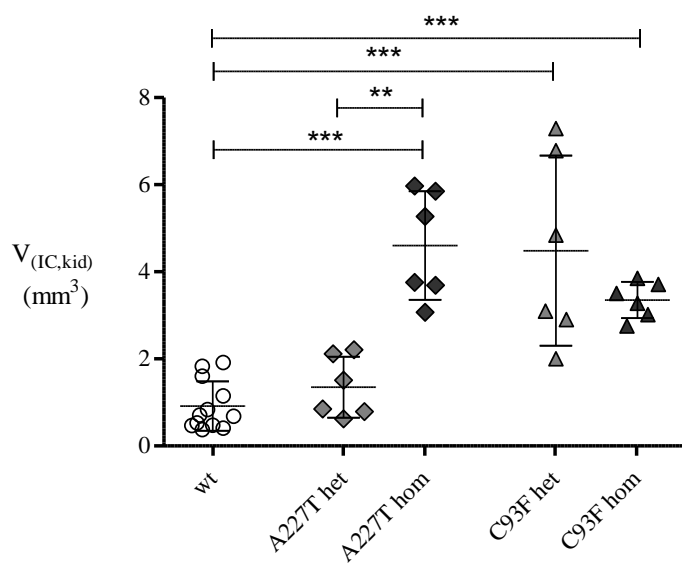


Figure 4.16: Total volumes of inflammatory cell infiltrates in kidneys ($V_{(IC,kid)}$) of 20-22-month-old $Umod^{A227T}$ and $Umod^{C93F}$ mice. Homozygous mutant mice of both lines as well as heterozygous $Umod^{C93F}$ mutant mice exhibited significantly higher total volume of inflammatory cell infiltrates than wild-type controls. Scatter dot plot lines represent mean \pm SD; number of animals analysed: n=12 wild-type mice, n=6 mutant mice per genotype and mouse line. wt: wild-type mice, het: heterozygous mutant mice, hom: homozygous mutant mice. Student's t-test with Bonferroni adjustment: *, p<0.01, **, p<0.001, ***, p<0.0001.

4.2.2.2.3 Inflammatory cell infiltrates in *Umod*^{C93F} mutant mice at different ages

Although there was a tendency towards an age-dependent increase in $V_{V(IC/kid)}$ within each genotype-group, only 20-22-month-old heterozygous *Umod*^{C93F} mutant mice exhibited a significantly higher $V_{V(IC/kid)}$ compared to genotype-matched mice at the age of 14 months. However, heterozygous *Umod*^{C93F} mutant mice at the age of 20-22 months constituted the group with the largest variation of $V_{V(IC/kid)}$ values (Figure 4.17).

In comparison, total volumes of inflammatory cell infiltrates in the kidneys ($V_{(IC,kid)}$) of 20-22-month-old wild-type and heterozygous *Umod*^{C93F} mutant mice were significantly higher than in the kidneys of genotype-matched 14-month-old mice. Older homozygous *Umod*^{C93F} mutant mice only showed a tendency towards an increase in ($V_{(IC,kid)}$) when compared to 14-month-old homozygous mutant mice. Again, heterozygous *Umod*^{C93F} mutant mice at an age of 14 months exhibited the largest variation of $V_{(IC,kid)}$ values (Figure 4.18).

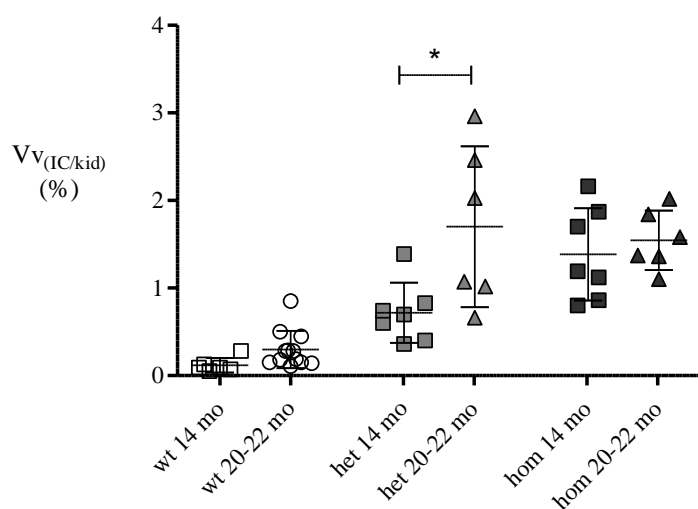


Figure 4.17: Volume fractions of inflammatory cell infiltrates in kidneys ($V_{V(IC/kid)}$) of *Umod*^{C93F} mice at different ages. Within each genotype group, $V_{V(IC/kid)}$ did not change significantly with age, with the exception of heterozygous *Umod*^{C93F} mutants. Scatter dot plot lines represent mean \pm SD; number of animals analysed: n=6-12 wild-type mice, n=6-7 mutants per genotype and mouse line. wt: wild-type mice, het: heterozygous mutant mice, hom: homozygous mutant mice. Student's t-test vs. genotype-matched mice at 14 months: *, p<0.05, **, p<0.01, ***, p<0.001.

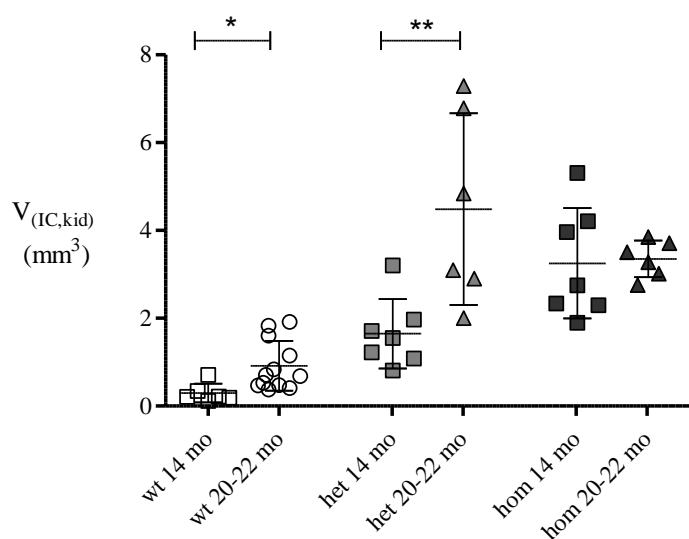


Figure 4.18: Total volumes of inflammatory cell infiltrates in kidneys ($V_{(IC,kid)}$) of $Umod^{C93F}$ mice at different ages. In wild-type and heterozygous mutant mice a marked increase of $V_{(IC,kid)}$ was detected with age. Scatter dot plot lines represent mean \pm SD; number of animals analysed: n=6-12 wild-type mice, n=6-7 mutant mice per genotype and mouse line. wt: wild-type mice, het: heterozygous mutant mice, hom: homozygous mutant mice. Student's t-test vs. genotype-matched mice at 14 months: *, $p < 0.05$, **, $p < 0.01$, ***, $p < 0.001$.

4.2.2.3 TALH cells

TALH cells were defined as those cells that were positive for anti-uromodulin immunohistochemical staining. In cases where only one cell of a tubule profile showed positivity for uromodulin, the remaining cells of the tubule profile were defined as TALH cells as well.

4.2.2.3.1 $Umod^{C93F}$ mutant mice at 14 months of age

TALH cell volume fractions ($V_{V(TALH/kid)}$) did not differ significantly between $Umod^{C93F}$ mutant mice and wild-type controls. However, heterozygous $Umod^{C93F}$ mutant mice showed a significantly higher mean $V_{V(TALH/kid)}$ than homozygous $Umod^{C93F}$ mutant mice ($p = 0.0057$) (Figure 4.24). Total TALH cell volumes ($V_{(TALH,kid)}$) revealed no significant difference between mutants and wild-type controls. Notably, $V_{(TALH,kid)}$ values tended to drop in homozygous mutant $Umod^{C93F}$ mice and the lowest $V_{(TALH,kid)}$ was measured in this group (Figure 4.20).

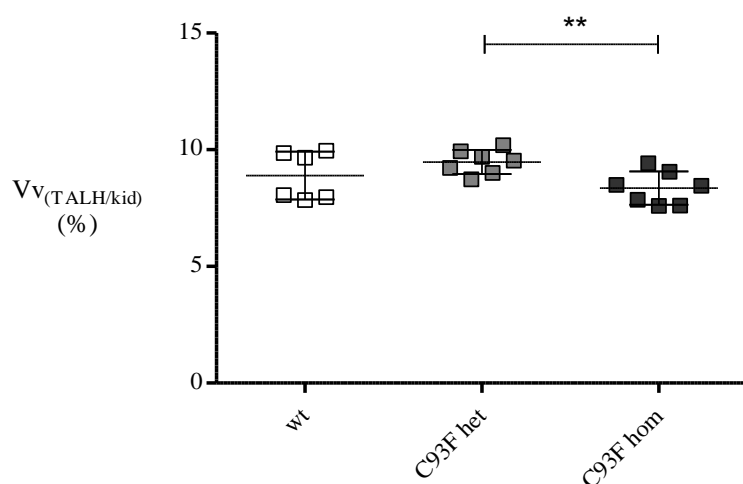


Figure 4.19: Volume fractions of TALH cells in kidneys ($Vv_{(TALH/kid)}$) of 14-month-old $Umod^{C93F}$ mice. Compared to wild-type littermates, mutants showed no significant decrease in $Vv_{(TALH/kid)}$. Homozygous mutant mice exhibited a significantly lower $Vv_{(TALH/kid)}$ than heterozygous mutant mice. Scatter dot plot lines represent mean \pm SD; n=6-7 per genotype. wt: wild-type mice, het: heterozygous mutant mice, hom: homozygous mutant mice. Student's t-test with Bonferroni adjustment: *, $p < 0.016$, **, $p < 0.01$, ***, $p < 0.001$.

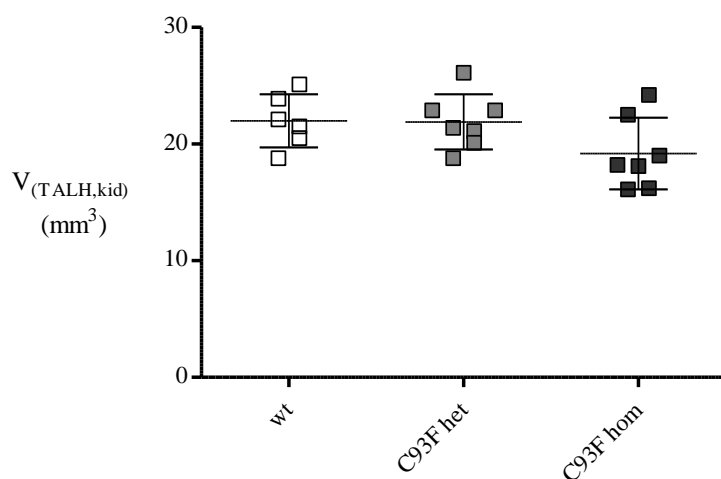


Figure 4.20: Total volumes of TALH cells in kidneys ($V_{(TALH,kid)}$) of 14-month-old $Umod^{C93F}$ mice. Compared to wild-type littermates, mutants showed no significant decrease in $V_{(TALH,kid)}$. There was a trend towards lower total TALH cell volumes in homozygous $Umod^{C93F}$ mutant mice. Scatter dot plot lines represent mean \pm SD; n=6-7 per genotype. wt: wild-type mice, het: heterozygous mutant mice, hom: homozygous mutant mice. Student's t-test with Bonferroni adjustment: *, $p < 0.016$, **, $p < 0.01$, ***, $p < 0.001$.

4.2.2.3.2 *Umod*^{C93F} and *Umod*^{A227T} mutant mice at 20-22 months of age

At 20-22 months of age, neither heterozygous *Umod*^{A227T} mutant nor heterozygous *Umod*^{C93F} mutant mice differed from age-matched wild-type controls with regard to TALH cell volume fractions. The kidneys of both homozygous *Umod*^{A227T} mutant and homozygous *Umod*^{C93F} mutant mice in this age group contained significantly lower fractional volumes of TALH cells when compared to wild-type controls (Figure 4.21).

Similarly, total volumes of TALH cells of heterozygous mutant mice of both lines were not significantly below those of wild-type controls. Homozygous *Umod*^{A227T} and *Umod*^{C93F} mutant kidneys, on the other hand, contained significantly lower total volumes of TALH cells when compared to wild-type controls (Figure 4.22).

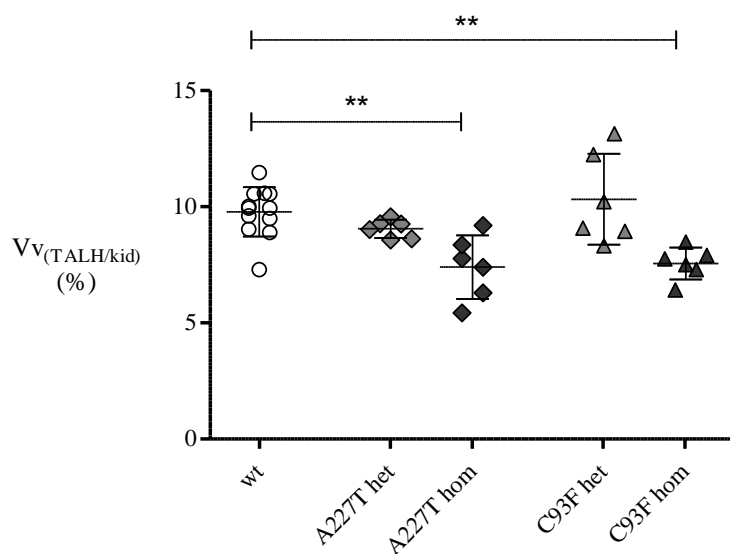


Figure 4.21: Volume fractions of TALH cells in the kidneys ($V_{v(TALH/kid)}$) of 20-22-month-old *Umod*^{A227T} and *Umod*^{C93F} mice. Compared to wild-type controls, homozygous mutant mice of both lines had significantly reduced renal $V_{v(TALH/kid)}$. Scatter dot plot lines represent mean \pm SD; number of animals analysed: n=12 wild-type mice, n=6 mutant mice per genotype and mouse line. wt: wild-type mice, het: heterozygous mutant mice, hom: homozygous mutant mice. Student's t-test with Bonferroni adjustment: *, p<0.01, **, p<0.001, ***, p<0.0001.

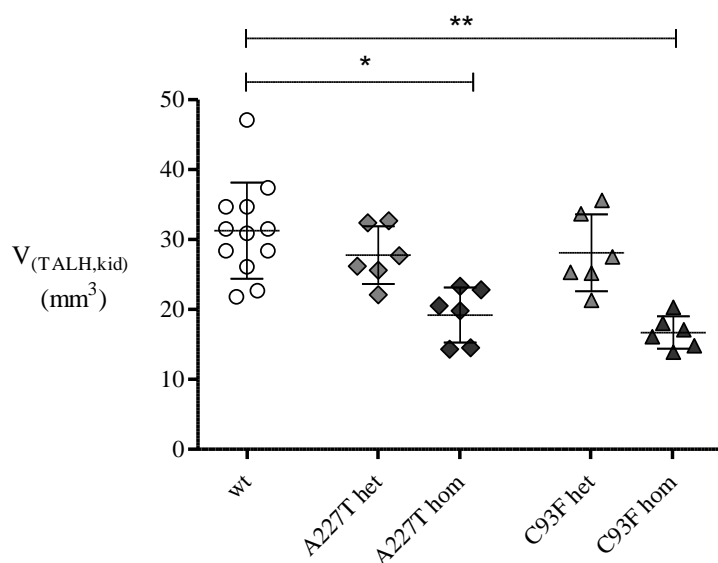


Figure 4.22: Total volumes of TALH cells ($V_{(TALH,kid)}$) in 20-22-month-old $Umod^{A227T}$ and $Umod^{C93F}$ mice. Compared to wild-type controls, heterozygous mutant mice of both lines exhibited similar $V_{(TALH,kid)}$. In contrast, the $V_{(TALH,kid)}$ of homozygous $Umod^{A227T}$ and $Umod^{C93F}$ mutant mice was significantly lower compared to age-matched wild-type controls. Scatter dot plot lines represent mean \pm SD; number of animals analysed: n=12 wild-type mice, n=6 mutant mice per genotype and mouse line. wt: wild-type mice, het: heterozygous mutant mice, hom: homozygous mutant mice. Student's t-test with Bonferroni adjustment: *, $p < 0.01$, **, $p < 0.001$, ***, $p < 0.0001$.

4.2.2.3.3 $V_{(TALH/kid)}$ and $V_{(TALH,kid)}$ in $Umod^{C93F}$ mutant mice at different ages

Neither wild-type nor heterozygous or homozygous $Umod^{C93F}$ mutant mice exhibited a significant change in fractional renal TALH cell volumes between the ages of 14 and 20-22 months. There was, however, a tendency towards an age-related rise of $V_{(TALH/kid)}$ values in wild-type and heterozygous mutant mice. In contrast, $V_{(TALH/kid)}$ slightly dropped with age in homozygous $Umod^{C93F}$ mutant mice (20-22 months of age compared to 14-month-old mice, $p=0.066$) (Figure 4.23).

Regarding total renal TALH cell volumes ($V_{(TALH,kid)}$), there was a significant increase with age in both wild-type and heterozygous $Umod^{C93F}$ mutant mice. In contrast, the mean $V_{(TALH,kid)}$ dropped in aged (20-22-month-old) homozygous mutant mice of this line but the decline remained insignificant ($p=0.1329$) (Figure 4.24).

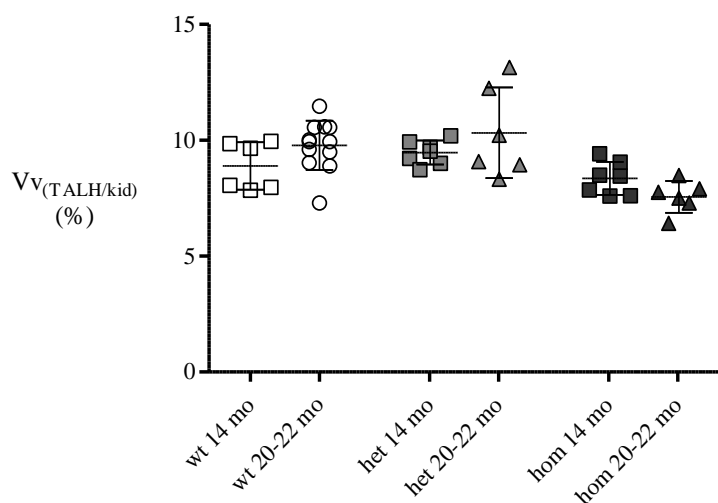


Figure 4.23: Volume fractions of TALH cells in kidneys ($V_{v(\text{TALH}/\text{kid})}$) of $Umod^{C93F}$ mice at different ages. Only homozygous mutant mice showed a tendency to a decreasing $V_{v(\text{TALH}/\text{kid})}$ value with age ($p=0.066$). Scatter dot plot lines represent mean \pm SD; number of animals analysed: $n=6-12$ wild-type, $n=6-7$ mutants per genotype and mouse line. wt: wild-type mice, het: heterozygous mutant mice, hom: homozygous mutant mice. Student's t-test vs. genotype-matched mice at 14 months: *, $p<0.05$, **, $p<0.01$, ***, $p<0.001$.

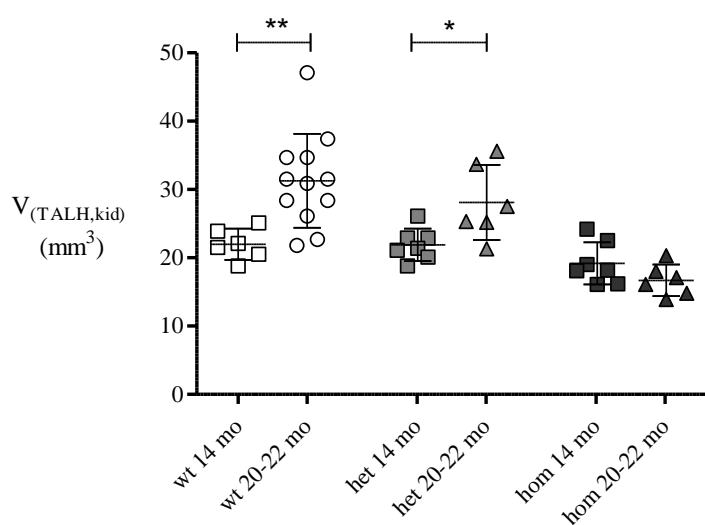


Figure 4.24: Total volumes of TALH cells in kidneys ($V_{(\text{TALH},\text{kid})}$) of $Umod^{C93F}$ mice at different ages. Homozygous $Umod^{C93F}$ mutant mice leaned towards lower $V_{(\text{TALH},\text{kid})}$ values at a higher age. The opposite was detected in heterozygous mutant mice and wild-type controls. Scatter dot plot lines represent mean \pm SD; number of animals analysed: $n=6-12$ wild-type, $n=6-7$ mutants per genotype and mouse line. wt: wild-type mice, het: heterozygous mutant mice, hom: homozygous mutant mice. Student's t-test vs. genotype-matched mice at 14 months: *, $p<0.05$, **, $p<0.01$, ***, $p<0.001$.

4.3 *In vivo* testing of two putative causative therapeutics for UAKD

After the mating of heterozygous mutant animals in each mouse line, genotyping of the litters was performed in order to select a total of 47 wild-type, 42 homozygous *Umod*^{A227T} mutant and 36 homozygous *Umod*^{C93F} mutant male mice for the therapy experiment. Each treatment group consisted of homozygous mutant mice from both mouse lines and of wild-type controls. 19 wild-type, 19 homozygous *Umod*^{A227T} mutant and 11 homozygous *Umod*^{C93F} mutant mice were given 4-PBA. The tempol treatment group consisted of 13 wild-type, 17 homozygous *Umod*^{A227T} mutant and 11 homozygous *Umod*^{C93F} mutant mice. 15 wild-type, 6 homozygous *Umod*^{A227T} mutant and 14 homozygous *Umod*^{C93F} mutant mice received drinking water only and thus constituted the placebo group. Having been divided into three treatment groups (4-PBA, tempol and placebo), all mice were compared with regard to body weight, clinical chemistry of blood plasma and urine, kidney function, urinary uromodulin excretion and renal histology (refer to section 3.5).

4.3.1 Body weight

During the 8 weeks of drug administration (4-PBA, tempol and placebo), the body weight of all mice was measured every 7 days. In all treatment groups and at all points of measurements, the lowest body weights were detected in homozygous *Umod*^{C93F} mutant mice, while the highest body weights were measured in wild-type mice. Of a total of 35 mice in the placebo treatment group, 10 animals were only tested at the age of 4 months and are therefore not included in the data presentation below (Figure 4.25).

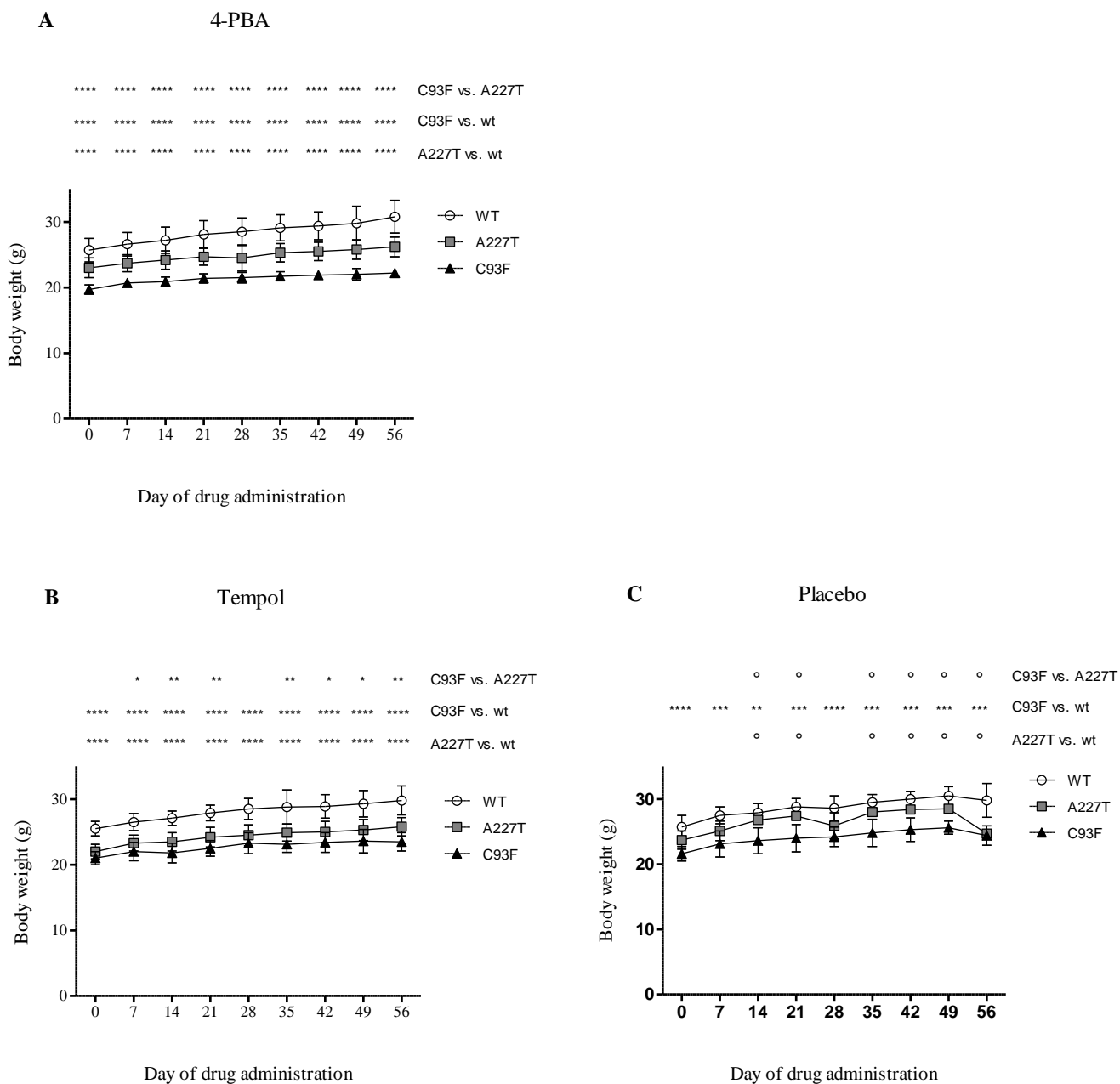


Figure 4.25: Body weights of homozygous $Umod^{A227T}$ mutant and homozygous $Umod^{C93F}$ mutant mice compared to wild-type controls between day 0 and day 56 of (A) 4-PBA, (B) tempol and (C) placebo treatment. In both the 4-PBA and the tempol treatment group the body weights of homozygous $Umod^{A227T}$ and $Umod^{C93F}$ mutant mice remained significantly below those of wild-type controls. Data are represented as mean \pm SD; number of animals analysed: n=9-19 wild-type, n=1-19 homozygous $Umod^{A227T}$ mutant mice, 3-11 homozygous $Umod^{C93F}$ mutant mice per treatment group. wt: wild-type mouse, A227T: homozygous $Umod^{A227T}$ mutant mice, C93F: homozygous $Umod^{C93F}$ mutant mice. Student's t-test with Bonferroni adjustment: *, $p < 0.016$, **, $p < 0.01$, ***, $p < 0.001$, ****, $p < 0.0001$. \circ $Umod^{A227T}$ body weight represents 1 animal only.

4.3.2 Clinical chemical analysis

ER storage of mutant uromodulin results in disturbed ER homeostasis and subsequently in renal dysfunction leading to elevated plasma urea levels, which is the major phenotypic characteristic of *Umod*^{A227T} and *Umod*^{C93F} mutant mice. At the ages of 2, 3 and 4 months, plasma urea levels and other clinical chemical parameters were compared between the different genotypes within each treatment group (homozygous *Umod*^{A227T} mutant and homozygous *Umod*^{C93F} mutant male mice as well as wild-type male mice). Blood plasma parameters of genotype-matched mice receiving different treatments (4-PBA, tempol or placebo) were compared as well. The principal purpose of this analysis was to answer the question whether 4-PBA or tempol application may decrease plasma urea values of homozygous *Umod*^{A227T} mutant and homozygous *Umod*^{C93F} mutant mice to a level similar to the values in wild-type mice (Tables 4.2, 4.3 and 4.4).

Regardless of treatment, the plasma urea levels of all mice increased with age. At all points of the analysis and within each treatment group, the plasma urea levels of homozygous *Umod*^{C93F} mutant mice and those of homozygous *Umod*^{A227T} mutant mice were significantly above wild-type mice levels.

At the age of 3 months, wild-type mice of the 4-PBA treatment group exhibited a significantly higher plasma urea concentration than those of the placebo group. Although plasma urea concentrations of both wild-type and homozygous *Umod*^{A227T} mutant mice in the 4-PBA treatment group were significantly higher than in genotype-matched mice of the tempol treatment group, this had already been the case at the start of treatment application (at 2 months of age). Similarly, plasma urea concentrations of 3-month-old homozygous *Umod*^{C93F} mutant mice tended to be highest in the 4-PBA and lowest in the tempol treatment group but differences were insignificant.

At 4 months of age, plasma urea concentrations were highest in mice receiving 4-PBA when compared to genotype-matched mice of other treatment groups (Figure 4.26).

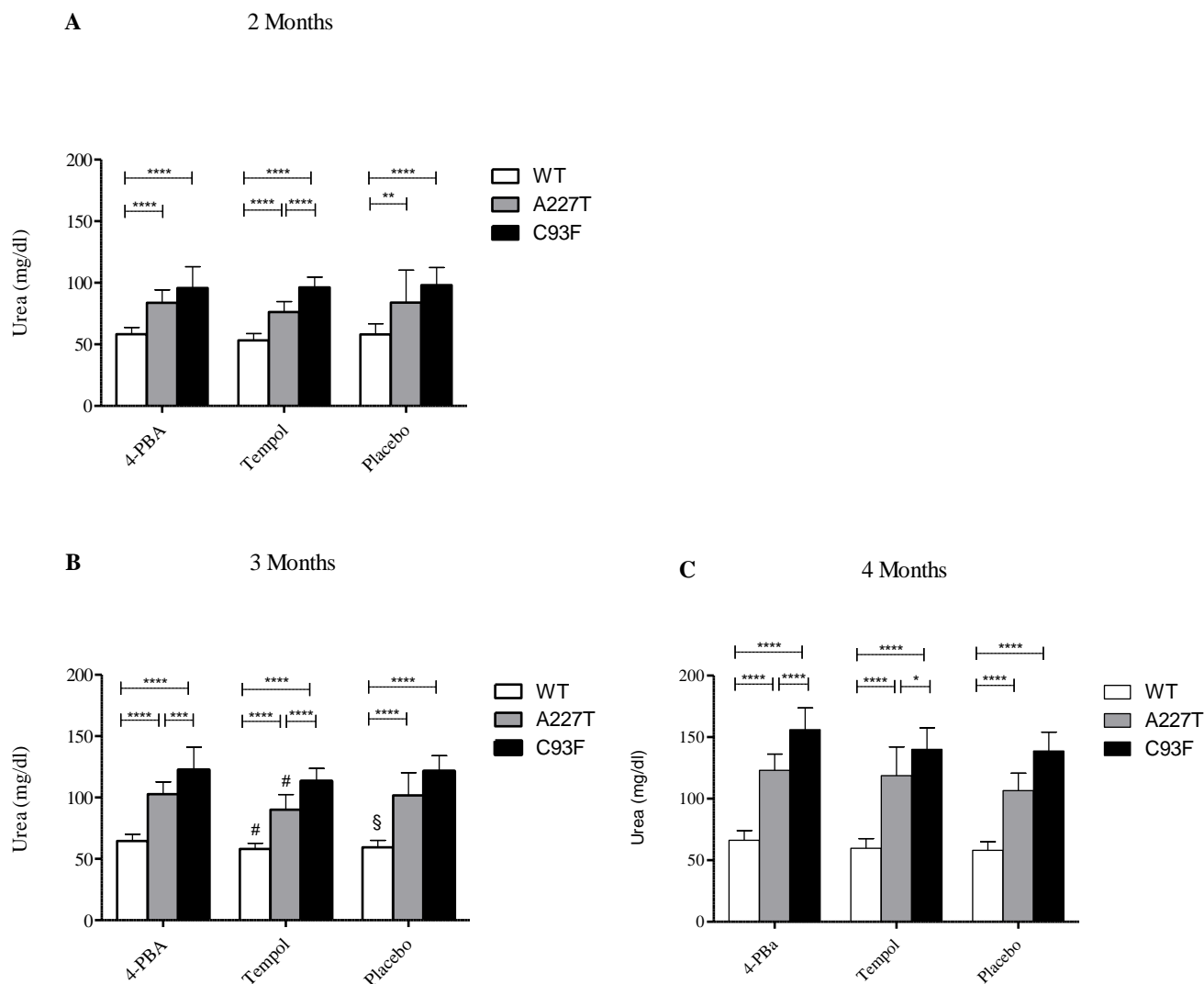


Figure 4.26: Plasma urea levels of homozygous *Umod*^{A227T} and *Umod*^{C93F} mutant mice as well as of wild-type controls of the different treatment groups at the ages of (A) 2 months, (B) 3 months and (C) 4 months. All genotypes and treatment groups exhibited an increase in plasma urea concentration over time. Plasma urea levels tended to be highest for each genotype in the 4-PBA treatment group. At the age of 4 months, mutant mice in all groups exhibited significantly higher plasma urea levels than wild-type controls. Data represents mean \pm SD. n=13-19 wild-type mice, n=3-19 homozygous *Umod*^{A227T} mutant mice, n=8-13 homozygous *Umod*^{C93F} mutant mice; wt: wild-type animal; *Umod*^{A227T}: homozygous *Umod*^{A227T} mutant animal; *Umod*^{C93F}: homozygous *Umod*^{C93F} mutant animal. Student's t-test with Bonferroni adjustment: p: *, <0.016; **, <0.01; ***, <0.001; ****, <0.0001. §p<0.05 vs. matching genotype in 4-PBA treatment group; #p<0.01 vs. matching genotype in 4-PBA treatment group.

Plasma uric acid concentrations did not differ between mice of different genotypes in any of the treatment groups.

Plasma cholesterol levels in *Umod* mutant mice tended to be decreased in all treatment groups at the ages of 2 and 3 months. At 4 months of age, both homozygous *Umod*^{A227T} mutant and homozygous *Umod*^{C93F} mutant mice reached cholesterol levels which were similar to those of wild-type controls within both the 4-PBA and the tempol treatment group. Plasma cholesterol values of wild-type and homozygous *Umod*^{A227T} mutant mice were highest in the tempol treatment group when compared to genotype-matched mice in the 4-PBA and placebo treatment groups (Figure 4.27).

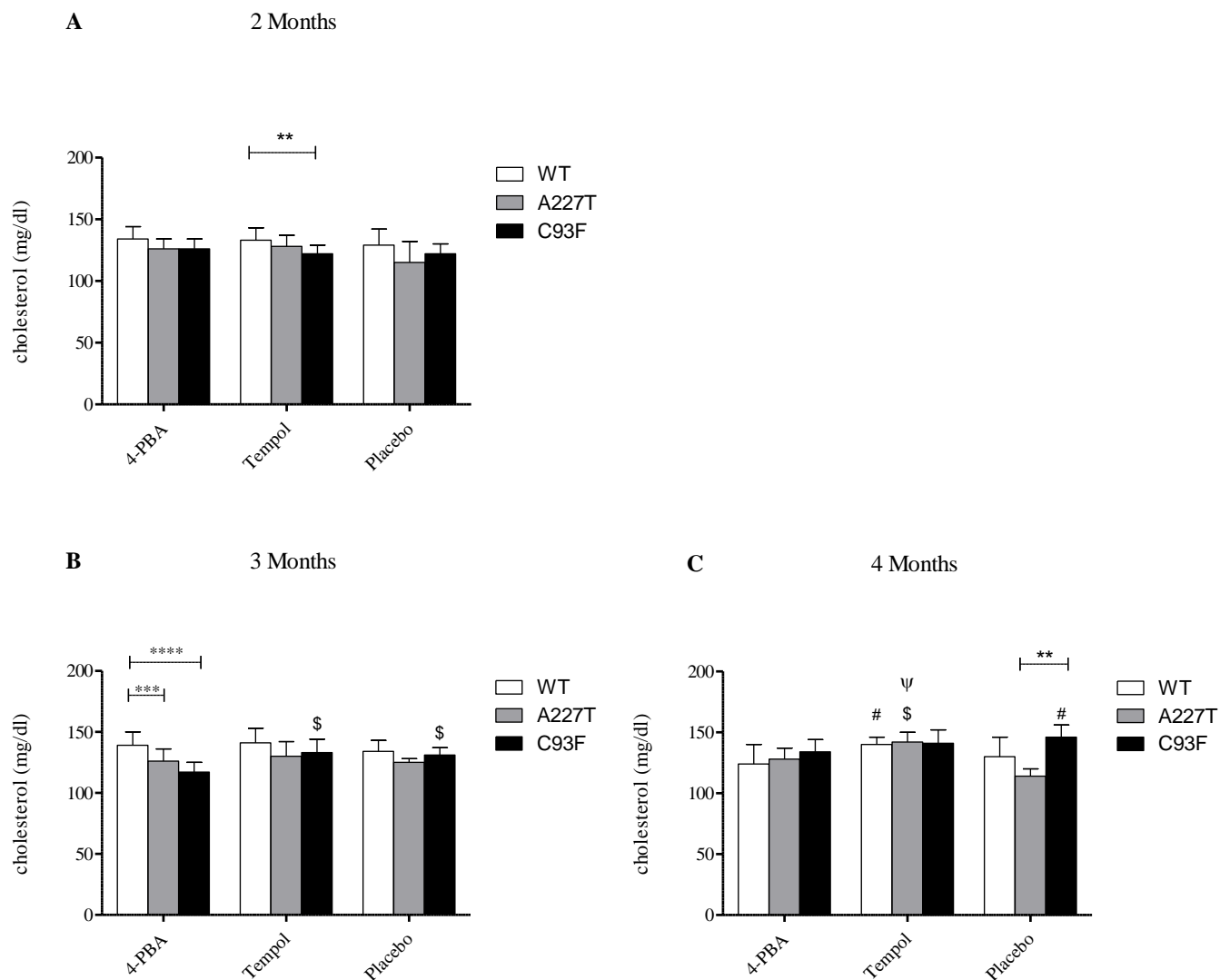


Figure 4.27: Plasma cholesterol levels of homozygous *Umod*^{A227T} mutant and homozygous *Umod*^{C93F} mutant mice as well as of wild-type controls of the different treatment groups at the ages of (A) 2 months, (B) 3 months and (C) 4 months. At the age of 2 and 3 months, homozygous mutant mice of both lines exhibited lower plasma cholesterol levels than wild-type controls. At 4 months of age, plasma cholesterol levels of mutant mice in the 4-PBA and the tempol treatment group showed no significant difference from those of wild-type mice. Mutants in the placebo group never exhibited significantly lower plasma cholesterol concentrations when compared to wild-type mice. Data represent mean \pm SD. n=13-19 wild-type mice, n=3-19 homozygous *Umod*^{A227T} mutant mice, n=8-13 homozygous *Umod*^{C93F} mutant mice. wt: wild-type animal; *Umod*^{A227T}: homozygous *Umod*^{A227T} mutant animal; *Umod*^{C93F}: homozygous *Umod*^{C93F} mutant animal. Student's t-test with Bonferroni adjustment: p*: <0.01; **, <0.001; ***, <0.0001. §p<0.016 vs. matching genotype in 4-PBA treatment group; #p<0.01 vs. matching genotype in 4-PBA treatment group; \$p<0.001 vs. matching genotype in 4-PBA treatment group, Ψp<0.01 vs. matching genotype in placebo group.

In all treatment groups, the plasma triglyceride concentrations of homozygous *Umod*^{A227T} mutant and homozygous *Umod*^{C93F} mutant mice were significantly beneath those of wild-type controls by the age of 3 months and remained low in 4-month-old mutant animals, regardless of the treatment received (Figure 4.28).

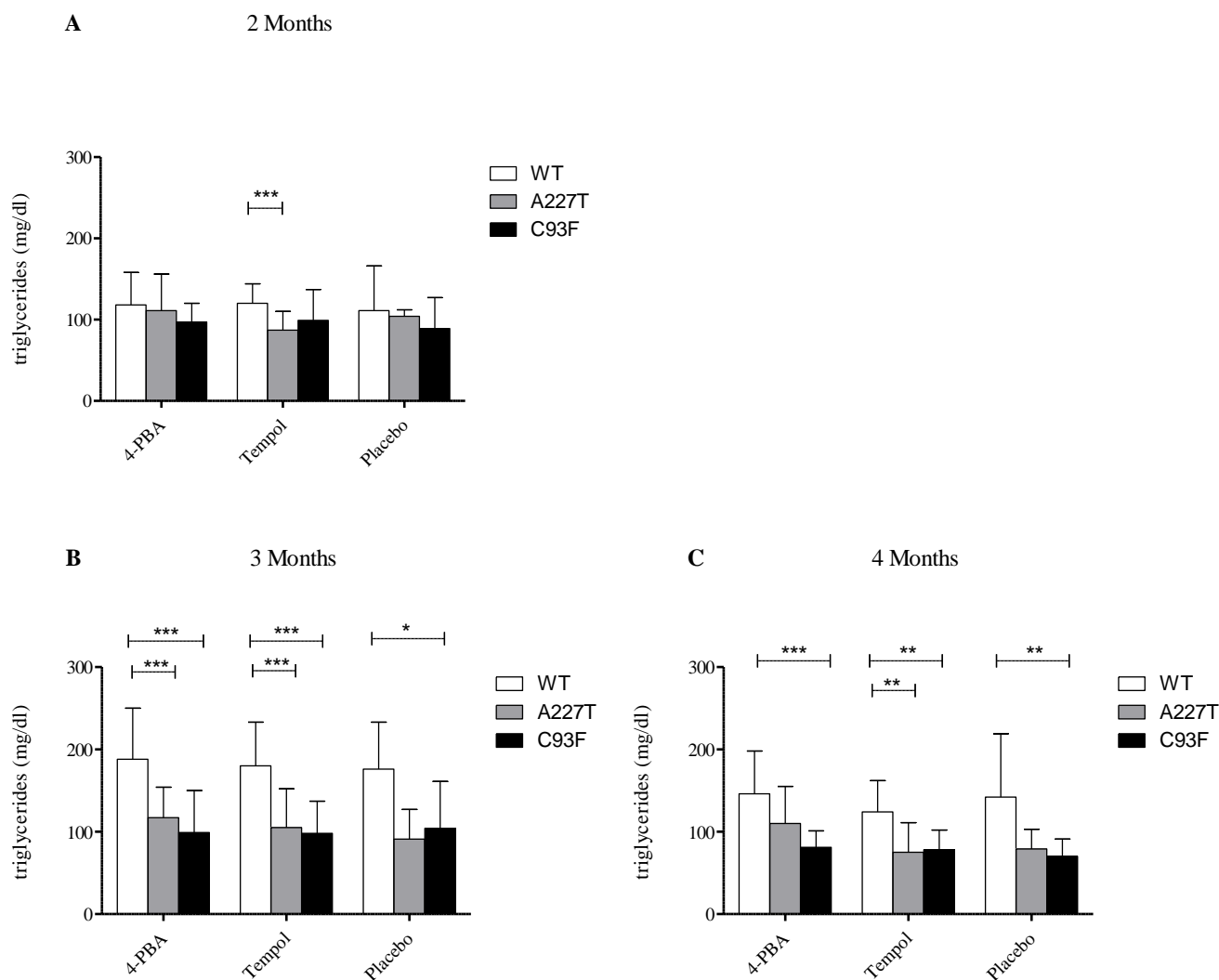


Figure 4.28: Plasma triglyceride levels of homozygous *Umod*^{A227T} and *Umod*^{C93F} mutant mice as well as of wild-type controls of the different treatment groups at the ages of (A) 2 months, (B) 3 months and (C) 4 months. In all treatment groups plasma triglyceride levels in homozygous mutant mice of both lines were significantly lower when compared to wild-type controls. Data represents mean \pm SD. n=13-19 wild-type mice, n=3-19 homozygous *Umod*^{A227T} mutant mice, n=8-13 homozygous *Umod*^{C93F} mutant mice; wt: wild-type animal; *Umod*^{A227T}: homozygous *Umod*^{A227T} mutant animal; *Umod*^{C93F}: homozygous *Umod*^{C93F} mutant animal. Student's t-test with Bonferroni adjustment: *, p<0.016; **, p<0.01; ***, p<0.001; ****p <0.0001.

Both Jaffe- and enzymatically measured plasma creatinine levels tended to be increased in homozygous *Umod*^{A227T} and *Umod*^{C93F} mutant mice at all times of measurement. After two months of treatment, 4-PBA-treated homozygous mutant mice of both lines showed significantly increased creatinine levels when compared to wild-type controls. Animals which had been given tempol or placebo showed no genotypic difference. After two months of treatment, creatinine levels did not differ significantly between genotype-matched mice of different treatment groups.

By the age of 4 months, plasma lipase activity was elevated in homozygous *Umod*^{C93F} mutant mice in the 4-PBA and placebo treatment group when compared to wild-type controls. The comparison of plasma lipase levels of genotype-matched mice receiving different treatments revealed no significant difference at this age.

In the tempol treatment group, 4-month-old homozygous mutant mice of both lines exhibited significantly higher plasma levels of α -amylase than wild-type controls. The same was detected for homozygous *Umod*^{C93F} mutant mice in the placebo treatment group and for homozygous *Umod*^{A227T} mutant mice in the 4-PBA treatment group. Compared to the other treatment groups, α -amylase concentrations of wild-type and homozygous *Umod*^{C93F} mutant mice were lowest in the 4-PBA treatment group.

	4-PBA					
	wt (n=19)	A227T (n=19)	C93F (n=11)	t-test		
				C93F vs A227T	C93F vs wt	A227T vs wt
Na (mmol/l)	149 ± 3	149 ± 3	149 ± 5			
K (mmol/l)	4.0 ± 0.4	4.2 ± 0.3	4.1 ± 0.2			
Ca (mmol/l)	2.4 ± 0.1	2.4 ± 0.1	2.4 ± 0.1			
Cl (mmol/l)	110 ± 2	110 ± 2	110 ± 4			
Pi (mmol/l)	2.6 ± 0.3	2.6 ± 0.4	2.4 ± 0.3			
Total protein (g/dl)	5.0 ± 0.3	4.8 ± 0.2	4.9 ± 0.2			*
Creatinine-J (mg/dl)	0.32 ± 0.05	0.33 ± 0.04	0.34 ± 0.02			
Creatinine-E (mg/dl)	0.10 ± 0.02	0.11 ± 0.02	0.10 ± 0.02			
Urea (mg/dl)	58 ± 6	84 ± 11	96 ± 17	****		****
Uric acid (mg/dl)	1.1 ± 0.5	1.0 ± 0.5	0.9 ± 0.5			
Cholesterol (mg/dl)	134 ± 10	126 ± 8	126 ± 8			
Triglycerides (mg/dl)	118 ± 40	111 ± 45	97 ± 23			
ALT (U/l)	27 ± 11	27 ± 7	36 ± 10	**		
AST (U/l)	43 ± 5	41 ± 5	48 ± 7	**		
Lipase (U/l)	53 ± 11	51 ± 11	55 ± 5			
Amylase (U/l)	515 ± 32	520 ± 55	532 ± 46			
	Tempol					
	wt (n=13)	A227T (n=17)	C93F (n=11)	t-test		
				C93F vs A227T	C93F vs wt	A227T vs wt
Na (mmol/l)	147 ± 3	148 ± 4	147 ± 4			
K (mmol/l)	4.0 ± 0.3	4.1 ± 0.3	3.8 ± 0.4			
Ca (mmol/l)	2.3 ± 0.1	2.3 ± 0.1	2.3 ± 0.1			
Cl (mmol/l)	110 ± 2	111 ± 2	110 ± 2			
Pi (mmol/l)	2.5 ± 0.4	2.5 ± 0.4	2.2 ± 0.2	*		
Total protein (g/dl)	4.9 ± 0.2	4.8 ± 0.2	4.9 ± 0.3			
Creatinine-J (mg/dl)	0.32 ± 0.03	0.31 ± 0.02	0.31 ± 0.02			
Creatinine-E (mg/dl)	0.10 ± 0.02	0.10 ± 0.02	0.09 ± 0.01			
Urea (mg/dl)	53 ± 6	76 ± 9	96 ± 8	****	****	****
Uric acid (mg/dl)	1.1 ± 0.7	0.8 ± 0.4	0.7 ± 0.2			
Cholesterol (mg/dl)	133 ± 10	128 ± 9	122 ± 7		**	
Triglycerides (mg/dl)	120 ± 24	87 ± 23	99 ± 38			***
ALT (U/l)	33 ± 10	35 ± 29	39 ± 23			
AST (U/l)	39 ± 6	39 ± 6	43 ± 7			
Lipase (U/l)	50 ± 9	56 ± 16	50 ± 5			
Amylase (U/l)	521 ± 50	524 ± 50	503 ± 30			
	Placebo ^{*)}					
	wt (n=14)	A227T (n=3)	C93F (n=8)	t-test		
				C93F vs A227T	C93F vs wt	A227T vs wt
Na (mmol/l)	148 ± 5	148 ± 2	148 ± 5			
K (mmol/l)	3.9 ± 0.3	4.5 ± 0.5	3.9 ± 0.4			
Ca (mmol/l)	2.3 ± 0.0	2.3 ± 0.0	2.3 ± 0.1			
Cl (mmol/l)	110 ± 2	108 ± 2	110 ± 3			
Pi (mmol/l)	2.6 ± 0.5	2.5 ± 0.3	2.3 ± 0.3			
Total protein (g/dl)	4.9 ± 0.3	4.7 ± 0.1	4.9 ± 0.3			
Creatinine-J (mg/dl)	0.29 ± 0.02	0.33 ± 0.01	0.33 ± 0.05			
Creatinine-E (mg/dl)	0.09 ± 0.02	0.11 ± 0.03	0.10 ± 0.02			
Urea (mg/dl)	58 ± 9	84 ± 26	98 ± 14	****		**
Uric acid (mg/dl)	0.8 ± 0.6	1.2 ± 1.2	0.8 ± 0.3			
Cholesterol (mg/dl)	129 ± 13	115 ± 17	122 ± 8			
Triglycerides (mg/dl)	111 ± 55	104 ± 8	89 ± 38			
ALT (U/l)	29 ± 9	57 ± 51	33 ± 10			
AST (U/l)	40 ± 3	44 ± 9	44 ± 4		*	
Lipase (U/l)	53 ± 10	57 ± 4	54 ± 12			
Amylase (U/l)	499 ± 31	518 ± 31	533 ± 76			

Treatment comparison								
4-PBA vs Placebo			Tempol vs Placebo			Tempol vs 4-PBA		
wt	A227T	C93F	wt	A227T	C93F	wt	A227T	C93F
								**
						**		

Table 4.2: Plasma clinical chemistry of homozygous *Umod*^{A227T} and *Umod*^{C93F} mutant mice and wild-type controls at the age of 2 months. Data presentation as means ± SD; SD: standard deviation. Student's t-test with Bonferroni adjustment: *, p<0.016; **, p<0.01; ***, p<0.001; ****p <0.0001. n: number of the animals analysed. A227T: homozygous *Umod*^{A227T} mutant mice, C93F: homozygous *Umod*^{C93F} mice wt: wild-type mice. *) 10 of the 35 mice in the placebo group were tested at the age of 4 months only.

	4-PBA					
	wt (n=19)	A227T (n=19)	C93F (n=11)	t-test		
				C93F vs A227T	C93F vs wt	A227T vs wt
Na (mmol/l)	153 ± 4	152 ± 3	150 ± 4			
K (mmol/l)	4.3 ± 0.5	4.2 ± 0.3	3.9 ± 0.3			
Ca (mmol/l)	2.3 ± 0.1	2.3 ± 0.1	2.3 ± 0.1			
Cl (mmol/l)	112 ± 4	113 ± 3	111 ± 2			
Pi (mmol/l)	2.2 ± 0.2	2.3 ± 0.3	2.2 ± 0.3			
Total protein (g/dl)	5.3 ± 0.3	5.2 ± 0.3	5.0 ± 0.2		*	
Creatinine-J (mg/dl)	0.31 ± 0.05	0.34 ± 0.03	0.35 ± 0.06		*	
Creatinine-E (mg/dl)	0.10 ± 0.02	0.11 ± 0.02	0.11 ± 0.01			**
Urea (mg/dl)	65 ± 5	103 ± 10	122 ± 19	***	****	****
Uric acid (mg/dl)	1.5 ± 1.2	1.1 ± 0.6	1.0 ± 0.6			
Cholesterol (mg/dl)	139 ± 11	126 ± 10	117 ± 8		****	***
Triglycerides (mg/dl)	188 ± 62	117 ± 37	99 ± 51		***	***
ALT (U/l)	35 ± 11	31 ± 7	32 ± 8			
AST (U/l)	48 ± 15	45 ± 6	50 ± 15			
Lipase (U/l)	49 ± 7	53 ± 7	54 ± 15			
Amylase (U/l)	515 ± 39	511 ± 47	512 ± 48			
	Tempol					
	wt (n=13)	A227T (n=17)	C93F (n=11)	t-test		
				C93F vs A227T	C93F vs wt	A227T vs wt
Na (mmol/l)	152 ± 3	153 ± 3	151 ± 3			
K (mmol/l)	4.1 ± 0.3	4.2 ± 0.3	4.0 ± 0.3			
Ca (mmol/l)	2.3 ± 0.1	2.3 ± 0.1	2.3 ± 0.1			
Cl (mmol/l)	110 ± 3	113 ± 2	111 ± 3			**
Pi (mmol/l)	2.1 ± 0.3	2.3 ± 0.3	1.9 ± 0.4			
Total protein (g/dl)	5.2 ± 0.20	5.0 ± 0.3	5.1 ± 0.3			
Creatinine-J (mg/dl)	0.30 ± 0.03	0.32 ± 0.02	0.31 ± 0.02			
Creatinine-E (mg/dl)	0.09 ± 0.02	0.11 ± 0.02	0.10 ± 0.02			
Urea (mg/dl)	58 ± 5	90 ± 12	113 ± 11	****	****	****
Uric acid (mg/dl)	1.5 ± 1.2	1.3 ± 0.7	1.8 ± 1.1			
Cholesterol (mg/dl)	141 ± 12	130 ± 12	133 ± 11			
Triglycerides (mg/dl)	180 ± 53	105 ± 47	98 ± 39		***	***
ALT (U/l)	35 ± 14	35 ± 37	35 ± 19			
AST (U/l)	40 ± 6	47 ± 35	43 ± 8			
Lipase (U/l)	50 ± 5	51 ± 10	54 ± 6			
Amylase (U/l)	521 ± 34	511 ± 51	515 ± 44			
	Placebo ^{*)}					
	wt (n=14)	A227T (n=3)	C93F (n=8)	t-test		
				C93F vs A227T	C93F vs wt	A227T vs wt
Na (mmol/l)	151 ± 3	149 ± 2	152 ± 1	*		
K (mmol/l)	4.1 ± 0.3	4.1 ± 0.1	4.0 ± 0.3			
Ca (mmol/l)	2.2 ± 0.1	2.3 ± 0.0	2.3 ± 0.1			
Cl (mmol/l)	110 ± 2	112 ± 1	111 ± 2			
Pi (mmol/l)	2.0 ± 0.3	2.1 ± 0.3	1.9 ± 0.4			
Total protein (g/dl)	5.1 ± 0.2	5.0 ± 0.1	5.1 ± 0.2			
Creatinine-J (mg/dl)	0.29 ± 0.02	0.29 ± 0.02	0.33 ± 0.06			
Creatinine-E (mg/dl)	0.09 ± 0.01	0.10 ± 0.01	0.10 ± 0.02			
Urea (mg/dl)	59 ± 5	102 ± 19	121 ± 13		****	****
Uric acid (mg/dl)	1.4 ± 1.0	0.4 ± 0.1	1.0 ± 0.7			
Cholesterol (mg/dl)	134 ± 9	125 ± 3	131 ± 6			
Triglycerides (mg/dl)	176 ± 57	91 ± 36	104 ± 57		*	
ALT (U/l)	33 ± 12	25 ± 7	38 ± 13			
AST (U/l)	40 ± 5	40 ± 5	40 ± 2			
Lipase (U/l)	52 ± 15	51 ± 14	49 ± 11			
Amylase (U/l)	514 ± 32	486 ± 35	514 ± 32			

Treatment comparison								
4-PBA vs Placebo			Tempol vs Placebo			Tempol vs 4-PBA		
wt	A227T	C93F	wt	A227T	C93F	wt	A227T	C93F
**								
	*						*	
*						**	**	
		***						***

Table 4.3: Plasma clinical chemistry of homozygous *Umod*^{A227T} and *Umod*^{C93F} mutant mice and wild-type controls at the age of 3 months. Data presentation as means ± SD; SD: standard deviation. Student's t-test with Bonferroni adjustment: *, p<0.016; **, p<0.01; ***, p<0.001; ****p <0.0001 n: number of the animals analysed. A227T: homozygous *Umod*^{A227T} mutant mice, C93F: homozygous *Umod*^{C93F} mutant mice. wt: wild-type mice. ALT: alanine aminotransferase; AST: aspartate aminotransferase. *) 10 of the 35 mice in the placebo group were tested at the age of 4 months only.

	4-PBA			t-test				
	wt (n=19)	A227T (n=19)	C93F (n=11)	C93F vs A227T	C93F vs wt	A227T vs wt		
	Na (mmol/l)	154 ± 4	156 ± 2	156 ± 1.9				
K (mmol/l)	3.9 ± 0.2	4.2 ± 0.3	4.0 ± 0.3			**		
Ca (mmol/l)	2.2 ± 0.1	2.3 ± 0.1	2.4 ± 0.1		***	****		
Cl (mmol/l)	114 ± 3	115 ± 2	116 ± 1	**	**			
Pi (mmol/l)	2.1 ± 0.3	1.9 ± 0.4	1.9 ± 0.3					
Total protein (g/dl)	5.1 ± 0.3	5.2 ± 0.2	5.3 ± 0.2					
Creatinine-J (mg/dl)	0.31 ± 0.03	0.34 ± 0.05	0.36 ± 0.05		**			
Creatinine-E (mg/dl)	0.09 ± 0.02	0.11 ± 0.02	0.11 ± 0.01		**	***		
Urea (mg/dl)	66 ± 8	123 ± 13	156 ± 18	****	****	****		
Uric acid (mg/dl)	0.9 ± 0.7	1.3 ± 0.6	0.9 ± 0.4					
Cholesterol (mg/dl)	124 ± 16	128 ± 9	134 ± 10					
Triglycerides (mg/dl)	146 ± 52	110 ± 45	81 ± 20		***			
ALT (U/l)	39 ± 24	43 ± 45	31 ± 5					
AST (U/l)	69 ± 49	72 ± 55	58 ± 8					
Lipase (U/l)	44 ± 8	50 ± 8	56 ± 5		***			
Amylase (U/l)	516 ± 73	577 ± 67	572 ± 26			*		
Tempol								
	wt (n=13)	A227T (n=17)	C93F (n=11)	t-test				
				C93F vs A227T	C93F vs wt	A227T vs wt		
Na (mmol/l)	157 ± 2	157 ± 3	157 ± 3					
K (mmol/l)	4.3 ± 1.1	4.1 ± 0.3	4.8 ± 1.6					
Ca (mmol/l)	2.3 ± 0.1	2.3 ± 0.0	2.4 ± 0.1					
Cl (mmol/l)	116 ± 2	115 ± 2	115 ± 2					
Pi (mmol/l)	2.3 ± 0.6	2.5 ± 0.5	2.5 ± 0.8					
Total protein (g/dl)	5.1 ± 0.2	5.2 ± 0.2	5.4 ± 0.2	**	**			
Creatinine-J (mg/dl)	0.31 ± 0.06	0.33 ± 0.04	0.36 ± 0.05					
Creatinine-E (mg/dl)	0.10 ± 0.02	0.11 ± 0.01	0.12 ± 0.02					
Urea (mg/dl)	60 ± 8	119 ± 23	140 ± 18	*	****	****		
Uric acid (mg/dl)	1.6 ± 1.3	1.2 ± 0.8	1.6 ± 1.1					
Cholesterol (mg/dl)	140 ± 6	142 ± 8	141 ± 11					
Triglycerides (mg/dl)	124 ± 38	75 ± 36	78 ± 24		**	**		
ALT (U/l)	35 ± 17	34 ± 13	34 ± 10					
AST (U/l)	59 ± 20	64 ± 21	113 ± 152					
Lipase (U/l)	47 ± 13	48 ± 10	53 ± 5					
Amylase (U/l)	559 ± 30	592 ± 33	610 ± 47		**	**		
Placebo [*]								
	wt (n=15)	A227T (n=6)	C93F (n=13)	t-test				
				C93F vs A227T	C93F vs wt	A227T vs wt		
Na (mmol/l)	147 ± 3	131 ± 7	156 ± 4					
K (mmol/l)	4.1 ± 0.3	4.4 ± 0.4	4.2 ± 0.6					
Ca (mmol/l)	2.3 ± 0.07	2.3 ± 0.2	2.4 ± 0.1					
Cl (mmol/l)	115 ± 1.9	112 ± 4	114 ± 4					
Pi (mmol/l)	2.4 ± 0.4	2.6 ± 0.7	2.3 ± 0.6					
Total protein (g/dl)	5.1 ± 0.2	5.0 ± 0.4	5.2 ± 0.2					
Creatinine-J (mg/dl)	1.25 ± 0.05	1.17 ± 0.05	0.35 ± 0.04					
Creatinine-E (mg/dl)	0.10 ± 0.02	0.11 ± 0.01	0.11 ± 0.02					
Urea (mg/dl)	58 ± 7	107 ± 14	139 ± 15		****	****		
Uric acid (mg/dl)	1.9 ± 0.5	1.9 ± 0.3	1.0 ± 0.6					
Cholesterol (mg/dl)	130 ± 16	114 ± 6	146 ± 10	**				
Triglycerides (mg/dl)	142 ± 77	79 ± 24	70 ± 21		**			
ALT (U/l)	31 ± 14	26 ± 9	28 ± 6					
AST (U/l)	56 ± 15	49 ± 5	66 ± 30					
Lipase (U/l)	46 ± 8	54 ± 6	56 ± 6		***			
Amylase (U/l)	578 ± 39	526 ± 50	642 ± 52		**			
Treatment comparison								
4-PBA vs Placebo		Tempol vs Placebo			Tempol vs 4-PBA			
wt	A227T	C93F	wt	A227T	C93F	wt	A227T	C93F
	*			**				
**			*			**		**
	**							***
			**		**	**	**	***
**	***							

Table 4.4: Plasma clinical chemistry of homozygous *Umod*^{A227T} and *Umod*^{C93F} mutant mice and wild-type controls at the age of 4 months. Data presentation as means ± SD; SD: standard deviation. Student's t-test with Bonferroni adjustment: *, p<0.016; **, p<0.01; ***, p<0.001; ****p <0.0001. n: number of the animals analysed. A227T: homozygous *Umod*^{A227T} mutant mice, C93F: homozygous *Umod*^{C93F} mutant mice wt: wild-type mice. ALT: alanine aminotransferase; AST: aspartate aminotransferase; *) 10 of the 35 mice in the placebo group were tested at the age of 4 months only. Due to a weight loss of >15 %, one homozygous *Umod*^{C93F} mutant mouse of the placebo group was excluded from the metabolic cage experiment

4.3.3 Metabolic cage analysis

After two months of treatment, metabolic cage analysis of the 4-month-old mice was carried out and data was collected every 24 hours over the course of two days. Corresponding to their respective treatment group, the application of 4-PBA, tempol or pure drinking water was continued (Table 4.5).

In all treatment groups homozygous *Umod*^{A227T} mutant and homozygous *Umod*^{C93F} mutant mice weighed significantly less than wild-type controls both at the start and throughout the metabolic cage experiment. Percent body weight change did not differ significantly between genotypes. Food intake per gram body weight did not vary between the three genotypes.

In both the 4-PBA and the tempol treatment group, the water intake per gram body weight tended to be highest in homozygous *Umod*^{C93F} mutant mice and lowest in wild-type controls. This trend reached a degree of significance only in the 4-PBA treatment group where homozygous *Umod*^{C93F} mutant mice showed a significantly higher water intake per gram body weight than wild-type controls ($p < 0.01$) on day 1.

Compared to wild-type controls, homozygous *Umod*^{A227T} mutant as well as homozygous *Umod*^{C93F} mutant mice excreted a significantly higher volume of urine per gram body weight in both the 4-PBA and the tempol treatment group (day 1 and 2). Urine volumes per gram body weight did not vary significantly between the different genotypes receiving placebo treatment (Figure 4.29 A).

On both days of the metabolic cage experiment, urine osmolality was significantly decreased in homozygous mutant mice of both lines in the 4-PBA and tempol treatment group. Urine osmolality was lowest in homozygous *Umod*^{C93F} mutant mice in both the 4-PBA and the tempol treatment group. In the placebo treatment group, the urine osmolality of wild-type and homozygous *Umod*^{A227T} mutant mice showed no significant difference. Homozygous *Umod*^{C93F} mutant mice showed a significantly reduced urine osmolality in this treatment group as well (Figure 4.29 B).

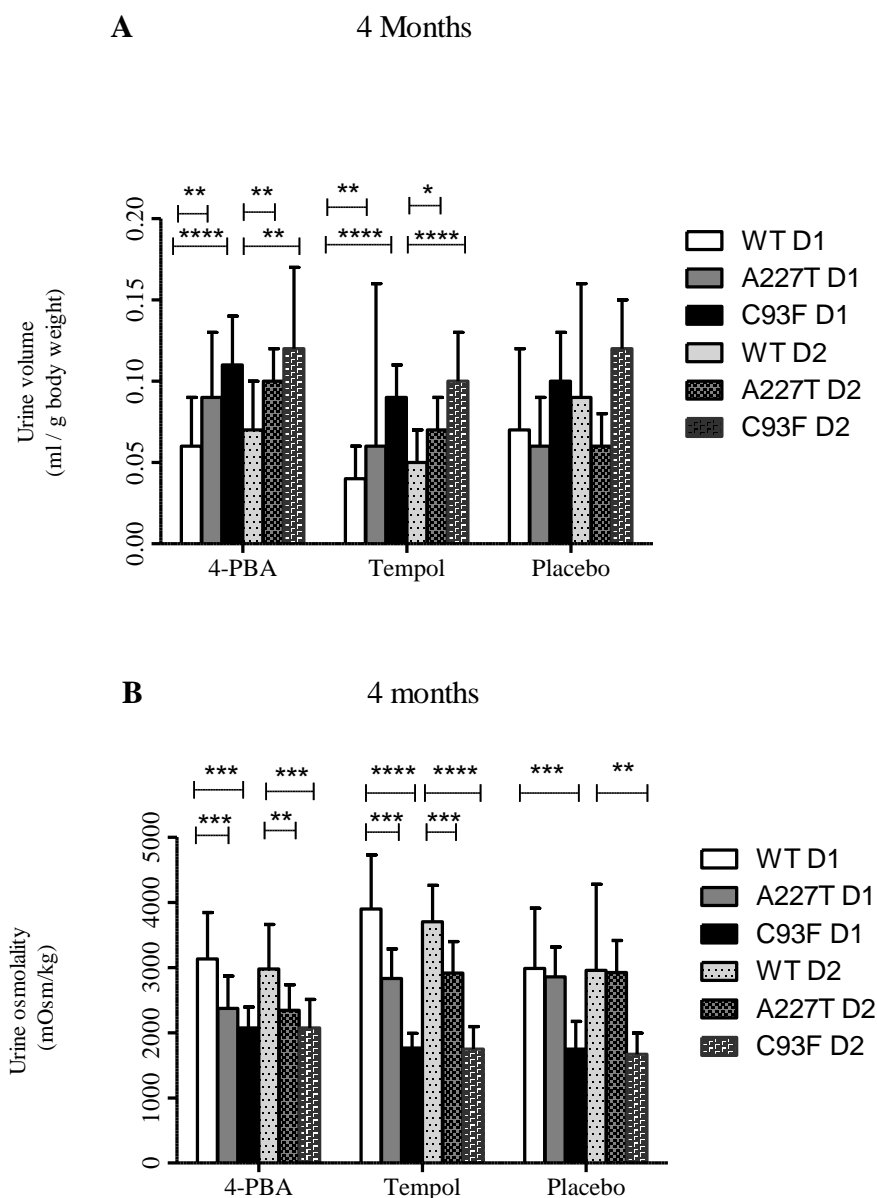


Figure 4.29: Urine volume and urine osmolality of 24h-urine of 4-month-old *Umod*^{A227T} and *Umod*^{C93F} mice. (A) In all treatment groups, homozygous *Umod*^{C93F} mutant mice excreted the highest volume of urine per gram body weight. (B) In the 4-PBA and tempol treatment group, urine osmolality was decreased significantly in homozygous mutant mice of both lines when compared to wild-type controls. In the placebo treatment group, urine osmolality was significantly reduced only in homozygous *Umod*^{C93F} mutant mice. wt: wild-type mice, A227T: homozygous *Umod*^{A227T} mutant mice, C93F: homozygous *Umod*^{C93F} mutant mice. D1: day 1 on the metabolic cage analysis. D2: day 2 of the metabolic cage analysis. Student's t-test with Bonferroni adjustment: *, p<0.016; **, p<0.01; ***, p<0.001; ****p <0.0001.

	Day	PBA				Tempol				Placebo						
		wt (n = 19)	A227T (n = 19)	t-test (A227T vs wt)	C93F (n = 11)	t-test (C93F vs wt)	wt (n = 13)	A227T (n = 17)	t-test (A227T vs wt)	C93F (n = 11)	t-test (C93F vs wt)	wt (n=15)	A227T (n = 6)	t-test (A227T vs wt)	C93F (n = 13)	t-test (C93F vs wt)
Body weight (g)	0	28.6 ± 2.5	25.0 ± 2.4	****	20.9 ± 1.5	****	29.4 ± 2.0	25.3 ± 1.7	****	23.8 ± 0.9	****	29.3 ± 1.7	25.8 ± 1.4	***	23.8 ± 1.9	****
	1	28.9 ± 2.1	25.4 ± 1.2	****	21.3 ± 1.3	****	29.3 ± 1.8	25.3 ± 1.5	****	23.7 ± 1.3	****	29.2 ± 1.7	25.9 ± 1.8	***	23.6 ± 1.9	****
	2	29.4 ± 2.1	25.9 ± 1.1	****	21.9 ± 0.9	****	28.9 ± 3.0	25.4 ± 1.5	***	24.1 ± 1.3	***	29.6 ± 1.5	26.3 ± 1.7	***	23.9 ± 1.9	****
Body weight change (%)	1	1.3 ± 2.8	1.6 ± 2.4		1.9 ± 2.4		- 0.2 ± 2.1	1.2 ± 2.3		- 0.5 ± 2.4		-0.5 ± 2.4	0.3 ± 2.7		- 0.8 ± 1.7	
	2	1.7 ± 2.0	2.0 ± 1.6		2.8 ± 3.1		-1.3 ± 9.0	0.6 ± 3.3		1.4 ± 2.1		1.5 ± 2.5	1.3 ± 1.7		1.4 ± 1.7	
Food intake (g/day)	1	4.4 ± 0.5	4.1 ± 0.6		3.5 ± 0.5	***	4.8 ± 0.5	4.2 ± 0.4	***	3.6 ± 0.3	****	4.4 ± 1.0	3.8 ± 0.7		3.3 ± 0.5	**
	2	4.5 ± 0.6	4.2 ± 0.4		3.7 ± 0.3	***	4.9 ± 0.5	4.1 ± 0.6	***	3.7 ± 0.2	****	4.5 ± 0.7	4.0 ± 0.6		3.6 ± 0.6	***
Food intake (g/g body weight)	1	0.16 ± 0.02	0.17 ± 0.03		0.17 ± 0.03		0.17 ± 0.02	0.17 ± 0.03		0.15 ± 0.01		0.15 ± 0.03	0.15 ± 0.02		0.14 ± 0.02	
	2	0.16 ± 0.03	0.17 ± 0.02		0.18 ± 0.02		0.17 ± 0.02	0.17 ± 0.03		0.16 ± 0.01		0.16 ± 0.02	0.15 ± 0.03		0.15 ± 0.02	
Water intake (g)	1	5.8 ± 2.2	6.7 ± 3.4		6.4 ± 1.6		8.7 ± 2.2	7.4 ± 1.7		8.6 ± 2.1		7.3 ± 5.7	4.8 ± 1.5		5.9 ± 1.8	
	2	6.6 ± 3.6	6.2 ± 1.6		6.1 ± 1.6		9.6 ± 3.0	8.1 ± 2.3		9.6 ± 2.9		10.4 ± 10.1	5.0 ± 1.0		7.3 ± 1.5	
Water intake (g/g body weight)	1	0.21 ± 0.09	0.27 ± 0.13		0.31 ± 0.08	**	0.30 ± 0.08	0.30 ± 0.07		0.36 ± 0.09		0.25 ± 0.19	0.18 ± 0.05		0.25 ± 0.07	
	2	0.24 ± 0.14	0.25 ± 0.07		0.29 ± 0.08		0.33 ± 0.11	0.32 ± 0.08		0.40 ± 0.13		0.35 ± 0.34	0.19 ± 0.03		0.31 ± 0.05	
Urine volume (ml)	1	1.6 ± 0.7	2.3 ± 1.1		2.2 ± 0.6		1.3 ± 0.5	1.6 ± 0.4		2.1 ± 0.4	***	2.0 ± 1.4	1.6 ± 0.7		2.4 ± 0.7	
	2	2.0 ± 0.9	2.4 ± 0.5		2.4 ± 0.9		1.4 ± 0.6	1.7 ± 0.5		2.5 ± 0.7	***	2.6 ± 2.0	1.7 ± 0.7		2.8 ± 0.7	
Urine volume (ml/g body weight)	1	0.06 ± 0.03	0.09 ± 0.04	**	0.11 ± 0.03	****	0.04 ± 0.02	0.06 ± 0.1	**	0.09 ± 0.02	****	0.07 ± 0.05	0.06 ± 0.03		0.10 ± 0.03	
	2	0.07 ± 0.03	0.10 ± 0.02	**	0.12 ± 0.05	**	0.05 ± 0.02	0.07 ± 0.02	*	0.10 ± 0.03	****	0.09 ± 0.07	0.06 ± 0.02		0.12 ± 0.03	
Urine osmolality (mOsm/kg)	1	3132 ± 713	2372 ± 496	***	2073 ± 322	***	3898 ± 831	2832 ± 453	***	1766 ± 222	****	2984 ± 928	2856 ± 458		1746 ± 428	***
	2	2979 ± 681	2345 ± 390	**	2073 ± 437	***	3702 ± 557	2914 ± 485	***	1747 ± 345	****	2956 ± 1319	2921 ± 494		1667 ± 327	**
Faeces excretion (g)	1	1.9 ± 0.4	1.7 ± 0.4		1.4 ± 0.3	***	2.1 ± 0.3	1.8 ± 0.2	**	1.7 ± 0.2	***	1.8 ± 0.4	1.3 ± 0.2	**	1.3 ± 0.3	***
	2	1.9 ± 0.4	1.7 ± 0.3		1.4 ± 0.3	***	2.1 ± 0.4	1.7 ± 0.3	**	1.6 ± 0.2	***	2.0 ± 0.3	1.4 ± 0.3	***	1.4 ± 0.3	****
Faeces excretion (g/g body weight)	1	0.07 ± 0.02	0.07 ± 0.02		0.07 ± 0.01		0.07 ± 0.02	0.07 ± 0.01		0.07 ± 0.01		0.06 ± 0.01	0.05 ± 0.01		0.05 ± 0.01	
	2	0.07 ± 0.01	0.07 ± 0.02		0.07 ± 0.01		0.07 ± 0.02	0.07 ± 0.01		0.07 ± 0.01		0.07 ± 0.01	0.06 ± 0.01		0.06 ± 0.01	*

Table 4.5: 24h-metabolic cage data of 4 month-old homozygous *Umod*^{A227T} and *Umod*^{C93F} mutant mice and wild-type controls. Data presentation as means ± SD; SD: standard deviation. Student's t-test, p<0.016, p<0.01, p<0.001 and p<0.0001. n: number of the animals analysed. A227T: homozygous *Umod*^{A227T} mutant mice. C93F: homozygous *Umod*^{C93F} mutant mice; wt: wild-type male mice.

4.3.4 Urine analysis

Western blot analysis was used to examine 24h-urine samples from the metabolic cage analysis for their respective uromodulin content. In addition, the 24h-urine collected in the metabolic cage experiment underwent clinical chemical analysis.

4.3.4.1 Western blot analysis of 24h-urine

Western blot analysis of uromodulin content in 24h-urine revealed that homozygous *Umod*^{C93F} mutant mice secreted a distinctly lower amount of the protein than both wild-type controls and homozygous *Umod*^{A227T} mutant mice, regardless of the treatment received. The urinary uromodulin content of homozygous *Umod*^{A227T} mutant mice also remained lower than that of wild-type controls after treatment application. Uromodulin appeared slightly reduced in the urine of 4-PBA-treated homozygous *Umod*^{A227T} mutant mice when compared to genotype-matched placebo-treated animals (Figure 4.30).

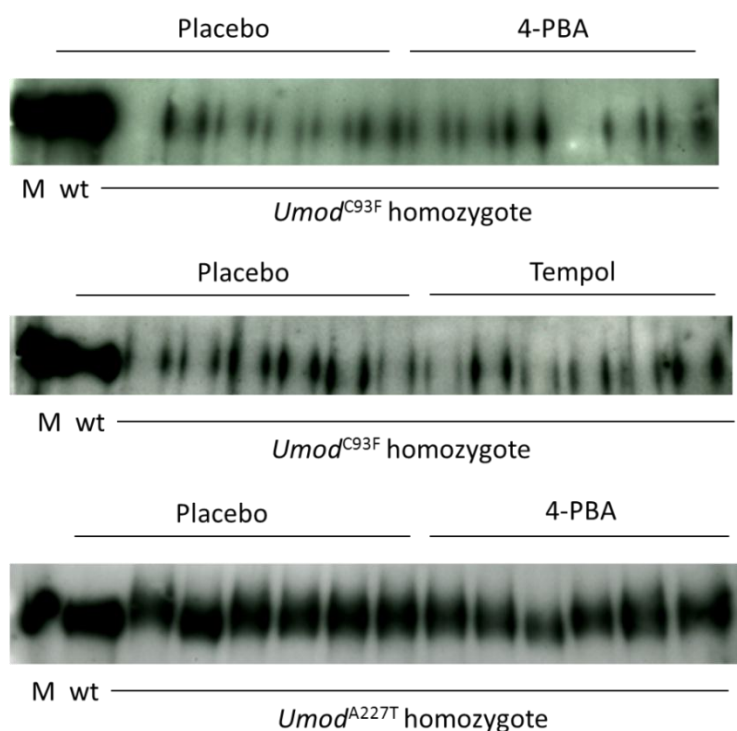


Figure 4.30: Western blot analysis of urinary uromodulin content in homozygous *Umod*^{C93F} mutant and homozygous *Umod*^{A227T} mutant mice compared to wild-type controls. Homozygous *Umod*^{C93F} mutant mice treated with (A) 4-PBA and (B) tempol excreted similarly low amounts of uromodulin as homozygous *Umod*^{C93F} mutant mice of the placebo treatment group. (C) Compared to homozygous *Umod*^{C93F} mutant mice, a distinctly higher urinary uromodulin content was detected in homozygous *Umod*^{A227T} mutant mice of both the 4-PBA and placebo treatment group but did not reach wild-type levels. M: MBI unstained protein marker; wt: wild-type.

4.3.4.2 Clinical chemistry of 24h-urine

24h-urine was collected on day 1 and 2 of the metabolic cage analysis for clinical chemical analysis. Urine parameters were standardized to 25 grams of body weight and compared between homozygous mutant mice of both lines and wild-type controls as well as between genotype-matched mice of the three treatment groups (Tables 4.6 and 4.7).

Placebo treatment group:

Compared to wild-type mice in this treatment group, urinary calcium excretion tended to be higher in homozygous *Umod*^{A227T} mutant and homozygous *Umod*^{C93F} mutant mice but this difference reached a degree of significance on day 1 only.

On both days, uric acid excretion tended to be highest in wild-type mice and lowest in homozygous *Umod*^{A227T} mutant mice but differences did not reach a degree of significance.

On both day 1 and 2, the total urinary protein excretion was significantly lower in mutants of both mouse lines than in wild-type controls, with homozygous *Umod*^{C93F} mutant mice excreting the least amount of protein.

On day 2, urinary albumin excretion of homozygous *Umod*^{A227T} mutant mice was significantly reduced versus wild-type controls and homozygous *Umod*^{C93F} mutant mice. On both days, the urinary albumin concentrations were lowest in homozygous *Umod*^{A227T} mutant and highest in wild-type mice.

4-PBA treatment group:

Urinary sodium excretion in this treatment group tended to be lowest in wild-type and highest in homozygous *Umod*^{C93F} mutant mice on both days of the metabolic cage analysis. On day 1 the difference in sodium excretion was significant between homozygous *Umod*^{C93F} mutant mice and wild-type controls. Compared to genotype-matched mice of the other treatment groups, 4-PBA-treated homozygous *Umod*^{C93F} mutant and homozygous *Umod*^{A227T} mutant mice exhibited the highest urinary sodium excretions.

On both days of analysis, urinary potassium excretion was significantly increased in *Umod*^{C93F} mutant mice when compared to wild-type controls. While potassium excretion was lowest in homozygous *Umod*^{A227T} mutant mice on day 1, the least amount of potassium was excreted by wild-type mice on day 2.

On both days of the metabolic cage analysis, homozygous mutant mice of both mouse lines showed a significantly increased urinary calcium excretion when compared to wild-type controls. Homozygous *Umod*^{C93F} mutant mice excreted the highest amount of calcium on day 1 and 2. On both days homozygous *Umod*^{C93F} mutant mice receiving 4-PBA also exhibited significantly increased urinary calcium concentrations when compared to genotype-matched mice in the placebo treatment group.

Urinary urea excretions were significantly elevated in homozygous *Umod*^{A227T} mutant and homozygous *Umod*^{C93F} mutant mice on day 1. On day 2, the same tendency was detected but urinary urea excretions did not differ significantly between the different genotypes. Urinary urea excretion of 4-PBA-treated homozygous *Umod* mutant mice of both lines tended to be higher when compared to genotype-matched mice in the tempol and placebo treatment groups.

Phosphate concentrations in the urine of homozygous *Umod*^{C93F} mutant mice of both lines were significantly lower than those of wild-type controls on both days of analysis.

Urinary excretion of enzymatically measured creatinine was significantly increased in homozygous *Umod*^{C93F} mutant mice of both lines on day 2. On both days of analysis, creatinine measured by the enzymatic and the Jaffe method tended to be increased in *Umod* mutant mice of both lines.

Tempol treatment group:

Urinary sodium excretion did not differ between genotypes within the tempol treatment group. However, urinary sodium excretion of homozygous *Umod* mutant and wild-type mice receiving tempol was significantly lower than those of 4-PBA-treated genotype-matched mice.

Urinary potassium excretion was lowest in wild-type mice on day 1 and 2. Compared to wild-type controls, potassium excretion was significantly increased in homozygous *Umod*^{A227T} mutant mice on day 1 and in homozygous *Umod*^{C93F} mutant mice on day 2 of analysis.

Homozygous mutant mice of both lines showed a significantly higher urinary calcium excretion on both days of the metabolic cage analysis when compared to wild-type controls. Compared to wild-type and homozygous *Umod*^{C93F} mutant mice in the 4-PBA treatment group, urinary calcium excretion of genotype-matched mice was significantly reduced in the tempol treatment group.

Total protein was decreased in the urine of both homozygous *Umod*^{A227T} mutant and homozygous *Umod*^{C93F} mutant mice versus wild-type controls. The difference between homozygous *Umod*^{C93F} mutant and wild-type mice was significant on both days of analysis.

Compared to wild-type controls, urinary magnesium excretion on day 2 was significantly increased in homozygous *Umod*^{C93F} mutant mice and significantly reduced in homozygous *Umod*^{A227T} mutant mice.

Homozygous *Umod*^{C93F} mutant mice showed an increased urinary glucose excretion when compared to wild-type mice on day 2 of analysis.

	PBA					
	wt (n=19)	A227T (n=19)	C93F (n=11)	t-test		
				C93F vs A227T	C93F vs wt	A227T vs wt
Urine volume (ml)	1.6 ± 0.7	2.3 ± 1.1	2.2 ± 0.6			
Urine osmolality (mOsm/kg)	3132 ± 713	2372 ± 496	2073 ± 322	***	***	
Na (µmol/day)	325 ± 91	340 ± 112	426 ± 115		*	
K (µmol/day)	497 ± 130	387 ± 194	702 ± 169	***		***
Ca (µmol/day)	3.1 ± 1.1	9.8 ± 5.5	10.3 ± 4.4	****		****
Cl (µmol/day)	462 ± 112	515 ± 118	517 ± 127			
Creatinine-J (µmol/day)	5.7 ± 1.7	7.5 ± 1.8	7.3 ± 2.4			**
Urea (mmol/day)	2.5 ± 0.6	3.1 ± 0.7	3.2 ± 0.5		**	**
Uric acid (nmol/day)	205 ± 157	133 ± 101	140 ± 45			
Total protein (µg/day)	14750 ± 3801	12401 ± 3375	6993 ± 2637	***	****	
Glucose (µmol/day)	4.5 ± 5.8	4.0 ± 1.8	4.0 ± 2.0			
Microalbumin (µg/day)	19.2 ± 4.8	19.1 ± 6.5	20.5 ± 5.5			
Mg (µmol/day)	36 ± 13	45 ± 18	49 ± 25			
Pi (µmol/day)	127 ± 58	86 ± 51	53 ± 62		**	
Creatinine-E (µmol/day)	3.0 ± 0.7	3.7 ± 1.0	3.7 ± 0.9			
	Tempol					
	wt (n=13)	A227T (n=17)	C93F (n=11)	t-test		
				C93F vs A227T	C93F vs wt	A227T vs wt
Urine volume (ml)	1.3 ± 0.5	1.6 ± 0.4	2.1 ± 0.4	**	***	
Urine osmolality (mOsm/kg)	3898 ± 831	2832 ± 453	1766 ± 222	***	***	
Na (µmol/day)	264 ± 66	301 ± 69	260 ± 56			
K (µmol/day)	445 ± 146	561 ± 103	530 ± 101			*
Ca (µmol/day)	2.1 ± 0.6	8.0 ± 2.6	6.2 ± 1.6		****	****
Cl (µmol/day)	470 ± 112	491 ± 96	412 ± 85			
Creatinine-J (µmol/day)	5.1 ± 1.9	6.6 ± 1.5	6.3 ± 1.6			
Urea (mmol/day)	2.4 ± 0.7	2.7 ± 0.4	2.4 ± 0.4			
Uric acid (nmol/day)	117 ± 76	90 ± 41	91 ± 32			
Total protein (µg/day)	13935 ± 4393	11424 ± 3080	8117 ± 2340	**	***	
Glucose (µmol/day)	2.6 ± 0.7	3.4 ± 1.4	4.8 ± 3.6			
Microalbumin (µg/day)	19.0 ± 6.7	16.7 ± 3.6	15.4 ± 4.3			
Mg (µmol/day)	25 ± 12	45 ± 13	40 ± 14			
Pi (µmol/day)	137 ± 58	131 ± 54	122 ± 65			
Creatinine-E (µmol/day)	2.3 ± 0.5	2.9 ± 0.5	3.1 ± 0.4			
	Placebo					
	wt (n=15)	A227T (n=6)	C93F (n=13)	t-test		
				C93F vs A227T	C93F vs wt	A227T vs wt
Urine volume (ml)	2.0 ± 1.4	1.6 ± 0.7	2.4 ± 0.7			
Urine osmolality (mOsm/kg)	2984 ± 928	2856 ± 458	1746 ± 428	***	***	
Na (µmol/day)	279 ± 99	279 ± 78	291.5 ± 53.1			
K (µmol/day)	517 ± 202	485 ± 167	594 ± 139			
Ca (µmol/day)	3.5 ± 2.6	6.7 ± 1.9	6.4 ± 1.9		**	*
Cl (µmol/day)	466 ± 139	431 ± 116	450 ± 77			
Creatinine-J (µmol/day)	5.7 ± 1.7	5.8 ± 1.3	6.1 ± 1.2			
Urea (mmol/day)	2.6 ± 0.7	2.6 ± 0.7	2.7 ± 0.5			
Uric acid (nmol/day)	298 ± 250	96 ± 34	134 ± 54			
Total protein (µg/day)	16522 ± 5358	10257 ± 3101	9257 ± 2964		***	*
Glucose (µmol/day)	3.2 ± 1.0	2.5 ± 0.6	3.3 ± 1.7			
Microalbumin (µg/day)	18.5 ± 6.1	13.2 ± 2.8	18.2 ± 3.7	**		
Mg (µmol/day)	34 ± 12	49 ± 37	43 ± 13			
Pi (µmol/day)	124 ± 37	113 ± 45	96 ± 42			
Creatinine-E (µmol/day)	3.0 ± 1.0	3.0 ± 0.6	3.5 ± 0.8			

Treatment comparison								
PBA vs Placebo			Tempol vs Placebo			Tempol vs PBA		
wt	A227T	C93F	wt	A227T	C93F	wt	A227T	C93F
		**				**	***	
						**	**	
	**					**	**	

								**
			**				*	
			**	**		**	**	**

Table 4.6: Clinical chemistry of 24h-urine from 4 month-old homozygous *Umod*^{A227T} mutant and homozygous *Umod*^{C93F} mutant mice and wild-type controls, day 1. Urine parameters are normalized to 25 g body weight and presented as means ± SD; SD: standard deviation. Student's t-test with Bonferroni adjustment: *, p<0.016; **, p<0.01; ***, p<0.001; ****p <0.0001. n: number of the animals analysed. A227T: homozygous *Umod*^{A227T} mutant mice. C93F: homozygous *Umod*^{C93F} mutant mice; wt: wild-type mice.

	PBA					
	wt (n=19)	A227T (n=19)	C93F (n=11)	t-test		
				C93F vs A227T	C93F vs wt	A227T vs wt
Urine volume (ml)	2.0 ± 0.9	2.4 ± 0.4	2.4 ± 0.9			
Urine osmolality (mOsm/kg)	2979 ± 681	2345 ± 390	2073 ± 437	***		**
Na (µmol/day)	368 ± 88	420 ± 90	456 ± 103			
K (µmol/day)	592 ± 137	692 ± 141	758 ± 178	**		
Ca (µmol/day)	3.8 ± 1.9	10.0 ± 3.6	11.3 ± 4.2	****		****
Cl (µmol/day)	513 ± 119	538 ± 561	546 ± 105			
Creatinine-J (µmol/day)	6.2 ± 2.1	7.2 ± 1.9	7.8 ± 1.9			
Urea (mmol/day)	2.8 ± 0.6	3.1 ± 0.6	3.3 ± 0.5			
Uric acid (nmol/day)	197 ± 113	146 ± 56	177 ± 111			
Total protein (µg/day)	17134 ± 4228	12626 ± 2375	7412 ± 2526	****	****	**
Glucose (µmol/day)	3.5 ± 1.3	3.8 ± 2.1	3.7 ± 3.3			
Microalbumin (µg/day)	19.2 ± 4.3	17.8 ± 4.1	20.9 ± 5.5			
Mg (µmol/day)	41 ± 24	40 ± 21	52 ± 19			
Pi (µmol/day)	103 ± 62	62 ± 46	22 ± 34		***	
Creatinine-E (µmol/day)	3.1 ± 0.5	3.6 ± 0.8	3.8 ± 0.5		***	
	Tempol					
	wt (n=13)	A227T (n=17)	C93F (n=11)	t-test		
				C93F vs A227T	C93F vs wt	A227T vs wt
Urine volume (ml)	1.4 ± 0.6	1.7 ± 0.5	2.5 ± 0.7	***	****	*
Urine osmolality (mOsm/kg)	3702 ± 557	2914 ± 485	1747 ± 345	****	****	***
Na (µmol/day)	271 ± 85	299 ± 68	305 ± 54			
K (µmol/day)	462 ± 156	563 ± 128	649 ± 138		**	
Ca (µmol/day)	2.3 ± 0.9	7.9 ± 2.6	8.1 ± 2.7		****	****
Cl (µmol/day)	478 ± 139	494 ± 102	499 ± 97			
Creatinine-J (µmol/day)	5.4 ± 2.0	6.6 ± 2.0	7.3 ± 2.0			
Urea (mmol/day)	2.4 ± 0.8	2.7 ± 0.6	2.9 ± 0.4			
Uric acid (nmol/day)	133 ± 54	94 ± 38	102 ± 47			
Total protein (µg/day)	14008 ± 4754	11916 ± 2863	9558 ± 2365		*	
Glucose (µmol/day)	2.8 ± 0.9	3.6 ± 2.7	4.3 ± 1.4		**	
Microalbumin (µg/day)	18.6 ± 5.8	16.0 ± 3.6	16.7 ± 3.9			
Mg (µmol/day)	26 ± 15	16.0 ± 3.6	48 ± 17		**	**
Pi (µmol/day)	136 ± 60	113 ± 62	115 ± 58			
Creatinine-E (µmol/day)	2.5 ± 0.7	2.9 ± 0.5	3.1 ± 0.4			
	Placebo ^{a)}					
	wt (n=15)	A227T (n=6)	C93F (n=13)	t-test		
				C93F vs A227T	C93F vs wt	A227T vs wt
Urine volume (ml)	2.6 ± 2.0	1.7 ± 0.7	2.8 ± 0.8	**		
Urine osmolality (mOsm/kg)	2956 ± 1319	2921 ± 494	1667 ± 327	****	**	
Na (µmol/day)	345 ± 199	302 ± 58	318 ± 50			
K (µmol/day)	626 ± 306	529 ± 156	662 ± 84			
Ca (µmol/day)	5.8 ± 6.6	8.1 ± 1.7	7.8 ± 2.3			
Cl (µmol/day)	569 ± 242	472 ± 92	492 ± 58			
Creatinine-J (µmol/day)	7.2 ± 4.6	6.2 ± 0.9	6.6 ± 0.7			
Urea (mmol/day)	3.0 ± 1.2	2.7 ± 0.6	3.0 ± 0.4			
Uric acid (nmol/day)	279 ± 244	97 ± 35	142 ± 60			
Total protein (µg/day)	19144 ± 5051	11241 ± 3278	9938 ± 2553		****	**
Glucose (µmol/day)	3.7 ± 1.8	2.4 ± 0.5	3.4 ± 1.6			
Microalbumin (µg/day)	22.4 ± 7.4	13.4 ± 3.1	17.7 ± 2.6	**		*
Mg (µmol/day)	46 ± 17	42 ± 16	47 ± 15			
Pi (µmol/day)	148 ± 48	100 ± 66	110 ± 60			
Creatinine-E (µmol/day)	3.3 ± 1.1	3.1 ± 0.5	3.7 ± 0.6			

Treatment comparison								
PBA vs Placebo			Tempol vs Placebo			Tempol vs PBA		
wt	A227T	C93F	wt	A227T	C93F	wt	A227T	C93F
**	***					**	***	***
		*					**	
								**
			*					
			**					
***						**	**	***
					**	**	**	**

Table 4.7: Clinical chemistry of 24h-urine from 4 month-old homozygous *Umod*^{A227T} mutant and homozygous *Umod*^{C93F} mutant mice and wild-type controls, day 2. Urine parameters are normalized to 25 g body weight and presented as means ± SD; SD: standard deviation. Student's t-test with Bonferroni adjustment: *, p<0.016; **, p<0.01; ***, p<0.001; ****, p<0.0001. n: number of the animals analysed. A227T: homozygous *Umod*^{A227T} mutant mice. C93F: homozygous *Umod*^{C93F} mutant mice; wt: wild-type mice.

4.3.4.3 Fractional excretion of urinary solutes

The fractional excretions (FE) of sodium (FE_{Na}), potassium (FE_K), urea (FE_{urea}), uric acid ($FE_{(uric\ acid)}$), chloride (FE_{Cl}), calcium (FE_{Ca}), potassium (Fe_K) and phosphate (FE_{Pi}) were evaluated in 24h-urine of day 2 of the metabolic cage analysis and compared between genotypes and treatment groups (Table 4.8).

In all three treatment groups, FE_{urea} was highest in wild-type and lowest in homozygous *Umod*^{C93F} mutant mice. The difference between mutant mice of both lines and wild-type controls was significant in all treatment groups. FE_{urea} did not differ between genotype-matched mice of different treatment groups (Figure 4.31 A).

In both the 4-PBA and the placebo treatment group $FE_{(uric\ acid)}$ was significantly decreased in homozygous *Umod*^{A227T} mutant mice when compared to wild-type controls. Genotypic differences remained insignificant otherwise but wild-type mice tended to show the highest $FE_{(uric\ acid)}$ in each treatment group (Figure 4.31 B).

There was no genotypic difference of FE_{Na} in any of the treatment groups. However, FE_{Na} was significantly increased in homozygous *Umod*^{C93F} mutant mice of the 4-PBA treatment group when compared to genotype-matched placebo-treated animals. FE_{Na} of homozygous *Umod*^{A227T} mutant and homozygous *Umod*^{C93F} mutant mice in the 4-PBA treatment group was also significantly higher than that of the corresponding genotypes in the tempol treatment group (Figure 4.31 C).

In each treatment group, FE_{Ca} was significantly increased in homozygous mutant mice of both lines when compared to wild-type mice. A comparison of genotype-matched mice receiving different treatments revealed no difference (Figure 4.31 D).

While the lowest FE_K was detected in wild-type mice in each treatment group, it was increased to a degree of significance only in homozygous *Umod*^{C93F} mutant mice of the placebo treatment group.

FE_{Pi} was significantly reduced in homozygous *Umod*^{C93F} mutant mice of the 4-PBA and the placebo treatment group. The same was detected for homozygous *Umod*^{A227T} mutant mice in the

placebo treatment group. 4-PBA-treated homozygous *Umod*^{C93F} mutant mice also showed a lower FE_{Pi} than genotype-matched mice in the tempol and placebo treatment groups.

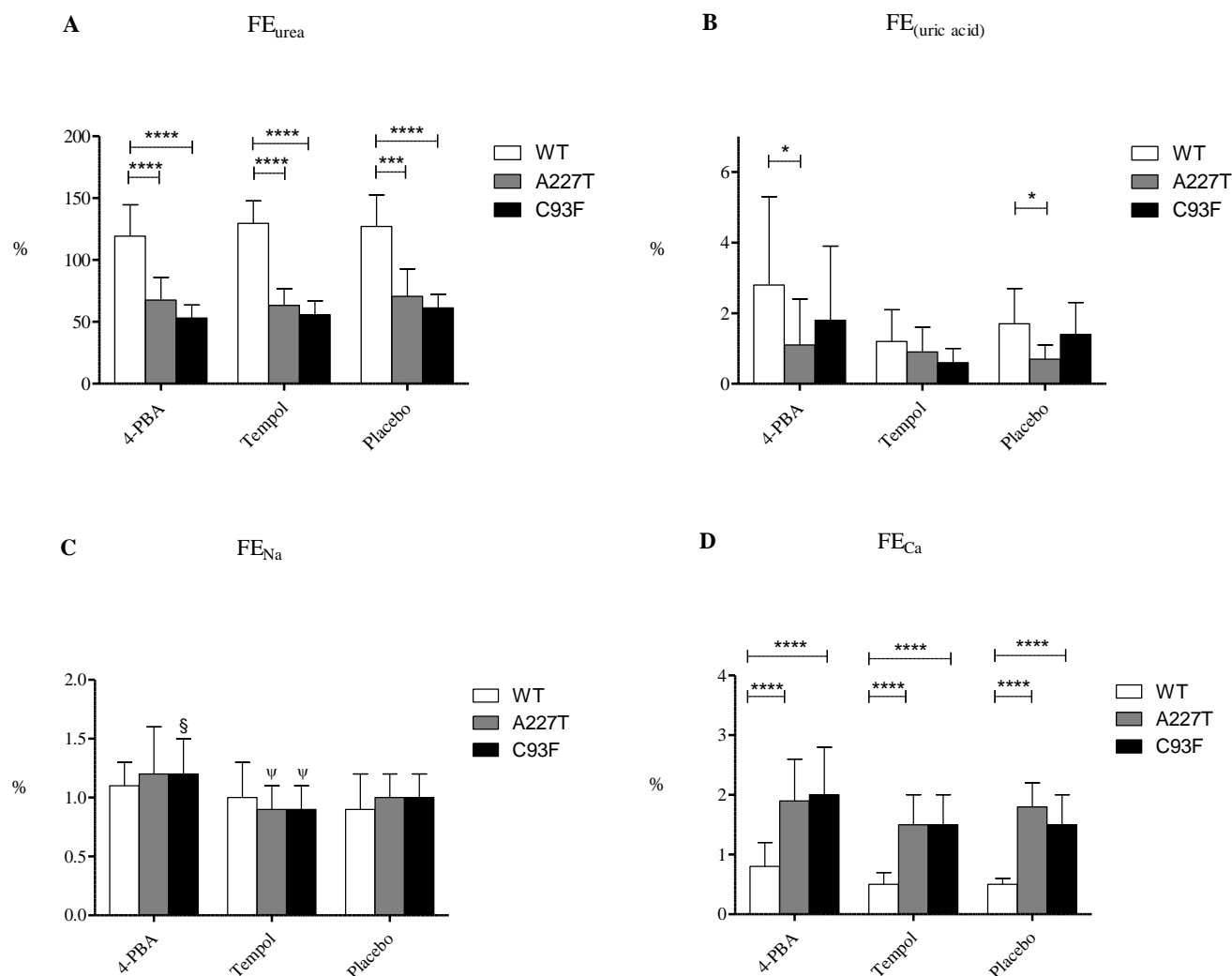


Figure 4.31: Fractional excretion (FE) of (A) urea, (B) uric acid, (C) sodium, and (D) calcium in the urine of homozygous *Umod*^{A227T} mutant and homozygous *Umod*^{C93F} mutant mice as well as of wild-type controls of different treatment groups. While FE_{urea} and $FE_{\text{(Uric acid)}}$ were significantly increased in wild-type mice of all treatment groups, genotypic differences in FE_{Na} remained insignificant. The fractional excretion of calcium was significantly increased in homozygous mutant animals of both mouse lines. Data represents mean \pm SD. n=13-19 wild-type mice, n=3-19 homozygous *Umod*^{A227T} mutant mice, n=8-13 homozygous *Umod*^{C93F} mutant; wt: wild-type mice; *Umod*^{A227T}: homozygous *Umod*^{A227T} mutant mice; *Umod*^{C93F}: homozygous *Umod*^{C93F} mutant mice. Student's t-test with Bonferroni adjustment: *, $p < 0.016$; **, $p < 0.01$; ***, $p < 0.001$; ****, $p < 0.0001$. § $p < 0.016$ vs. matching genotype in placebo treatment group; $\psi p < 0.01$ vs. matching genotype in 4-PBA treatment group.

Fractional excretion	PBA					
	wt (n=19)	A227T (n=19)	C93F (n=11)	t-test		
				C93F vs A227T	C93F vs wt	A227T vs wt
Na (%)	1.1 ± 0.2	1.2 ± 0.4	1.2 ± 0.3			
K (%)	69.3 ± 14.2	74.3 ± 24.1	78.4 ± 18.0			
Urea (%)	119.2 ± 25.3	67.5 ± 18.4	53.1 ± 10.5		****	****
Uric acid (%)	2.8 ± 2.5	1.1 ± 1.3	1.8 ± 2.1			*
Cl (%)	2.1 ± 0.4	2.1 ± 0.5	1.9 ± 0.4			
Ca (%)	0.8 ± 0.4	1.9 ± 0.7	2.0 ± 0.8		****	****
Pi (%)	23.8 ± 16.5	16.2 ± 15.9	4.7 ± 6.9		**	
Fractional excretion	Tempol					
	wt (n=13)	A227T (n=17)	C93F (n=11)	t-test		
				C93F vs A227T	C93F vs wt	A227T vs wt
Na (%)	1.0 ± 0.3	0.9 ± 0.2	0.9 ± 0.2			
K (%)	58.3 ± 15.1	61.2 ± 10.3	63.7 ± 18.9			
Urea (%)	129.6 ± 18.1	63.3 ± 13.4	55.7 ± 11.2		****	****
Uric acid (%)	1.2 ± 0.9	0.9 ± 0.7	0.6 ± 0.4			
Cl (%)	2.3 ± 0.7	2.0 ± 0.5	1.9 ± 0.4			
Ca (%)	0.5 ± 0.2	1.5 ± 0.5	1.5 ± 0.5		****	****
Pi (%)	35.3 ± 17.5	23.6 ± 17.2	23.7 ± 17.5			
Fractional excretion	Placebo ^{*)}					
	wt (n=15)	A227T (n=6)	C93F (n=13)	t-test		
				C93F vs A227T	C93F vs wt	A227T vs wt
Na (%)	0.9 ± 0.3	1.0 ± 0.2	1.0 ± 0.2			
K (%)	57.9 ± 11.6	66.2 ± 20.7	74.9 ± 15.7		**	
Urea (%)	127.0 ± 25.6	70.6 ± 22.2	61.3 ± 10.8		****	***
Uric acid (%)	1.7 ± 1.0	0.7 ± 0.4	1.4 ± 0.9			*
Cl (%)	2.2 ± 0.6	2.2 ± 0.4	2.0 ± 0.4			
Ca (%)	0.5 ± 0.1	1.8 ± 0.4	1.5 ± 0.5		****	****
Pi (%)	33.9 ± 8.2	18.8 ± 10.4	22.1 ± 10.2		**	**

	Treatment comparison								
	PBA vs Placebo			Tempol vs Placebo			Tempol vs PBA		
	wt	A227T	C93F	wt	A227T	C93F	wt	A227T	C93F
Na (%)			*				**	**	
K (%)									
Urea (%)									
Uric acid (%)									
Cl (%)									
Ca (%)									
Pi (%)			***						**

Table 4.8: Fractional excretion of urine parameters of 24h-urine from 4-month-old A227T and C93F homozygotes and wild-type controls, day 2. Fractional excretions are presented as means ± SD; SD: standard deviation. Student's t-test with Bonferroni adjustment: *, p<0.016; **, p<0.01; ***, p<0.001; ****, p<0.0001. n: number of the animals analysed. A227T: homozygous *Umod*^{A227T} mutant mice. C93F: homozygous *Umod*^{C93F} mutant male mice; wt: wild-type male mice. *) Due to a weight loss of >15 %, one mouse of the placebo group was excluded from the metabolic cage experiment.

4.3.5 Histopathology

4.3.5.1 Light microscopic analysis

Uromodulin accumulation in perinuclear clusters was demonstrated by immunohistochemical analysis in TALH cells of homozygous *Umod*^{C93F} mutant and homozygous *Umod*^{A227T} mutant mice after both 4-PBA and tempol treatment. In contrast, TALH cells of wild-type controls exhibited a diffuse cytosolic distribution pattern of uromodulin with an apically reinforced signal. Renal histology of mutants from both lines and treatment groups showed no further alterations compared to wild-type controls (Figure 4.32).

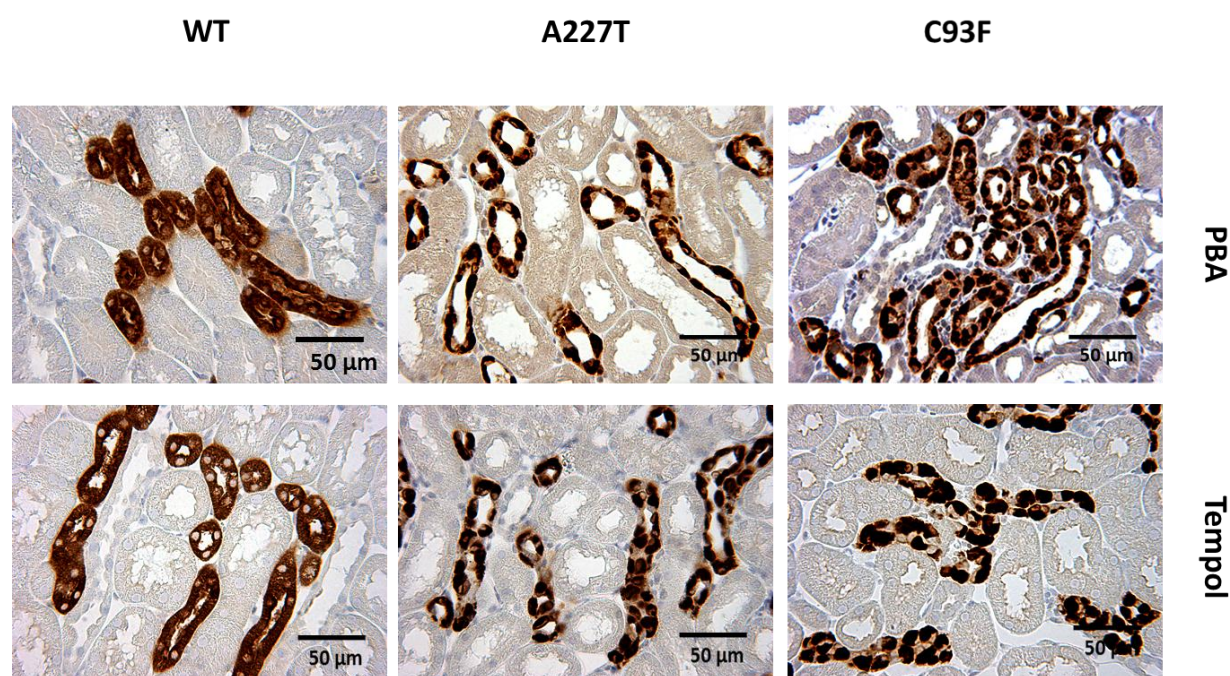


Figure 4.32: TALH cells of wild-type, homozygous *Umod*^{A227T} mutant and homozygous *Umod*^{C93F} mutant mice of the 4-PBA and of the tempol treatment group: Representative TALH profiles of the indicated genotype and treatment group. Immunohistochemical staining for uromodulin.

4.3.5.2 TEM analysis

Irrespective of their treatment, TALH cell nuclei of both homozygous *Umod*^{A227T} mutant and homozygous *Umod*^{C93F} mutant mice were surrounded by membranous piles that were interspersed with granular bodies (Figure 4.33).

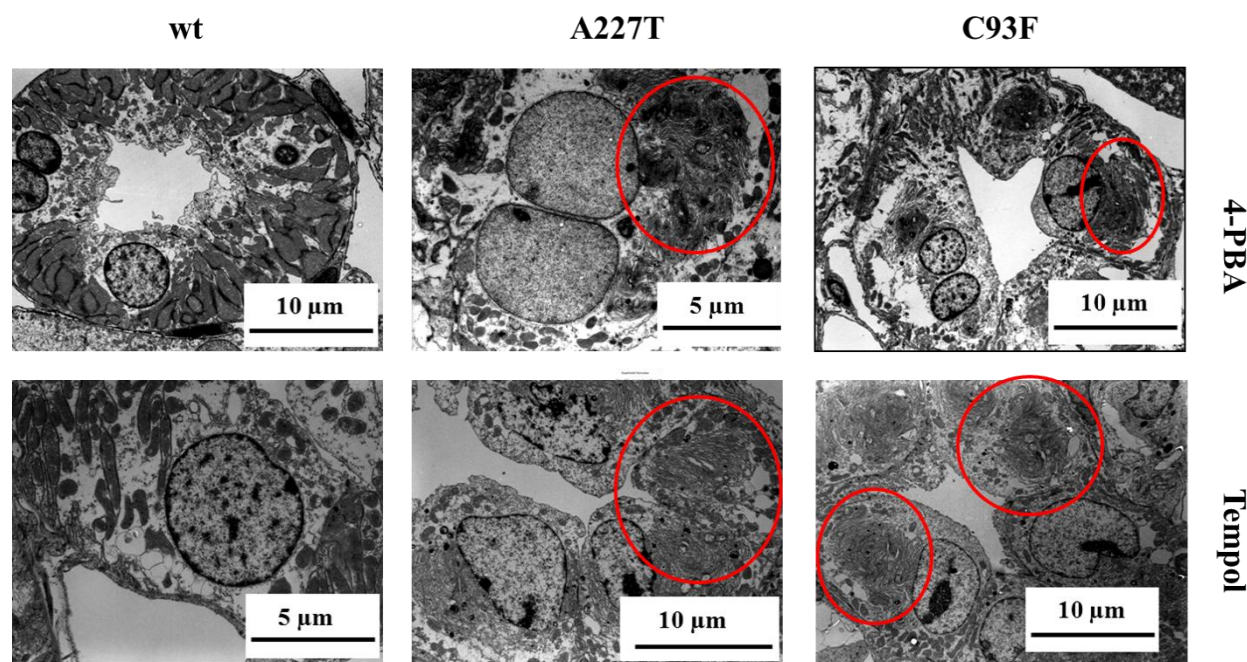


Figure 4.33: TALH cells of wild-type, homozygous *Umod*^{A227T} mutant and homozygous *Umod*^{C93F} mutant mice of the 4-PBA and the tempol treatment group. Ultrastructural analysis of TALH cells of mice of the 4-PBA and tempol treatment group revealed distinct perinuclear, lamellated membrane stacks (red circles) in TALH cells of homozygous *Umod*^{A227T} mutant and homozygous *Umod*^{C93F} mutant mice. wt: wild-type mice, A227T: homozygous *Umod*^{A227T} mutant mouse, C93F: homozygous *Umod*^{C93F} mutant mouse. 4-PBA, tempol: treatment groups.

5 Discussion

5.1 Uromodulin-associated kidney disease

Uromodulin-associated kidney disease (UAKD) is a human renal disease of autosomal dominant inheritance that is caused by mutations in the *UMOD* gene. Frequent symptoms include hyperuricaemia and gout as well as defective urine concentrating ability. UAKD patients develop renal lesions leading to end-stage renal disease (ESRD) between the third and seventh decade of life (Kumar, 2007; Rampoldi *et al.*, 2011). The clinical phenotype of UAKD shows heterogeneity regarding the onset as well as the severity of chronic kidney disease, even within affected families. Likewise, corticomedullary and glomerular cysts are inconsistently found in kidneys of UAKD patients (Rampoldi *et al.*, 2003; Bleyer *et al.*, 2011). UAKD patients are hitherto treated symptomatically for hyperuricaemia and gout with allopurinol but causative therapies for the disease remain to be found.

Mutant uromodulin is misfolded and precipitates in the endoplasmic reticulum (ER) of TALH cells. Thus, intracellular trafficking and full maturation of both wild-type and mutant uromodulin is impaired. A gain of toxic function of mutant uromodulin in TALH cells is hypothesized. However, the exact pathophysiologic mechanisms of UAKD are incompletely understood and are subject to continued *in vitro* and *in vivo* research (Dahan *et al.*, 2003; Rampoldi *et al.*, 2003).

The objective of this study was twofold. For one, the aim was to quantify histologic alterations in the kidneys of mice harbouring a mutation in the murine *Umod* gene and to compare the severity thereof with regard to different genotypes and ages. Secondly, the chemical chaperone 4-PBA as well as the superoxide dismutase mimetic tempol were tested as causative therapies at the onset of UAKD. Both parts of the study were conducted on mice of the *Umod*^{A227T} and the *Umod*^{C93F} mouse lines.

5.2 *Umod* mutant mouse lines as a murine model for UAKD

Two ENU-induced missense point mutations of autosomal dominant inheritance were identified in the *Umod* gene of the mouse lines *Umod*^{A227T} and *Umod*^{C93F}. Mutant mice of both lines mirror the clinical phenotype of human UAKD regarding impaired urinary concentrating ability, azotaemia and reduced fractional excretion of uric acid. Furthermore, the ER storage of

uromodulin detected in TALH cells of *Umod* mutant mice resembles the findings in kidney biopsies of UAKD patients. Both the *Umod*^{A227T} and the *Umod*^{C93F} mutation cause an increase in plasma urea levels in juvenile and young adult mice, with homozygous mutant mice of both lines exhibiting the maximal plasma urea concentrations at the age of 20-22 months. However, the two lines differ with regard to onset and severity of plasma urea elevation which was detected earlier in *Umod*^{C93F} mutant than in *Umod*^{A227T} mutant mice. Also, the clinical phenotype depends on the allelic status of animals and is expressed more severely by homozygous mutant than by heterozygous mutant mice in each line. Thus, the phenotype of homozygous *Umod*^{A227T} mutant mice compares to that of heterozygous *Umod*^{C93F} mutant mice (Kemter *et al.*, 2009; Prueckl, 2011; Kemter, 2012). Similarly, UAKD phenotypes described for humans depend on the location of the *UMOD* mutation and on the allelic status of patients (Rezende-Lima *et al.*, 2004; Williams *et al.*, 2009)

At the age of 6 months, mutant mice of both lines showed no alterations of renal histology, except for perinuclear uromodulin accumulations in TALH cells. Upon ultra-structural evaluation, hyperplastic membranous bundles were detected in TALH cells of these animals. This suggests ER stress and disturbed ER homeostasis as a probable cause of TALH cell dysfunction. In addition to these abnormalities, aged *Umod* mutant mice exhibited renal IFTA as well as interstitial infiltrates of lymphocytes and plasma cells. Therefore, quantitative stereology was used to investigate whether renal pathology of *Umod*^{A227T} and *Umod*^{C93F} mutant mice was correlated to their age- and genotype-dependent clinical phenotype.

5.3 Tubulointerstitial lesions in *Umod* mutant mice

In chronic kidney disease, irreversible tissue scarring is commonly marked by tubular atrophy as well as by interstitial fibrosis. Consequently, both parameters have been summarized as the term IFTA and, in this study, were evaluated as such (Bröcker *et al.*, 2010; Farris & Colvin, 2012).

At 20-22 months of age, renal IFTA was distinctly increased in homozygous *Umod*^{C93F} mutant and homozygous *Umod*^{A227T} mutant mice when compared to both heterozygous mutant and wild-type mice of the corresponding mouse line. While the presence of IFTA was comparably low in wild-type and heterozygous *Umod*^{A227T} mutant mice, homozygous *Umod*^{A227T} mutant mice showed IFTA levels similar to those measured in the kidneys of heterozygous *Umod*^{C93F} mutant

mice. Inflammatory cell infiltration of wild-type and heterozygous *Umod*^{A227T} mutant kidneys was similarly low at 20-22 months as well. In comparison, the presence of lymphocytes and plasma cells was distinctly increased in the renal interstitium of both homozygous *Umod*^{A227T} mutant and of heterozygous and homozygous *Umod*^{C93F} mutant mice. Clearly, the occurrence of both IFTA and inflammatory cell infiltration relates to both the location of the murine *Umod* mutation and to the genotype of the animal. This finding is in accordance with previous studies comparing the clinical phenotypes of these two lines (Prueckl, 2011).

As in this study, chronic inflammatory cell infiltrates such as lymphocytes and plasma cells frequently accompany renal interstitial fibrosis. Whether fibrosis triggers inflammation or vice versa is subject to continued discussion, though (Bröcker *et al.*, 2010). To gather further insight into the pathomechanism of UAKD, renal volumes of IFTA and inflammatory cell infiltrates were quantified in the kidneys of 14-month-old *Umod*^{C93F} mutant mice. *Umod*^{A227T} mutant mice were not analysed at this age since the occurrence of IFTA and inflammatory cell infiltrates in heterozygous *Umod*^{A227T} mutant mice at 20-22 months of age was still comparable to that measured in wild-type controls. Compared to wild-type controls, 14-month-old heterozygous and homozygous *Umod*^{C93F} mutant mice showed significantly increased IFTA and inflammatory cell infiltration. Homozygous *Umod*^{C93F} mutant mice showed no significant difference in either parameter between 14 and 20-22 months of age. In contrast, the kidneys of 14-month-old heterozygous *Umod*^{C93F} mutant mice were significantly less infiltrated by lymphocytes and plasma cells than those of 20-22-month-old animals. IFTA was present to a similar degree at 14 and 20-22 months of age in heterozygous *Umod*^{C93F} mutant mice. These findings indicate that the occurrence of IFTA is an earlier event and is followed by inflammatory cell infiltration in the kidneys of UAKD affected mutant mice. As described by Prueckl in 2011, the clinical phenotype of *Umod*^{C93F} mutant mice manifests itself later in heterozygous than in homozygous mutant animals. This could explain why inflammation in the kidneys of homozygous *Umod*^{C93F} mutant mice did not progress between 14 and 20-22 months of age.

Bohle *et al.* were among the first to point out a close correlation between the degree of interstitial fibrosis and the loss of renal urine concentrating ability in chronic kidney disease, regardless of the primary pathologic event (Schainuck *et al.*, 1970; Bohle *et al.*, 1977; Bohle *et al.*, 1987). Therefore, the IFTA measurements described above (refer to 4.1.1.2) agree with the deterioration

of urine concentration ability with UAKD progression described for mutant mice of both lines (Kemter *et al.*, 2009; Prueckl, 2011; Kemter, 2012). From the increased amount of IFTA and inflammatory cell infiltrates in *Umod* mutant murine kidneys, a parallel to biopsy findings of human UAKD patients can be drawn, where both interstitial fibrosis and infiltrates of lymphocytes indicate chronic tubulointerstitial nephropathy (Nasr *et al.*, 2008; Smith *et al.*, 2011). IFTA and interstitial inflammation were also detected in the kidneys of Tg^{*Umod*C147W} mice. However, Bernascone *et al.* (2010) described an upregulation of markers for macrophages and granulocytes which pointed to a more acute process of inflammation (Ackermann, 2009). Beyond the necrosis of TALH cells, the authors listed the release of uromodulin into the renal interstitium as possible proinflammatory trigger (Bernascone *et al.*, 2010). Moreover, the elevated uromodulin serum levels detected in UAKD patients with interstitial uromodulin deposits were associated with an increase in serum concentrations of pro-inflammatory cytokines and growth factors (Jennings *et al.*, 2007; Prajczek *et al.*, 2010). Despite the absence of interstitial uromodulin in *Umod* mutant mice, a comparable pathomechanism in the process of renal inflammation cannot be excluded.

5.4 Renal TALH cell volumes and tubular atrophy

At the age of 20-22 months, both heterozygous and homozygous *Umod*^{A227T} mutant and homozygous and heterozygous *Umod*^{C93F} mutant mice exhibited irregular aggregates of uromodulin in the cytoplasm of TALH cells. This observation was analogous to previously described alterations in immunohistochemically stained kidney sections of 3-6 month-old homozygous *Umod*^{A227T} mutant and heterozygous *Umod*^{C93F} mutant mice (Kemter *et al.*, 2009; Prueckl, 2011). However, the immunohistochemical staining pattern of uromodulin in TALH cells of aged mutant mice appeared more heterogeneous than in younger mutants, as there were some intensely stained TALH cells and also TALH cells with irregular weak or absent uromodulin signal in the same TALH section profile. Signs of intracellular uromodulin accumulation have also been detected in the kidneys of 3- and 6-month-old Tg^{*Umod*C147W} mice as well as in humans harbouring a *UMOD* mutation (Dahan *et al.*, 2003; Rampoldi *et al.*, 2003; Nasr *et al.*, 2008; Bernascone *et al.*, 2010). Both *in vivo* and *in vitro* immunofluorescence findings favour the ER as the location of uromodulin retention (Vylet'al *et al.*, 2006; Bernascone *et al.*, 2010). Whether the above described tubular atrophy affected predominantly TALH-

segments was investigated by the stereological analysis of the renal TALH volumes in *Umod* mutant mice in comparison to age-matched wild-type controls. Further, genotype-matched mice of the *Umod*^{Umod^{C93F}} line were compared with regard to age-dependent alterations of renal TALH cell contents.

At the age 20-22 months, both the fractional and total volume of TALH cells was significantly reduced in homozygous *Umod*^{A227T} mutant and homozygous *Umod*^{C93F} mutant mice when compared to wild-type controls. The comparison of 14-month-old wild-type mice to age-matched homozygous *Umod*^{C93F} mutant mice showed the same tendency. However, differences were still insignificant at that age. This suggests that, with age, a permanent, ever-increasing ER stress due to uromodulin accumulation in the TALH cells cannot be compensated for by the unfolded protein response alone, leaving cell death as the final pathway (Shore *et al.*, 2011; Moore & Hollien, 2012). Decreased renal TALH cell contents are not only reciprocated by an increase in IFTA but also reflect the situation in UAKD patients where cells undergo ER stress and eventually become atrophic (Rampoldi *et al.*, 2003; Bleyer & Hart, 2007). A consequent release of uromodulin into the renal interstitium has been described in UAKD patients (Resnick *et al.*, 1978; Zager *et al.*, 1978; Chambers *et al.*, 1986) but was not detected in either of the two *Umod* mutant mouse lines (refer to 5.3). Nonetheless, a reduction in TALH cells did not necessarily seem to be strongly linked to the occurrence of IFTA since the latter was also detected in 20-22-month-old *Umod* mutant mice exhibiting renal TALH cell volumes at wild-type level. This may suggest either that a signal for uromodulin can still be detected in early apoptotic cells, or that nephron segments other than the TALH are affected by tubular atrophy as well. It has been proposed that the gain-of-toxic effect of mutant uromodulin is compensated for by other nephron segments, which may ultimately lead to ER stress and apoptosis in the epithelium of proximal tubules or the collecting duct (Gersch *et al.*; Scolari *et al.*, 2004).

5.5 Age-related lesions in *Umod* mutant mice

Between the ages of 14 and 20-22 months, neither the loss of TALH volume nor the increase of IFTA progressed to a degree of significance in heterozygous or homozygous *Umod*^{C93F} mutant mice. Regarding inflammatory cell infiltrates, both their fractional and total volumes increased in aged heterozygous *Umod*^{C93F} mutant mice compared to middle-aged 14-month-old heterozygous

mutant mice. However, as explained beforehand, standard deviation is high in this group so a general trend is hardly assessable. The mild increase in inflammatory cell infiltrates in 20-22-month-old wild-type mice leads to the assumption that, with age, some of the nephritic processes detected occur independently to UAKD. Considering the results of this study together with the fact that *Umod* mutant mice showed no light microscopic histopathological alterations at 3-6 months of age (Kemter *et al.*, 2009), it seems likely that UAKD-associated alterations in mutant kidneys set in at some point between 6 and 14 months and that the progression of histopathology largely takes place in this space of time.

5.6 Sporadic renal histopathology in *Umod* mutant mice

In contrast to IFTA and inflammatory infiltrates, dilated or cystic tubules and Bowman capsules represented sporadic findings. Therefore, they were described solely qualitatively. Their occasional presence in mutants of both mouse lines, especially in the 20-22-month age group, parallels pathologic features described for humans suffering from UAKD. Upon ultrasound examination, dilated tubules and cysts were inconsistently detected in these patients, particularly at the corticomedullary junction and, similar to the findings in *Umod* mutant mice, as a comparatively late phenomenon (Scolari *et al.*, 1998; Dahan *et al.*, 2001; Dahan *et al.*, 2003; Nasr *et al.*, 2008). Focal glomerulosclerosis was also described in humans expressing mutant uromodulin (Williams *et al.*, 2009; Smith *et al.*, 2011). Intraluminal cast formation was detected in the *Umod* mutant mice of this study as well as in Tg^{*Umod*C147W} mice and constitutes another similarity to UAKD. Bernascone *et al.* suggested that mutant uromodulin is released into the lumen from cellular debris or that some of it skirts ER quality control and is secreted (Bernascone *et al.*, 2010; Schaeffer *et al.*, 2012). This may serve as an explanation for the absence of interstitial uromodulin deposits in *Umod*^{A227T} and *Umod*^{C93F} mutants.

5.7 UAKD therapy approach

So far, a causative therapy for human UAKD does not exist. Allopurinol and uricosuric drugs are in use to reduce hyperuricaemia or to increase the urinary excretion of uric acid, respectively (Pacher *et al.*, 2006; Schaffer *et al.*, 2010). However, the origin of UAKD presumably lies in ER retention of misfolded uromodulin and subsequent ER stress in TALH cells (Dahan *et al.*, 2003; Rampoldi *et al.*, 2011). Neither allopurinol nor uricosurics tackle the maturation retardation and

the resulting renal dysfunction on cellular and, eventually, on organ level. Thus, the administration of allopurinol ameliorates gout as a symptom of hyperuricaemia while the underlying kidney disease continues to progress (Bleyer & Hart, 2003). To date, renal transplantation presents the only effective cure for UAKD (Labriola *et al.*, 2007; Rampoldi *et al.*, 2011). *In vitro* studies proved that the chemical chaperone 4-PBA was beneficial in promoting the maturation of mutant uromodulin in transfected human embryonic kidney 293 cells, in immortalized TALH cells and in Madin-Darby canine kidney cells. It increased the translocation of mutant uromodulin from the ER to the cell membrane, thereby improving cell viability. Allopurinol, on the other hand, was found to have no such effect (Choi *et al.*, 2005b; Ma *et al.*, 2012). Based on these studies, we hypothesized that 4-PBA might act in a similar way upon TALH cells of *Umod* mutant mice *in vivo* and that, consequently, the renal plasma and urine parameters of *Umod* mutant mice might assimilate to those of wild-type littermates.

Reactive oxygen species are increasingly formed during chronic kidney disease (Hasselwander & Young, 1998; Martin-Mateo *et al.*, 1999; Banday *et al.*, 2005). Regarding the TALH-segment in particular, the free radical superoxide is hypothesized to reduce the bioavailability of nitroxide which is an important regulator of sodium chloride absorption in the TALH. *In vitro* perfusion of this nephron segment with tempol enhanced the release of nitroxide (Ortiz & Garvin, 2002). Therefore, the administration of the radical scavenger tempol to a second treatment group was expected to counteract an increase in reactive oxygen species in dysfunctional TALH cells of *Umod* mutant mice and to ameliorate their clinical and histopathological phenotype.

Since male and female mice differ significantly in some blood and urine parameters, for instance in urine osmolality (Kemter *et al.*, 2009), and to exclude hormonal influences of ovarian cycle of female mice the treatment assay was conducted on male mice.

5.8 Treatment of *Umod* mutant mice with 4-PBA and tempol

Starting at 2 months of age, sodium 4-PBA was continuously administered via drinking solution to homozygous *Umod*^{A227T} mutant and homozygous *Umod*^{C93F} mutant male mice at a dosage of 1 g per kg of body weight. A second treatment group was orally given 2mM tempol in drinking solution *ad libitum*. Plasma and urine parameters as well as body weights were compared

between mutant and wild-type mice in each group. Animals receiving regular drinking water without drug supplements served as a placebo treatment group.

Contrary to the initial hypothesis, plasma urea levels of homozygous *Umod* mutant mice of both lines and treatment assays rose above those of wild-type controls. A hypertonic medullary interstitium is essential for the urine concentrating ability of the kidney. It results mainly from the tubular reabsorption of sodium and urea (Yang & Bankir, 2005). Since renal urea transport occurs in the thin descending limb and the collecting duct (Yang & Bankir, 2005; Fenton & Knepper, 2007), these results suggest that TALH cell dysfunction may be compensated by increased urea reabsorption in other nephron segments to keep up the medullary hyperosmolality. This effect did not seem to be ameliorated by 4-PBA or tempol. 4-PBA-treated mutant and wild-type mice tended to exhibit the highest plasma urea levels and the lowest fractional excretion of urea when compared to genotype-matched mice in the other treatment groups. This implies a potential adverse effect of 4-PBA on the function of various renal cell types to reabsorb urea and ions in order to maintain an efficient countercurrent mechanism.

Hyperuricaemia due to reduced fractional excretion of uric acid is a major symptom of UAKD (Hart *et al.*, 2002). Possibly an impaired sodium reabsorption in TALH cells is compensated for by the proximal tubule where sodium reabsorption triggers the reabsorption of urate (Scolari *et al.*, 2004). In neither treatment group, plasma concentrations of uric acid differed between *Umod* mutant mice and wild-type controls. Different from humans, mice express uricase as a functional active enzyme which is a catalyst in the conversion of uric acid to allantoin (Choi *et al.*, 2005a) and which might explain the unaltered plasma levels of uric acid in *Umod* mutant mice.

UAKD patients frequently exhibit low urine osmolality and sometimes polyuria, which gives rise to the assumption that defective uromodulin trafficking may interfere with the functionality of TALH-located ion transporters such as the NKCC2 co-transporter (Rampoldi *et al.*, 2003). Together with other ion transporters, NKCC2 regulates the exchange and reabsorption of sodium, potassium, and chloride and, consequently, is essential for the creation and maintenance of a hypertonic interstitium of the renal medulla and thus for the urine concentration capability of the kidney. It also plays an important role in the paracellular reabsorption of magnesium and calcium (Figure 5.1) (Greger, 1985; Gamba, 2005). Thus, ion transport of TALH cells build up

an electric gradient between luminal side and blood side, which in turn enables the passive paracellular transport of divalent cations by this electric gradient.

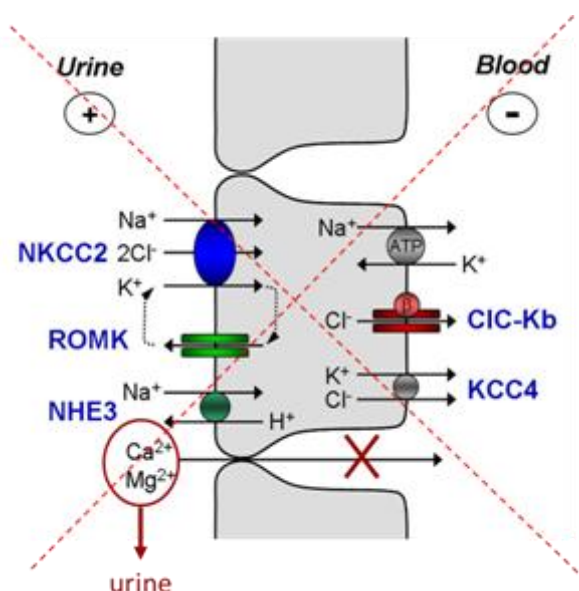


Figure 5.1: Scheme of the hypothesized impairment of ion exchange in TALH cells expressing mutant uromodulin. The reduced reabsorption of sodium, magnesium and divalent cations leads to an increased urinary excretion thereof.

Calcium excretion in the 24h-urine of 4-PBA- and tempol-treated homozygous *Umod*^{A227T} and *Umod*^{C93F} mutant mice was significantly elevated versus wild-type levels. Overall, calcium excretion was highest in animals of the 4-PBA treatment group when compared to genotype-matched mice receiving tempol or pure drinking water. Again, these results point to an adverse effect of 4-PBA on TALH cells and on their salt transport in particular. While deficiencies in sodium reabsorption in the TALH cells might be enhanced, they might also be compensated for to a substantial extent in other nephron segments. Calcium reabsorption on the other hand, is largely dependent on TALH functionality (Silbernagl & Lang, 2005; Gamba & Friedman, 2009) and therefore TALH dysfunction has a greater effect on FE_{Ca} than on FE_{Na}.

The resulting loss of urine concentrating ability has previously been described for mutant mice of both lines (Kemter *et al.*, 2009; Prueckl, 2011). An increased urine volume as well as reduced

urine osmolalities persisted in homozygous *Umod* mutant mice of both lines under the treatment with 4-PBA and tempol and rendered no evidence for an effect of either drug on urine concentrating ability.

Regardless of treatment group, the total protein excretion in the 24h-urine of homozygous *Umod*^{A227T} mutant and homozygous *Umod*^{C93F} mutant mice lay distinctly below wild-type levels. In all treatment groups, homozygous *Umod*^{C93F} mutant mice showed the lowest concentration of total urinary protein, which is in line with results from the western blot analysis where minimal urinary uromodulin excretion was detected in homozygous *Umod*^{C93F} mutant mice. In comparison, more urinary uromodulin was excreted by homozygous *Umod*^{A227T} mutant mice of all treatment groups but did not reach wild-type levels. Mutations in the human *UMOD* gene result in comparably reduced urinary uromodulin excretion (Wei *et al.*, 2012). In contrast to *in vitro* results, the administration of 4-PBA did not seem to improve the intracellular trafficking of uromodulin in *Umod* mutant mice.

Reduced body weight as well as a disturbed lipid metabolism have been described for both mouse lines in former studies and were interpreted as secondary alterations to renal malfunction (Kemter *et al.*, 2009; Prueckl, 2011). Compared to wild-type controls, neither 4-PBA nor tempol affected the decrease in plasma triglyceride levels in homozygous mutant mice of both lines. In analogy, the body weight of 4-PBA and tempol-treated homozygous *Umod*^{C93F} mutant and homozygous *Umod*^{A227T} mutant mice remained significantly below that of age-matched wild-type mice throughout the experiment.

From a young age, uromodulin retention and ER hyperplasia were detected in *Umod* mutant mice. Immunohistochemical and ultrastructural analysis showed similar alterations to those observed in renal biopsies of UAKD patients and present the hallmark of ER storage of mutant uromodulin (Nasr *et al.*, 2008; Kemter *et al.*, 2009). Contrary to the initial hypothesis, clusters of uromodulin as well as hyperplastic bundles of ER remained apparent in the kidneys of homozygous *Umod*^{A227T} mutant and homozygous *Umod*^{C93F} mutant mice after both 4-PBA and tempol treatment.

Unexpectedly and contrary to the published *in vitro* effects, both 4-PBA and tempol failed to bring the clinical and histological phenotypes of homozygous *Umod* mutant mice closer to those

of wild-type controls. Alterations such as reduced uromodulin excretion and increased urinary calcium excretion even appeared to be accentuated after 4-PBA treatment. To gain further insight behind the outcome of our treatment assay, a closer look at possible metabolic pathways of 4-PBA and tempol *in vivo* might be of help.

5.9 Metabolic pathways and efficacy of 4-PBA as a chemical chaperone

In the mammalian organism, the liver is the main location where 4-PBA is broken down into other compounds (Yu *et al.*, 2001). Phenylacetylglutamine, phenylbutyrylglutamine, phenylacetate and phenylbutyryl are four major metabolites of 4-PBA which are excreted in human urine (Comte *et al.*, 2002). However, they only constitute less than 50% of the amount of ingested PBA (Kasumov *et al.*, 2004). 4-PBA-metabolism in non-primates differs in that phenylacetyl-CoA is conjugated to glycine rather than glutamine. Yet, new PBA-metabolites were discovered in both rats and humans by Kasimov *et al.* (2004). From their results, the authors suggest that further, potentially toxic, metabolites remain to be searched for. Fractions of phenylacetate and phenylbutyryl glucuronides in the livers of *ad libitum*-fed rats were elevated compared to urine from humans who had fasted prior to 4-PBA administration. Thus, the intake of food may enhance the formation of compounds that do not act as chemical chaperones in the organism (Kasumov *et al.*, 2004). This assumption might be of relevance since all mice in this study were fed *ad libitum* and 4-PBA ingestion with the drinking water occurred throughout the whole day. This may have decreased the efficacy of 4-PBA as a chemical chaperone. In addition, it was found that, at a dosage of 0.4 - 0.6 g per kg and day, the sodium of Na 4-PBA increases extracellular fluid volume in cancer patients. Kasumov *et al.* point to the risk this constitutes to people with impaired heart and kidney function. Considering that 4-PBA was administered as a highly soluble sodium salt at a dosage of 1g per kg and day and that renal ion transport is already disturbed in *Umod* mutant mice, the form of application may have factored into the outcome of the 4-PBA treatment assay. Na 4-PBA is rapidly absorbed in the intestine and may have been converted to ineffective metabolites before entering the systemic circulation (McGuire *et al.*, 2010). Beyond the positive effect on uromodulin maturation *in vitro*, an amelioration of various other ER stress-induced conditions including diabetic nephropathy and adipogenesis has been reported for 4-PBA. Two of the studies were performed on mice and one on rats and in all three of them 4-PBA was administered at a dosage of 1g per kg of body weight (Basseri *et al.*, 2009;

Luo *et al.*, 2010; Qi *et al.*, 2011). However, the expression of unfolded-protein-response-related proteins in TALH cells may differ from the affected cell types used in the abovementioned studies. Thus, 4-PBA might not exert a regulating effect on TALH-specific unfolded protein response proteins (Dihazi *et al.*, 2005; Comes *et al.*, 2007).

5.10 Metabolization of tempol

Investigations of tempol pharmacokinetics in rats revealed that, at a fixed dose, tempol was reduced more quickly in the kidney than in the liver, due to a higher mitochondrial density in kidney cells (Kamataria *et al.*, 2002). These observations were made after intravenous injection of a bolus, however, and were sought to be prevented by continuously providing tempol as a drinking solution in this study. At the same time, it is important to note that renal reduction of tempol occurs primarily in the mitochondria and that this reaction is impaired by renal damage (Kamataria *et al.*, 2002; Ueda *et al.*, 2002; Oteki *et al.*, 2005). Yet, tempol administration has proved to ameliorate renal disorders in murine models such as insulin receptor knockout mice (Li *et al.*, 2012) and conditions caused by hypoxia in mice with reduced renal mass (Lai *et al.*, 2012). Again, it is noteworthy that other mouse strains were used in these studies and that tempol is likely to be oxidized in other, or additional, cells types than TALH cells.

The results discussed above indicate that, beyond the proper function of ion transport in TALH cells, mitochondrial metabolism might be affected by ER stress in uromodulin storage disease. Also, oxidative stress may not be a driving factor in the progression of UAKD and potential amelioration of oxidative stress by tempol might have been outweighed by other pathomechanisms.

5.11 Conclusion and outlook

Histopathological evaluation of the ENU mutant mouse lines *Umod*^{A227T} and *Umod*^{C93F} has now shown that *Umod* mutant mice exhibit distinct renal alterations compared to wild-type controls. Moreover, quantitative stereological kidney findings show that the degree of lesions correlates with the kind of mutation and thus with the degree of maturation retardation of mutant uromodulin as well as with the allelic status of the animal. It can further be concluded that renal morphological alterations progress largely between 6 and 14 months of age, rather than later on.

The findings described herein, together with previous phenotypic characterizations, validate the *Umod*^{A227T} and *Umod*^{C93F} mouse lines as useful animal models for UAKD.

The evaluation of causative treatment approaches for UAKD will remain subject to further investigations, ideally involving toxic dose low establishments and minimal interference of the metabolization of the drug with its efficacy in the kidney.

6 Summary

Pathomorphologic analysis and therapeutic *in-vivo* assay on two murine models of uromodulin-associated kidney disease

Uromodulin-associated kidney disease (UAKD) is a human renal disorder caused by mutations in the *UMOD* gene. *UMOD* encodes uromodulin, which is the most abundantly present protein in mammalian urine. Uromodulin, a GPI-anchored glycoprotein, is expressed in the cells of the thick ascending limb of the loop of Henle (TALH) and early parts of the distal convoluted tubule, exclusive of macula densa cells. To date, the complete functional scope of uromodulin remains to be clarified. Mutant, immature uromodulin aggregates in the endoplasmic reticulum of cells of the thick ascending limb of Henle. UAKD patients develop chronic kidney disease and end-stage renal failure between the third and seventh decade in their lives. Increasing ER stress leading to TALH cell dysfunction is regarded as the underlying pathomechanism. Despite their common genetic origin, clinical phenotypes vary with regard to onset, severity and renal morphologic alterations, depending on the localization of the mutation in the *UMOD* gene and the allelic status of the affected individual. Symptomatic heterogeneity occurs even within affected families. Most patients develop hyperuricaemia and gout, along with deficient urine concentrating ability. To date, UAKD cannot be cured. Therapy is limited to symptom amelioration by allopurinol or uricosuric drugs. Besides *in vitro* studies, *in vivo* research on UAKD has hitherto been performed on murine models. The mutant mouse lines, *Umod*^{A227T} and *Umod*^{C93F}, were developed in the Munich ENU mouse mutagenesis project and both harbour an autosomal dominant missense mutation in the murine *Umod* gene. Mutant mice of both lines exhibit elevated plasma urea levels, defective urinary concentrating ability and an increased excretion of bivalent cations, with *Umod*^{C93F} mutant mice expressing a stronger phenotype.

The first aim of this study was to qualify and quantify histomorphological alterations in the kidneys of *Umod*^{A227T} and *Umod*^{C93F} mutant mice of different allelic status and age in order to relate the findings to the onset, expression and progression of their clinical phenotype.

Secondly, the efficacy of two differently acting drugs as a causative treatment for UAKD was tested on homozygous mutant mice of the two mouse lines. Oral administration of the chemical chaperone 4-phenylbutyric acid and the antioxidant tempol to two different treatment groups was

aimed at evaluating their effect on *Umod* mutant mice. To this end, the clinical and histopathological phenotype of treated mutant mice was compared to treated wild-type controls as well as to animals of a placebo treatment group.

Interstitial fibrosis and tubular atrophy (IFTA) as well as inflammatory infiltrates were consistent findings in mutant mice and their quantification revealed a similar increase of both parameters in homozygous *Umod*^{A227T} mutant and in heterozygous *Umod*^{C93F} mutant mice at 20-22 months of age. IFTA had developed to the greatest extent in 20-22-month-old homozygous *Umod*^{C93F} mutant mice. Between the ages of 14 and 20-22 months, progressive inflammatory cell infiltration was detected in heterozygous *Umod*^{C93F} mutant mice. Homozygous mutant mice of both lines showed a tendency towards a loss of TALH cells at 20-22 months of age. Renal cysts and glomerulosclerosis were sporadically detected in *Umod* mutant mice of both lines.

Elevated plasma urea levels, impaired urine concentrating ability and increased urinary calcium excretion remained eminent in homozygous *Umod* mutant mice of both lines after two months of treatment with both 4-PBA and tempol. ER retention of uromodulin and, consequently, reduced urinary uromodulin excretion equally persisted after the application of either drug. Compared to untreated and tempol-treated mice, 4-PBA treatment appeared to stress clinical alterations in homozygous *Umod* mutant mice.

Quantification of renal histologic alterations of *Umod* mutant mice revealed that the expression and progression of alterations was dependent on age, line, and genotype. Comparable observations had been made for the clinical phenotype of *Umod* mutant mice. Moreover, the results indicated that, in the pathogenesis of tubulointerstitial nephropathy in *Umod* mutant mice, interstitial fibrosis and tubular atrophy preceded inflammation. The results of 4-PBA treatment suggest a minimally toxic effect on TALH cells, since plasma urea levels and the fractional excretion of sodium and calcium were most elevated in mice of this treatment group. Urinary uromodulin excretion appeared further diminished by 4-PBA treatment in homozygous mutant mice. Tempol treatment showed that, if there was a reduction of oxidative stress in the kidneys of *Umod* mutant mice, it was overshadowed by other pathological processes. Due to numerous clinical and histopathological analogies to the human disease, *Umod*^{A227T} and *Umod*^{C93F} mutant mice present a suitable murine model for further *in vivo* UAKD therapy assays.

7 Zusammenfassung

Pathomorphologische Untersuchung und *in vivo* Therapieversuch an zwei Mausmodellen für die Uromodulin-assoziierte Nierenerkrankung

Die Uromodulin-assoziierte Nierenerkrankung ist eine Nierenerkrankung des Menschen, die durch Mutationen des *UMOD* Gens verursacht wird. *UMOD* kodiert für Uromodulin, das auch unter dem Namen Tamm-Horsfall-Protein bekannt ist, und das am häufigsten vorgefundene Protein im Harn von Säugetieren darstellt. Bei Uromodulin handelt es sich um ein GPI-gebundenes Glykoprotein, das von den Zellen des dicken aufsteigenden Schenkels der Henle Schleife (TALH) sowie in frühen Abschnitten des distalen gewundenen Tubulus, ausgenommen Macula densa Zellen, exprimiert wird. Die gesamte Bandbreite der Funktion von Uromodulin bleibt bisher ungeklärt. Mutiertes, unreifes Uromodulin reichert sich im endoplasmatischen Retikulum (ER) von Zellen des TALH an. Zwischen der dritten und siebten Lebensdekade entwickeln UAKD Patienten chronische Niereninsuffizienz und terminales Nierenversagen. Man nimmt an, dass ansteigender endoplasmatischer Retikulum (ER)-Stress in den Zellen des TALH eine Fehlfunktion derselben nach sich zieht und somit den der UAKD zu Grunde liegenden Pathomechanismus darstellt. Trotz ihres gemeinsamen genetischen Ursprungs unterscheiden sich die klinischen Phänotypen der UAKD hinsichtlich Krankheitsbeginn und –schweregrad sowie in Bezug auf die Morphologie und Ausprägung der Nierenveränderungen, abhängig von der Lokalisation der Mutation im *UMOD* Gen und vom Allelstatus der betroffenen Person. Dabei treten selbst intrafamiliär heterogene Symptome auf. Bei den meisten Menschen kommt es zu Hyperurikämie und Gicht, sowie zu einer beeinträchtigten Harnkonzentrierungsfähigkeit. Bisher kann UAKD nicht geheilt werden. Therapien beschränken sich auf die Linderung von Symptomen durch Allopurinol und Urikosurika. Neben *in vitro* Studien wurde UAKD *in vivo* bisher an Mausmodellen untersucht. Die beiden *Umod* mutanten Linien, *Umod*^{A227T} und *Umod*^{C93F} entstanden aus dem Münchener ENU Maus Mutagenese Projekt und tragen jeweils eine autosomal dominante Missense-Mutation im murinen *Umod* Gen. Mutante Mäuse beider Linien haben erhöhte Plasmaharnstoffwerte, eine eingeschränkte Harnkonzentrierungsfähigkeit

und scheiden vermehrt bivalente Kationen aus, wobei *Umod*^{C93F} mutante Mäuse einen stärkeren Phänotyp zeigen.

Der erste Teil dieser Arbeit verfolgte das Ziel der qualitativen und quantitativen Bestimmung von histomorphologischen Nierenveränderungen bei *Umod*^{A227T} und *Umod*^{C93F} mutanten Mäusen von unterschiedlichem Allelstatus und Alter, um diese in Relation zu Beginn, Ausprägung und Progression ihres klinischen Phänotyps zu setzen.

Des Weiteren wurden zwei unterschiedlich agierende Medikamente hinsichtlich ihrer Wirksamkeit als Kausaltherapie für UAKD an homozygot mutanten Mäusen beider Linien getestet. Orale Abgabe des chemischen Chaperones 4-Phenylbutyrat und des Antioxidans Tempol an zwei verschiedene Behandlungsgruppen diente der Ermittlung ihrer Wirkung auf *Umod* mutante Mäuse. Hierzu wurden behandelte mutante Mäuse hinsichtlich ihres klinischen und histopathologischen Phänotyps mit gleich behandelten Wildtypkontrollen sowie mit Tieren aus einer Placebo-Gruppe verglichen.

Interstitielle Fibrose und tubuläre Atrophie (IFTA) sowie Entzündungszellinfiltrate stellten konstante pathologische Befunde in mutanten Mäusen beider Linien dar und ihre Quantifizierung zeigte einen ähnlichen Anstieg beider Parameter in den Nieren homozygot *Umod*^{A227T} mutanter und heterozygot *Umod*^{C93F} mutanter Mäuse im Alter von 20-22 Monaten. Homozygot *Umod*^{C93F} mutante Mäuse zeigten die stärkste Ausprägung von IFTA. In den Nieren von heterozygot *Umod*^{C93F} mutanten Mäusen wurde eine Progression der Entzündungszellinfiltration zwischen den Altersstufen von 14 und 20-22 Monaten festgestellt. Im Alter von 20-22 Monaten zeigen homozygot mutante Mäuse beider Linien eine Tendenz zu TALH-Zellverlust. Zysten und Glomerulosklerose wurden sporadisch in den Nieren mutanter Mäuse aus beiden Linien identifiziert.

Erhöhte Plasmaharnstoffwerte, verringerte Harnkonzentrierungsfähigkeit und vermehrte Kalziumausscheidung mit dem Urin blieben sowohl nach der Behandlung mit 4-PBA als auch mit Tempol bestehen. Gleichmaßen persistierten ER-Retention von Uromodulin und die dadurch bedingte verringerte Uromodulin-Ausscheidung im Harn nach Gabe beider Medikamente. Im Vergleich zu Tempol-behandelten und unbehandelten Tieren, erschienen die

klinischen Veränderungen in homozygot *Umod* mutanten Mäusen durch die 4-PBA-Behandlung verstärkt zu werden.

Die Quantifizierung histopathologischer Nierenveränderungen *Umod* mutanter Mäuse zeigte, dass deren Ausprägung und Progression vom Alter, der Mauslinie und dem Genotyp abhängen. Vergleichbare Beobachtungen wurden bereits für den klinischen Phänotyp gemacht. Darüber hinaus ging aus den Ergebnissen hervor, dass bei Pathogenese der tubulointerstitiellen Nephropathie von *Umod* mutanten Mäusen interstitielle Fibrose und tubuläre Atrophie der Infiltration durch Entzündungszellen vorangingen. Die Ergebnisse der Behandlung von Mäusen mit 4-PBA weisen auf einen minimal toxischen Effekt auf TALH-Zellen hin, da die Plasmaharstoffwerte und die fraktionelle Ausscheidung von Natrium und Kalzium sowohl bei Mäusen in dieser Behandlungsgruppe am höchsten lagen. Zudem schien die Ausscheidung von Uromodulin im Harn homozygot mutanter Tiere in dieser Behandlungsgruppe zusätzlich verringert. Sollte Tempol den oxidativen Stress in den Nieren von *Umod* mutanten Mäusen verringert haben, so wurde dieser Effekt von anderen pathologischen Prozessen überschattet. Aufgrund zahlreicher klinischer und histopathologischer Übereinstimmungen zur Erkrankung beim Menschen stellen *Umod*^{A227T} und *Umod*^{C93F} mutante Mäuse ein geeignetes Modell für weitere *in vivo* Therapieversuche für UAKD dar.

(<http://www.uniprot.org/uniprot/P07911>) Available at: (accessed

- Ackermann, M.R. (2009) Akute Entzündung. *Pahtologie der Haustiere: Allgemeine, spezielle und funktionelle Veterinärpathologie* (ed. by M.D. McGavin and J.F. Zachary), pp. 94-141. Elsevier GmbH, Urban & Fischer Verlag, Lektorat Veterinärmedizin, Karlstraße 45, 80333 München, München.
- Adam, J., Bollee, G., Fougeray, S., Noel, L.H., Antignac, C., Knebelman, B. & Pallet, N. (2012) Endoplasmic reticulum stress in UMOD-related kidney disease: a human pathologic study. *Am J Kidney Dis*, **59**, 117-21.
- Aigner, B., Rathkolb, B., Herbach, N., Kemter, E., Schessl, C., Klawns, M., Klempt, M., de Angelis, M.H., Wanke, R. & Wolf, E. (2007) Screening for increased plasma urea levels in a large-scale ENU mouse mutagenesis project reveals kidney disease models. *Am J Physiol Renal Physiol*, **292**, 30.
- Ananthan, J., Goldberg, A.L. & Voellmy, R. (1986) Abnormal proteins serve as eukaryotic stress signals and trigger the activation of heat shock genes. *Science*, **232**, 522-4.
- Anfinsen, C.B. (1973) Principles that govern the folding of protein chains. *Science*, **181**, 223-30.
- Bachmann, S., Metzger, R. & Bunnemann, B. (1990) Tamm-Horsfall protein-mRNA synthesis is localized to the thick ascending limb of Henle's loop in rat kidney. *Histochemistry*, **94**, 517-23.
- Banday, A.A., Marwaha, A., Tallam, L.S. & Lokhandwala, M.F. (2005) Tempol reduces oxidative stress, improves insulin sensitivity, decreases renal dopamine D1 receptor hyperphosphorylation, and restores D1 receptor-G-protein coupling and function in obese Zucker rats. *Diabetes*, **54**, 2219-26.
- Barnett, B.J. & Stephens, D.S. (1997) Urinary tract infection: an overview. *Am J Med Sci*, **314**, 245-9.
- Basseri, S., Lhotak, S., Sharma, A.M. & Austin, R.C. (2009) The chemical chaperone 4-phenylbutyrate inhibits adipogenesis by modulating the unfolded protein response. *J Lipid Res*, **50**, 2486-501.
- Bates, J.M., Raffi, H.M., Prasad, K., Mascarenhas, R., Laszik, Z., Maeda, N., Hultgren, S.J. & Kumar, S. (2004) Tamm-Horsfall protein knockout mice are more prone to urinary tract infection: rapid communication. *Kidney Int*, **65**, 791-7.
- Bayer, M.E. (1964) An Electron Microscope Examination of Urinary Mucoprotein and Its Interaction with Influenza Virus. *J Cell Biol*, **21**, 265-74.
- Benting, J.H., Rietveld, A.G. & Simons, K. (1999) N-Glycans mediate the apical sorting of a GPI-anchored, raft-associated protein in Madin-Darby canine kidney cells. *J Cell Biol*, **146**, 313-20.

- Bernascone, I., Janas, S., Ikehata, M., Trudu, M., Corbelli, A., Schaeffer, C., Rastaldi, M.P., Devuyst, O. & Rampoldi, L. (2010) A transgenic mouse model for uromodulin-associated kidney diseases shows specific tubulo-interstitial damage, urinary concentrating defect and renal failure. *Hum Mol Genet*, **19**, 2998-3010.
- Bernascone, I., Vavassori, S., Di Pentima, A., Santambrogio, S., Lamorte, G., Amoroso, A., Scolari, F., Ghiggeri, G.M., Casari, G., Polishchuk, R. & Rampoldi, L. (2006) Defective intracellular trafficking of uromodulin mutant isoforms. *Traffic*, **7**, 1567-79.
- Bleyer, A.J. & Hart, T.C. (2003) *Familial juvenile hyperuricaemic nephropathy*. QJM. 2003 Nov;96(11):867-8.
- Bleyer, A.J. & Hart, P.S. (2007) UMOD-Associated Kidney Disease. In: *Gene Review*, Internet.
- Bleyer, A.J., Zivna, M. & Knoch, S. (2011) Uromodulin-associated kidney disease. *Nephron Clin Pract*, **118**, 11.
- Bleyer, A.J., Trachtman, H., Sandhu, J., Gorry, M.C. & Hart, T.C. (2003) Renal manifestations of a mutation in the uromodulin (Tamm Horsfall protein) gene. *Am J Kidney Dis*, **42**, E20-6.
- Bleyer, A.J., Hart, T.C., Willingham, M.C., Iskandar, S.S., Gorry, M.C. & Trachtman, H. (2005) Clinico-pathologic findings in medullary cystic kidney disease type 2. *Pediatr Nephrol*, **20**, 824-7.
- Boger, C.A. & Heid, I.M. (2011) Chronic kidney disease: novel insights from genome-wide association studies. *Kidney Blood Press Res*, **34**, 225-34.
- Bohle, A., Mackensen-Haen, S. & von Gise, H. (1987) Significance of tubulointerstitial changes in the renal cortex for the excretory function and concentration ability of the kidney: a morphometric contribution. *Am J Nephrol*, **7**, 421-33.
- Bohle, A., Grund, K.E., Mackensen, S. & Tolon, M. (1977) Correlations between renal interstitium and level of serum creatinine. Morphometric investigations of biopsies in perimembranous glomerulonephritis. *Virchows Arch A Pathol Anat Histol*, **373**, 15-22.
- Bollee, G., Dahan, K., Flamant, M., Moriniere, V., Pawtowski, A., Heidet, L., Lacombe, D., Devuyst, O., Pirson, Y., Antignac, C. & Knebelmann, B. (2011) Phenotype and outcome in hereditary tubulointerstitial nephritis secondary to UMOD mutations. *Clin J Am Soc Nephrol*, **6**, 2429-38.
- Bröcker, V., Kreipe, H. & Haller, H. (2010) Tubulointerstitielle Fibrose. *Der Nephrologe*, **5**, 284-292.
- Brown, C.R., Hong-Brown, L.Q., Biwersi, J., Verkman, A.S. & Welch, W.J. (1996) Chemical chaperones correct the mutant phenotype of the delta F508 cystic fibrosis transmembrane conductance regulator protein. *Cell Stress Chaperones*, **1**, 117-25.

- Brown, D.A. & Rose, J.K. (1992) Sorting of GPI-anchored proteins to glycolipid-enriched membrane subdomains during transport to the apical cell surface. *Cell*, **68**, 533-44.
- Brusilow, S.W. (1991) Phenylacetylglutamine may replace urea as a vehicle for waste nitrogen excretion. *Pediatr Res*, **29**, 147-50.
- Bukau, B. & Horwich, A.L. (1998) The Hsp70 and Hsp60 chaperone machines. *Cell*, **92**, 351-66.
- Cai, H., Griendling, K.K. & Harrison, D.G. (2003) The vascular NAD(P)H oxidases as therapeutic targets in cardiovascular diseases. *Trends Pharmacol Sci*, **24**, 471-8.
- Carducci, M.A., Gilbert, J., Bowling, M.K., Noe, D., Eisenberger, M.A., Sinibaldi, V., Zabelina, Y., Chen, T.L., Grochow, L.B. & Donehower, R.C. (2001) A Phase I clinical and pharmacological evaluation of sodium phenylbutyrate on an 120-h infusion schedule. *Clin Cancer Res*, **7**, 3047-55.
- Chambers, R., Groufsky, A., Hunt, J.S., Lynn, K.L. & McGiven, A.R. (1986) Relationship of abnormal Tamm-Horsfall glycoprotein localization to renal morphology and function. *Clin Nephrol*, **26**, 21-6.
- Chamcheu, J.C., Navsaria, H., Pihl-Lundin, I., Liovic, M., Vahlquist, A. & Torma, H. (2011) Chemical chaperones protect epidermolysis bullosa simplex keratinocytes from heat stress-induced keratin aggregation: involvement of heat shock proteins and MAP kinases. *J Invest Dermatol*, **131**, 1684-91.
- Choi, H.K., Mount, D.B. & Reginato, A.M. (2005a) Pathogenesis of gout. *Ann Intern Med*, **143**, 499-516.
- Choi, S.W., Ryu, O.H., Choi, S.J., Song, I.S., Bleyer, A.J. & Hart, T.C. (2005b) Mutant tamm-horsfall glycoprotein accumulation in endoplasmic reticulum induces apoptosis reversed by colchicine and sodium 4-phenylbutyrate. *J Am Soc Nephrol*, **16**, 3006-14.
- Choppin, P.W. (2007) Igor Tamm 1922-1995. *A Biographical Memoir*. In, pp. 1-17. National Academy of Sciences
- Christensen, F.H., Stankevicius, E., Hansen, T., Jorgensen, M.M., Valverde, V.L., Simonsen, U. & Buus, N.H. (2007) Flow- and acetylcholine-induced dilatation in small arteries from rats with renovascular hypertension--effect of tempol treatment. *Eur J Pharmacol*, **566**, 160-6.
- Collins, A.F., Pearson, H.A., Giardina, P., McDonagh, K.T., Brusilow, S.W. & Dover, G.J. (1995) Oral sodium phenylbutyrate therapy in homozygous beta thalassemia: a clinical trial. *Blood*, **85**, 43-9.
- Comes, F., Matrone, A., Lastella, P., Nico, B., Susca, F.C., Bagnulo, R., Ingravallo, G., Modica, S., Lo Sasso, G., Moschetta, A., Guanti, G. & Simone, C. (2007) A novel cell type-specific role of p38alpha in the control of autophagy and cell death in colorectal cancer cells. *Cell Death Differ*, **14**, 693-702.

- Comte, B., Kasumov, T., Pierce, B.A., Puchowicz, M.A., Scott, M.E., Dahms, W., Kerr, D., Nissim, I. & Brunengraber, H. (2002) Identification of phenylbutyrylglutamine, a new metabolite of phenylbutyrate metabolism in humans. *J Mass Spectrom*, **37**, 581-90.
- Couet, W.R., Brasch, R.C., Sosnovsky, G. & Tozer, T.N. (1985) Factors affecting nitroxide reduction in ascorbate solution and tissue homogenates. *Magn Reson Imaging*, **3**, 83-8.
- Craig, E.A. & Gross, C.A. (1991) Is hsp70 the cellular thermometer? *Trends Biochem Sci*, **16**, 135-40.
- Cummings, R.D. & Kornfeld, S. (1982) Characterization of the structural determinants required for the high affinity interaction of asparagine-linked oligosaccharides with immobilized *Phaseolus vulgaris* leucoagglutinating and erythroagglutinating lectins. *J Biol Chem*, **257**, 11230-4.
- Dahan, K., Fuchshuber, A., Adamis, S., Smaers, M., Kroiss, S., Loute, G., Cosyns, J.P., Hildebrandt, F., Verellen-Dumoulin, C. & Pirson, Y. (2001) Familial juvenile hyperuricemic nephropathy and autosomal dominant medullary cystic kidney disease type 2: two facets of the same disease? *J Am Soc Nephrol*, **12**, 2348-57.
- Dahan, K., Devuyst, O., Smaers, M., Vertommen, D., Loute, G., Poux, J.M., Viron, B., Jacquot, C., Gagnadoux, M.F., Chauveau, D., Buchler, M., Cochat, P., Cosyns, J.P., Mougnot, B., Rider, M.H., Antignac, C., Verellen-Dumoulin, C. & Pirson, Y. (2003) A cluster of mutations in the UMOD gene causes familial juvenile hyperuricemic nephropathy with abnormal expression of uromodulin. *J Am Soc Nephrol*, **14**, 2883-93.
- Dihazi, H., Asif, A.R., Agarwal, N.K., Doncheva, Y. & Muller, G.A. (2005) Proteomic analysis of cellular response to osmotic stress in thick ascending limb of Henle's loop (TALH) cells. *Mol Cell Proteomics*, **4**, 1445-58.
- Dikalova, A., Clempus, R., Lassegue, B., Cheng, G., McCoy, J., Dikalov, S., San Martin, A., Lyle, A., Weber, D.S., Weiss, D., Taylor, W.R., Schmidt, H.H., Owens, G.K., Lambeth, J.D. & Griendling, K.K. (2005) Nox1 overexpression potentiates angiotensin II-induced hypertension and vascular smooth muscle hypertrophy in transgenic mice. *Circulation*, **112**, 2668-76.
- Dobson, C.M. & Karplus, M. (1999) The fundamentals of protein folding: bringing together theory and experiment. *Curr Opin Struct Biol*, **9**, 92-101.
- Dover, G.J., Brusilow, S. & Samid, D. *Increased fetal hemoglobin in patients receiving sodium 4-phenylbutyrate*. *N Engl J Med*. 1992 Aug 20;327(8):569-70.
- Dover, G.J., Brusilow, S. & Charache, S. (1994) Induction of fetal hemoglobin production in subjects with sickle cell anemia by oral sodium phenylbutyrate. *Blood*, **84**, 339-43.
- El-Achkar, T.M., Wu, X.R., Rauchman, M., McCracken, R., Kiefer, S. & Dagher, P.C. (2008) Tamm-Horsfall protein protects the kidney from ischemic injury by decreasing inflammation and altering TLR4 expression. *Am J Physiol Renal Physiol*, **295**, 21.

- Ellgaard, L. & Helenius, A. (2003) Quality control in the endoplasmic reticulum. *Nat Rev Mol Cell Biol*, **4**, 181-91.
- Ellgaard, L., Molinari, M. & Helenius, A. (1999) Setting the standards: quality control in the secretory pathway. *Science*, **286**, 1882-8.
- Ellis, R.J. (2006) Molecular chaperones: assisting assembly in addition to folding. *Trends Biochem Sci*, **31**, 395-401.
- Fairbanks, L.D., Cameron, J.S., Venkat-Raman, G., Rigden, S.P., Rees, L., Van, T.H.W., Mansell, M., Pattison, J., Goldsmith, D.J. & Simmonds, H.A. (2002) Early treatment with allopurinol in familial juvenile hyperuricaemic nephropathy (FJHN) ameliorates the long-term progression of renal disease. *Qjm*, **95**, 597-607.
- Farris, A.B. & Colvin, R.B. (2012) Renal interstitial fibrosis: mechanisms and evaluation. *Curr Opin Nephrol Hypertens*, **21**, 289-300.
- Feng, M.G., Dukacz, S.A. & Kline, R.L. (2001) Selective effect of tempol on renal medullary hemodynamics in spontaneously hypertensive rats. *Am J Physiol Regul Integr Comp Physiol*, **281**, R1420-5.
- Fenton, R.A. & Knepper, M.A. (2007) Urea and renal function in the 21st century: insights from knockout mice. *J Am Soc Nephrol*, **18**, 679-88.
- Ferguson, M.A. & Williams, A.F. (1988) Cell-surface anchoring of proteins via glycosyl-phosphatidylinositol structures. *Annu Rev Biochem*, **57**, 285-320.
- Fewell, S.W., Travers, K.J., Weissman, J.S. & Brodsky, J.L. (2001) The action of molecular chaperones in the early secretory pathway. *Annu Rev Genet*, **35**, 149-91.
- Fletcher, A.P., Neuberger, A. & Ratcliffe, W.A. (1970) Tamm-Horsfall urinary glycoprotein. The chemical composition. *Biochem J*, **120**, 417-24.
- Friedlander, R., Jarosch, E., Urban, J., Volkwein, C. & Sommer, T. (2000) A regulatory link between ER-associated protein degradation and the unfolded-protein response. *Nat Cell Biol*, **2**, 379-84.
- Gamba, G. (2005) Molecular physiology and pathophysiology of electroneutral cation-chloride cotransporters. *Physiol Rev*, **85**, 423-93.
- Gamba, G. & Friedman, P.A. (2009) Thick ascending limb: the Na(+):K (+):2Cl (-) cotransporter, NKCC2, and the calcium-sensing receptor, CaSR. *Pflugers Arch*, **458**, 61-76.
- Garvin, J.L. & Hong, N.J. (2008) Cellular stretch increases superoxide production in the thick ascending limb. *Hypertension*, **51**, 488-93.

- Gersch, M., Mutig, K., Bachmann, S., Kumar, S., Ouyang, X. & Johnson, R. *Is salt-wasting the long awaited answer to the hyperuricaemia seen in uromodulin storage diseases?* *Nephrol Dial Transplant*. 2006 Jul;21(7):2028-9. Epub 2006 Jan 18.
- Gething, M.J. & Sambrook, J. (1992) Protein folding in the cell. *Nature*, **355**, 33-45.
- Gething, M.J., McCammon, K. & Sambrook, J. (1986) Expression of wild-type and mutant forms of influenza hemagglutinin: the role of folding in intracellular transport. *Cell*, **46**, 939-50.
- Ghosh, M., Wang, H.D. & McNeill, J.R. (2004) Role of oxidative stress and nitric oxide in regulation of spontaneous tone in aorta of DOCA-salt hypertensive rats. *Br J Pharmacol*, **141**, 562-73.
- Gottschalk, A. (1952) Carbohydrate Residue of a Urine Mucoprotein inhibiting Influenza Virus Haemagglutination. *Nature*, **170**, 662-663.
- Grant, A.M. & Neuberger, A. (1973) The development of a radioimmunoassay for the measurement of urinary Tamm-Horsfall glycoprotein in the presence of sodium dodecyl sulphate. *Clin Sci*, **44**, 163-79.
- Greger, R. (1985) Ion transport mechanisms in thick ascending limb of Henle's loop of mammalian nephron. *Physiol Rev*, **65**, 760-97.
- Gundersen, H.J. & Jensen, E.B. (1987) The efficiency of systematic sampling in stereology and its prediction. *J Microsc*, **147**, 229-63.
- Guron, G.S., Grimberg, E.S., Basu, S. & Herlitz, H. (2006) Acute effects of the superoxide dismutase mimetic tempol on split kidney function in two-kidney one-clip hypertensive rats. *J Hypertens*, **24**, 387-94.
- Gusmano, R., Caridi, G., Marini, M., Perfumo, F., Ghiggeri, G.M., Piaggio, G., Ceccherini, I. & Seri, M. (2002) Glomerulocystic kidney disease in a family. *Nephrol Dial Transplant*, **17**, 813-8.
- Hambali, Z., Ahmad, Z., Arab, S. & Khazaai, H. (2011) Oxidative stress and its association with cardiovascular disease in chronic renal failure patients. *Indian J Nephrol*, **21**, 21-5.
- Hamlin, L.M. & Fish, W.W. (1977) Physical properties of Tamm-Horsfall glycoprotein and its glycopolyptide. *Int J Pept Protein Res*, **10**, 270-6.
- Hammarstrom, S., Hammarstrom, M.L., Sundblad, G., Arnarp, J. & Lonngren, J. (1982) Mitogenic leucoagglutinin from *Phaseolus vulgaris* binds to a pentasaccharide unit in N-acetyllactosamine-type glycoprotein glycans. *Proc Natl Acad Sci U S A*, **79**, 1611-5.
- Hammond, C. & Helenius, A. (1995) Quality control in the secretory pathway. *Curr Opin Cell Biol*, **7**, 523-9.

- Harding, H.P., Zhang, Y. & Ron, D. (1999) Protein translation and folding are coupled by an endoplasmic-reticulum-resident kinase. *Nature*, **397**, 271-4.
- Hart, T.C., Gorry, M.C., Hart, P.S., Woodard, A.S., Shihabi, Z., Sandhu, J., Shirts, B., Xu, L., Zhu, H., Barmada, M.M. & Bleyer, A.J. (2002) Mutations of the UMOD gene are responsible for medullary cystic kidney disease 2 and familial juvenile hyperuricaemic nephropathy. *J Med Genet*, **39**, 882-92.
- Hartl, F.U. & Hayer-Hartl, M. (2002) Molecular chaperones in the cytosol: from nascent chain to folded protein. *Science*, **295**, 1852-8.
- Hasselwander, O. & Young, I.S. (1998) Oxidative stress in chronic renal failure. *Free Radic Res*, **29**, 1-11.
- Hees, H. & Sinowatz, F. (2000) Harnorgane. *Histologie: Kurzlehrbuch der Zytologie und mikroskopischen Anatomie*, pp. 285-298. Deutscher Ärzte-Verlag, Köln.
- Herbach, N., Goeke, B., Schneider, M., Hermanns, W., Wolf, E. & Wanke, R. (2005) Overexpression of a dominant negative GIP receptor in transgenic mice results in disturbed postnatal pancreatic islet and beta-cell development. *Regul Pept*, **125**, 103-17.
- Hirono, Y., Yoshimoto, T., Suzuki, N., Sugiyama, T., Sakurada, M., Takai, S., Kobayashi, N., Shichiri, M. & Hirata, Y. (2007) Angiotensin II receptor type 1-mediated vascular oxidative stress and proinflammatory gene expression in aldosterone-induced hypertension: the possible role of local renin-angiotensin system. *Endocrinology*, **148**, 1688-96.
- Hirst, G.K. (1979) Frank Lippin Horsfall, Jr. 1906-1971. A Biographical Memoir. In, pp. 231-267. National Academy of Sciences, Washington D.C. .
- Horton, J.K., Davies, M., Topley, N., Thomas, D. & Williams, J.D. (1990) Activation of the inflammatory response of neutrophils by Tamm-Horsfall glycoprotein. *Kidney Int*, **37**, 717-26.
- Hoyer, J.R. & Seiler, M.W. (1979) Pathophysiology of Tamm-Horsfall protein. *Kidney Int*, **16**, 279-89.
- Hoyer, J.R., Sisson, S.P. & Vernier, R.L. (1979) Tamm-Horsfall glycoprotein: ultrastructural immunoperoxidase localization in rat kidney. *Lab Invest*, **41**, 168-73.
- Hrabe de Angelis, M.H., Flaswinkel, H., Fuchs, H., Rathkolb, B., Soewarto, D., Marschall, S., Heffner, S., Pargent, W., Wuensch, K., Jung, M., Reis, A., Richter, T., Alessandrini, F., Jakob, T., Fuchs, E., Kolb, H., Kremmer, E., Schaeble, K., Rollinski, B., Roscher, A., Peters, C., Meitinger, T., Strom, T., Steckler, T., Holsboer, F., Klopstock, T., Gekeler, F., Schindewolf, C., Jung, T., Avraham, K., Behrendt, H., Ring, J., Zimmer, A., Schughart, K., Pfeiffer, K., Wolf, E. & Balling, R. (2000) Genome-wide, large-scale production of mutant mice by ENU mutagenesis. *Nat Genet*, **25**, 444-7.

- http://www.genenames.org/data/hgnc_data.php?hgnc_id=12559 *UMOD*. Available at: http://www.genenames.org/data/hgnc_data.php?hgnc_id=12559 (accessed
- <http://www.uniprot.org/uniprot/Q91X17> <http://www.uniprot.org/uniprot/Q91X17>. Available at: (accessed
- Hubbard, S.C. & Ivatt, R.J. (1981) Synthesis and processing of asparagine-linked oligosaccharides. *Annu Rev Biochem*, **50**, 555-83.
- Hurtley, S.M. & Helenius, A. (1989) Protein oligomerization in the endoplasmic reticulum. *Annu Rev Cell Biol*, **5**, 277-307.
- Iannitti, T. & Palmieri, B. (2011) Clinical and experimental applications of sodium phenylbutyrate. *Drugs R D*, **11**, 227-49.
- Iannone, A., Bini, A., Swartz, H.M., Tomasi, A. & Vannini, V. (1989) Metabolism in rat liver microsomes of the nitroxide spin probe tempol. *Biochem Pharmacol*, **38**, 2581-6.
- Ishikawa, T., Taniguchi, Y., Okada, T., Takeda, S. & Mori, K. (2011) Vertebrate unfolded protein response: mammalian signaling pathways are conserved in Medaka fish. *Cell Struct Funct*, **36**, 247-59.
- Iwai, N., Kajimoto, K., Kokubo, Y. & Tomoike, H. (2006) Extensive genetic analysis of 10 candidate genes for hypertension in Japanese. *Hypertension*, **48**, 901-7.
- Jennings, P., Aydin, S., Kotanko, P., Lechner, J., Lhotta, K., Williams, S., Thakker, R.V. & Pfaller, W. (2007) Membrane targeting and secretion of mutant uromodulin in familial juvenile hyperuricemic nephropathy. *J Am Soc Nephrol*, **18**, 264-73.
- Jovine, L., Qi, H., Williams, Z., Litscher, E. & Wassarman, P.M. (2002) The ZP domain is a conserved module for polymerization of extracellular proteins. *Nat Cell Biol*, **4**, 457-61.
- Kamatani, N., Moritani, M., Yamanaka, H., Takeuchi, F., Hosoya, T. & Itakura, M. (2000) Localization of a gene for familial juvenile hyperuricemic nephropathy causing underexcretion-type gout to 16p12 by genome-wide linkage analysis of a large family. *Arthritis Rheum*, **43**, 925-9.
- Kamatania, M., Yasui, H., Ogata, T. & Sakurai, H. (2002) Local pharmacokinetic analysis of a stable spin probe in mice by in vivo L-band ESR with surface-coil-type resonators. *Free Radic Res*, **36**, 1115-25.
- Kasumov, T., Brunengraber, L.L., Comte, B., Puchowicz, M.A., Jobbins, K., Thomas, K., David, F., Kinman, R., Wehrli, S., Dahms, W., Kerr, D., Nissim, I. & Brunengraber, H. (2004) New secondary metabolites of phenylbutyrate in humans and rats. *Drug Metab Dispos*, **32**, 10-9.
- Kemter, E. (2012) Personal communication. In:

- Kemter, E., Rathkolb, B., Rozman, J., Hans, W., Schrewe, A., Landbrecht, C., Klaften, M., Ivandic, B., Fuchs, H., Gailus-Durner, V., Klingenspor, M., de Angelis, M.H., Wolf, E., Wanke, R. & Aigner, B. (2009) Novel missense mutation of uromodulin in mice causes renal dysfunction with alterations in urea handling, energy, and bone metabolism. *Am J Physiol Renal Physiol*, **297**, 19.
- Klausner, R.D. & Sitia, R. (1990) Protein degradation in the endoplasmic reticulum. *Cell*, **62**, 611-4.
- König, H.E., Maierl, J. & Liebich, H.G. (2002) Harnorgane (Organa urinaria). *Anatomie der Haussäugetiere: Lehrbuch und Farbatlas für Studium und Praxis* (ed. by H.E. König and H.G. Liebich), pp. 103-118. Schattauer, Stuttgart.
- Kornfeld, R. & Kornfeld, S. (1985) Assembly of asparagine-linked oligosaccharides. *Annu Rev Biochem*, **54**, 631-64.
- Kottgen, A., Yang, Q., Shimmin, L.C., Tin, A., Schaeffer, C., Coresh, J., Liu, X., Rampoldi, L., Hwang, S.J., Boerwinkle, E., Hixson, J.E., Kao, W.H. & Fox, C.S. (2012) Association of estimated glomerular filtration rate and urinary uromodulin concentrations with rare variants identified by UMOD gene region sequencing. *PLoS One*, **7**, 31.
- Kozutsumi, Y., Segal, M., Normington, K., Gething, M.J. & Sambrook, J. (1988) The presence of malfolded proteins in the endoplasmic reticulum signals the induction of glucose-regulated proteins. *Nature*, **332**, 462-4.
- Kreft, B., Jabs, W.J., Laskay, T., Klinger, M., Solbach, W., Kumar, S. & van Zandbergen, G. (2002) Polarized expression of Tamm-Horsfall protein by renal tubular epithelial cells activates human granulocytes. *Infect Immun*, **70**, 2650-6.
- Krishna, M.C., Grahame, D.A., Samuni, A., Mitchell, J.B. & Russo, A. (1992) Oxoammonium cation intermediate in the nitroxide-catalyzed dismutation of superoxide. *Proc Natl Acad Sci U S A*, **89**, 5537-41.
- Krishna, M.C., Russo, A., Mitchell, J.B., Goldstein, S., Dafni, H. & Samuni, A. (1996) Do nitroxide antioxidants act as scavengers of O₂⁻. or as SOD mimics? *J Biol Chem*, **271**, 26026-31.
- Kudo, E., Kamatani, N., Tezuka, O., Taniguchi, A., Yamanaka, H., Yabe, S., Osabe, D., Shinohara, S., Nomura, K., Segawa, M., Miyamoto, T., Moritani, M., Kunika, K. & Itakura, M. (2004) Familial juvenile hyperuricemic nephropathy: detection of mutations in the uromodulin gene in five Japanese families. *Kidney Int*, **65**, 1589-97.
- Kuhlmann, U., Walb, D., Böhler, J. & Luft, F.C. (2008) *Nephrologie: Pathophysiologie - Klinik - Nierenersatzverfahren*. Georg Thieme Verlag KG, Stuttgart.
- Kumar, S. (2007) Mechanism of injury in uromodulin-associated kidney disease. In. *J Am Soc Nephrol*. 2007 Jan;18(1):10-2. Epub 2006 Dec 20.

- Kumar, S. & Muchmore, A. (1990) Tamm-Horsfall protein--uromodulin (1950-1990). *Kidney Int*, **37**, 1395-401.
- Labriola, L., in Dahan, K. & Pirson, Y. (2007) Outcome of kidney transplantation in familial juvenile hyperuricaemic nephropathy. *Nephrol Dial Transplant*, **22**, 3070-3.
- Lai, E.Y., Luo, Z., Onozato, M.L., Rudolph, E.H., Solis, G., Jose, P.A., Wellstein, A., Aslam, S., Quinn, M.T., Griendling, K., Le, T., Li, P., Palm, F., Welch, W.J. & Wilcox, C.S. (2012) Effects of the antioxidant drug tempol on renal oxygenation in mice with reduced renal mass. *Am J Physiol Renal Physiol*, **303**, 4.
- Lee, S. & Tsai, F.T. (2005) Molecular chaperones in protein quality control. *J Biochem Mol Biol*, **38**, 259-65.
- Lens, X.M., Banet, J.F., Outeda, P. & Barrio-Lucia, V. (2005) A novel pattern of mutation in uromodulin disorders: autosomal dominant medullary cystic kidney disease type 2, familial juvenile hyperuricemic nephropathy, and autosomal dominant glomerulocystic kidney disease. *Am J Kidney Dis*, **46**, 52-7.
- Li, L., Garikepati, R.M., Tsukerman, S., Tiwari, S. & Ecelbarger, C.M. (2012) Salt sensitivity of nitric oxide generation and blood pressure in mice with targeted knockout of the insulin receptor from the renal tubule. *Am J Physiol Regul Integr Comp Physiol*, **303**, 18.
- Luo, Z.F., Feng, B., Mu, J., Qi, W., Zeng, W., Guo, Y.H., Pang, Q., Ye, Z.L., Liu, L. & Yuan, F.H. (2010) Effects of 4-phenylbutyric acid on the process and development of diabetic nephropathy induced in rats by streptozotocin: regulation of endoplasmic reticulum stress-oxidative activation. *Toxicol Appl Pharmacol*, **246**, 49-57.
- Ma, L., Liu, Y., El-Achkar, T.M. & Wu, X.R. (2012) Molecular and cellular effects of Tamm-Horsfall protein mutations and their rescue by chemical chaperones. *J Biol Chem*, **287**, 1290-305.
- Ma, Y. & Hendershot, L.M. (2002) The mammalian endoplasmic reticulum as a sensor for cellular stress. *Cell Stress Chaperones*, **7**, 222-9.
- Malagolini, N., Cavallone, D. & Serafini-Cessi, F. (1997) Intracellular transport, cell-surface exposure and release of recombinant Tamm-Horsfall glycoprotein. *Kidney Int*, **52**, 1340-50.
- Malhotra, J.D. & Kaufman, R.J. (2007) Endoplasmic reticulum stress and oxidative stress: a vicious cycle or a double-edged sword? *Antioxid Redox Signal*, **9**, 2277-93.
- Malo, A., Kruger, B., Goke, B. & Kubisch, C.H. (2012) 4-Phenylbutyric Acid Reduces Endoplasmic Reticulum Stress, Trypsin Activation, and Acinar Cell Apoptosis While Increasing Secretion in Rat Pancreatic Acini. *Pancreas*, **10**, 10.
- Martin-Mateo, M.C., Sanchez-Portugal, M., Iglesias, S., de Paula, A. & Bustamante, J. (1999) Oxidative stress in chronic renal failure. *Ren Fail*, **21**, 155-67.

- Martinez, I.M. & Chrispeels, M.J. (2003) Genomic analysis of the unfolded protein response in *Arabidopsis* shows its connection to important cellular processes. *Plant Cell*, **15**, 561-76.
- Martinez, J.J., Mulvey, M.A., Schilling, J.D., Pinkner, J.S. & Hultgren, S.J. (2000) Type 1 pilus-mediated bacterial invasion of bladder epithelial cells. *Embo J*, **19**, 2803-12.
- McGavin, M.D. & Zachary, J.F. (2009) Harnorgane. *Pathologie der Haustiere* (ed. by M.D. McGavin and J.F. Zachary), pp. 571-582. Elsevier GmbH, München, Munich.
- McGuire, B.M., Zupanets, I.A., Lowe, M.E., Xiao, X., Sypliy, V.A., Monteleone, J., Gargosky, S., Dickinson, K., Martinez, A., Mokhtarani, M. & Scharschmidt, B.F. (2010) Pharmacology and safety of glycerol phenylbutyrate in healthy adults and adults with cirrhosis. *Hepatology*, **51**, 2077-85.
- Mercuri, E., Bertini, E., Messina, S., Pelliccioni, M., D'Amico, A., Colitto, F., Mirabella, M., Tiziano, F.D., Vitali, T., Angelozzi, C., Kinali, M., Main, M. & Brahe, C. (2004) Pilot trial of phenylbutyrate in spinal muscular atrophy. *Neuromuscul Disord*, **14**, 130-5.
- Misawa, T., Hayashi, H., Sugiyama, Y. & Hashimoto, Y. (2012) Discovery and structural development of small molecules that enhance transport activity of bile salt export pump mutant associated with progressive familial intrahepatic cholestasis type 2. *Bioorg Med Chem*, **20**, 2940-9.
- Mo, L., Huang, H.Y., Zhu, X.H., Shapiro, E., Hasty, D.L. & Wu, X.R. (2004a) Tamm-Horsfall protein is a critical renal defense factor protecting against calcium oxalate crystal formation. *Kidney Int*, **66**, 1159-66.
- Mo, L., Zhu, X.H., Huang, H.Y., Shapiro, E., Hasty, D.L. & Wu, X.R. (2004b) Ablation of the Tamm-Horsfall protein gene increases susceptibility of mice to bladder colonization by type 1-fimbriated *Escherichia coli*. *Am J Physiol Renal Physiol*, **286**, 9.
- Mo, L., Liaw, L., Evan, A.P., Sommer, A.J., Lieske, J.C. & Wu, X.R. (2007) Renal calcinosis and stone formation in mice lacking osteopontin, Tamm-Horsfall protein, or both. *Am J Physiol Renal Physiol*, **293**, 26.
- Moldave, K. & Meister, A. (1957) Synthesis of phenylacetylglutamine by human tissue. *J Biol Chem*, **229**, 463-76.
- Moonen, P. & Williamson, K. *Bioassay for interleukin-1 inhibitors*. *J Immunol Methods*. 1987 Sep 24;102(2):283-4.
- Moore, K.A. & Hollien, J. (2012) The Unfolded Protein Response in Secretory Cell Function. *Annu Rev Genet*, **28**, 28.
- Moro, F., Simmonds, H.A., Cameron, J.S., Ogg, C.S., Williams, G.D., McBride, M.B. & Davis, P.M. (1991) Does allopurinol affect the progression of familial juvenile gouty nephropathy? *Adv Exp Med Biol*, 199-202.

- Muchmore, A.V. & Decker, J.M. (1985) Uromodulin: a unique 85-kilodalton immunosuppressive glycoprotein isolated from urine of pregnant women. *Science*, **229**, 479-81.
- Mulisch, M. & Welsch, U. (2010) *Romeis - Mikroskopische Technik*. Spektrum Akademischer Verlag.
- Nasr, S.H., Lucia, J.P., Galgano, S.J., Markowitz, G.S. & D'Agati, V.D. (2008) Uromodulin storage disease. *Kidney Int*, **73**, 971-6.
- Nie, J. & Hou, F.F. (2012) Role of reactive oxygen species in the renal fibrosis. *Chin Med J*, **125**, 2598-602.
- Nishikawa, S., Brodsky, J.L. & Nakatsukasa, K. (2005) Roles of molecular chaperones in endoplasmic reticulum (ER) quality control and ER-associated degradation (ERAD). *J Biochem*, **137**, 551-5.
- Okamoto, K. & Aoki, K. (1963) Development of a strain of spontaneously hypertensive rats. *Jpn Circ J*, **27**, 282-93.
- Olczak, T., Olczak, M., Kubicz, A., Dulawa, J. & Kokot, F. (1999a) Composition of the sugar moiety of Tamm-Horsfall protein in patients with urinary diseases. *Int J Clin Lab Res*, **29**, 68-74.
- Olczak, T., Olczak, M., Dereniowska, M., Strzelczyk, R. & Kubicz, A. (1999b) Alterations of the sugar moiety of Tamm-Horsfall protein in children with malignancies of lymphoid cells. *Electrophoresis*, **20**, 1382-9.
- Ortiz, P.A. & Garvin, J.L. (2002) Interaction of O₂(-) and NO in the thick ascending limb. *Hypertension*, **39**, 591-6.
- Oteki, T., Nagase, S., Yokoyama, H., Ohya, H., Akatsuka, T., Tada, M., Ueda, A., Hirayama, A. & Koyama, A. (2005) Evaluation of adriamycin nephropathy by an in vivo electron paramagnetic resonance. *Biochem Biophys Res Commun*, **332**, 326-31.
- Ozcan, U., Yilmaz, E., Ozcan, L., Furuhashi, M., Vaillancourt, E., Smith, R.O., Gorgun, C.Z. & Hotamisligil, G.S. (2006) Chemical chaperones reduce ER stress and restore glucose homeostasis in a mouse model of type 2 diabetes. *Science*, **313**, 1137-40.
- Pacher, P., Nivorozhkin, A. & Szabo, C. (2006) Therapeutic effects of xanthine oxidase inhibitors: renaissance half a century after the discovery of allopurinol. *Pharmacol Rev*, **58**, 87-114.
- Padmanabhan, S., Melander, O., Johnson, T., Di Blasio, A.M., Lee, W.K., Gentilini, D., Hastie, C.E., Menni, C., Monti, M.C., Delles, C., Laing, S., Corso, B., Navis, G., Kwakernaak, A.J., van der Harst, P., Bochud, M., Maillard, M., Burnier, M., Hedner, T., Kjeldsen, S., Wahlstrand, B., Sjogren, M., Fava, C., Montagnana, M., Danese, E., Torffvit, O., Hedblad, B., Snieder, H., Connell, J.M., Brown, M., Samani, N.J., Farrall, M., Cesana,

- G., Mancina, G., Signorini, S., Grassi, G., Eyheramendy, S., Wichmann, H.E., Laan, M., Strachan, D.P., Sever, P., Shields, D.C., Stanton, A., Vollenweider, P., Teumer, A., Volzke, H., Rettig, R., Newton-Cheh, C., Arora, P., Zhang, F., Soranzo, N., Spector, T.D., Lucas, G., Kathiresan, S., Siscovick, D.S., Luan, J., Loos, R.J., Wareham, N.J., Penninx, B.W., Nolte, I.M., McBride, M., Miller, W.H., Nicklin, S.A., Baker, A.H., Graham, D., McDonald, R.A., Pell, J.P., Sattar, N., Welsh, P., Munroe, P., Caulfield, M.J., Zanchetti, A. & Dominiczak, A.F. (2010) Genome-wide association study of blood pressure extremes identifies variant near UMOD associated with hypertension. *PLoS Genet*, **6**
- Pak, J., Pu, Y., Zhang, Z.T., Hasty, D.L. & Wu, X.R. (2001) Tamm-Horsfall protein binds to type 1 fimbriated *Escherichia coli* and prevents *E. coli* from binding to uroplakin Ia and Ib receptors. *J Biol Chem*, **276**, 9924-30.
- Pakula, T.M., Laxell, M., Huuskonen, A., Uusitalo, J., Saloheimo, M. & Penttila, M. (2003) The effects of drugs inhibiting protein secretion in the filamentous fungus *Trichoderma reesei*. Evidence for down-regulation of genes that encode secreted proteins in the stressed cells. *J Biol Chem*, **278**, 45011-20.
- Patel, K., Chen, Y., Dennehy, K., Blau, J., Connors, S., Mendonca, M., Tarpey, M., Krishna, M., Mitchell, J.B., Welch, W.J. & Wilcox, C.S. (2006) Acute antihypertensive action of nitroxides in the spontaneously hypertensive rat. *Am J Physiol Regul Integr Comp Physiol*, **290**, 22.
- Pennica, D., Kohr, W.J., Kuang, W.J., Glaister, D., Aggarwal, B.B., Chen, E.Y. & Goeddel, D.V. (1987) Identification of human uromodulin as the Tamm-Horsfall urinary glycoprotein. *Science*, **236**, 83-8.
- Pollak, V.E. & Arbel, C. (1969) The distribution of Tamm Horsfall mucoprotein (uromucoid) in the human nephron. *Nephron*, **6**, 667-72.
- Prajczek, S., Heidenreich, U., Pfaller, W., Kotanko, P., Lhotta, K. & Jennings, P. (2010) Evidence for a role of uromodulin in chronic kidney disease progression. *Nephrol Dial Transplant*, **25**, 1896-903.
- Prueckl, P. (2011) *Untersuchung zweier ENU-induzierter mutanter Mauslinien mit Fokus auf eine Linie mit einer Punktmutation im Uromodulin-Gen*. Ludwig-Maximilians-University Munich, Munich.
- Qi, W., Mu, J., Luo, Z.F., Zeng, W., Guo, Y.H., Pang, Q., Ye, Z.L., Liu, L., Yuan, F.H. & Feng, B. (2011) Attenuation of diabetic nephropathy in diabetes rats induced by streptozotocin by regulating the endoplasmic reticulum stress inflammatory response. *Metabolism*, **60**, 594-603.
- Qi, X., Hosoi, T., Okuma, Y., Kaneko, M. & Nomura, Y. (2004) Sodium 4-phenylbutyrate protects against cerebral ischemic injury. *Mol Pharmacol*, **66**, 899-908.

- Racusen, L.C., Solez, K., Colvin, R.B., Bonsib, S.M., Castro, M.C., Cavallo, T., Croker, B.P., Demetris, A.J., Drachenberg, C.B., Fogo, A.B., Furness, P., Gaber, L.W., Gibson, I.W., Glotz, D., Goldberg, J.C., Grande, J., Halloran, P.F., Hansen, H.E., Hartley, B., Hayry, P.J., Hill, C.M., Hoffman, E.O., Hunsicker, L.G., Lindblad, A.S., Yamaguchi, Y. & et al. (1999) The Banff 97 working classification of renal allograft pathology. *Kidney Int*, **55**, 713-23.
- Raffi, H.S., Bates, J.M., Jr., Laszik, Z. & Kumar, S. (2005) Tamm-Horsfall protein acts as a general host-defense factor against bacterial cystitis. *Am J Nephrol*, **25**, 570-8.
- Rambourg, A. & Leblond, C.P. (1967) Staining of basement membranes and associated structures by the periodic acid-Schiff and periodicacid-silver methenamine techniques. *J Ultrastruct Res*, **20**, 306-9.
- Rampoldi, L., Scolari, F., Amoroso, A., Ghiggeri, G. & Devuyst, O. (2011) The rediscovery of uromodulin (Tamm-Horsfall protein): from tubulointerstitial nephropathy to chronic kidney disease. *Kidney Int*, **80**, 338-47.
- Rampoldi, L., Caridi, G., Santon, D., Boaretto, F., Bernascone, I., Lamorte, G., Tardanico, R., Dagnino, M., Colussi, G., Scolari, F., Ghiggeri, G.M., Amoroso, A. & Casari, G. (2003) Allelism of MCKD, FJHN and GCKD caused by impairment of uromodulin export dynamics. *Hum Mol Genet*, **12**, 3369-84.
- Rathkolb, B., Fuchs, E., Kolb, H.J., Renner-Muller, I., Krebs, O., Balling, R., Hrabe de Angelis, M. & Wolf, E. (2000a) Large-scale N-ethyl-N-nitrosourea mutagenesis of mice--from phenotypes to genes. *Exp Physiol*, **85**, 635-44.
- Rathkolb, B., Decker, T., Fuchs, E., Soewarto, D., Fella, C., Heffner, S., Pargent, W., Wanke, R., Balling, R., Hrabe de Angelis, M., Kolb, H.J. & Wolf, E. (2000b) The clinical-chemical screen in the Munich ENU Mouse Mutagenesis Project: screening for clinically relevant phenotypes. *Mamm Genome*, **11**, 543-6.
- Reilly, R.F. & Ellison, D.H. (2000) Mammalian distal tubule: physiology, pathophysiology, and molecular anatomy. *Physiol Rev*, **80**, 277-313.
- Resnick, J.S., Sisson, S. & Vernier, R.L. (1978) TAMM-HORSFALL PROTEIN ABNORMAL LOCALIZATION IN RENAL-DISEASE. *Laboratory Investigation*, **38**, 550-555.
- Rezende-Lima, W., Parreira, K.S., Garcia-Gonzalez, M., Riveira, E., Banet, J.F. & Lens, X.M. (2004) Homozygosity for uromodulin disorders: FJHN and MCKD-type 2. *Kidney Int*, **66**, 558-63.
- Rhodes, D.C., Hinsman, E.J. & Rhodes, J.A. (1993) Tamm-Horsfall glycoprotein binds IgG with high affinity. *Kidney Int*, **44**, 1014-21.
- Rindler, M.J., Naik, S.S., Li, N., Hoops, T.C. & Peraldi, M.N. (1990) Uromodulin (Tamm-Horsfall glycoprotein/uromuoid) is a phosphatidylinositol-linked membrane protein. *J Biol Chem*, **265**, 20784-9.

- Rubenstein, R.C. & Zeitlin, P.L. (2000) Sodium 4-phenylbutyrate downregulates Hsc70: implications for intracellular trafficking of DeltaF508-CFTR. *Am J Physiol Cell Physiol*, **278**, C259-67.
- Rutkowski, D.T. & Kaufman, R.J. (2004) A trip to the ER: coping with stress. *Trends Cell Biol*, **14**, 20-8.
- Santambrogio, S., Cattaneo, A., Bernascone, I., Schwend, T., Jovine, L., Bachi, A. & Rampoldi, L. (2008) Urinary uromodulin carries an intact ZP domain generated by a conserved C-terminal proteolytic cleavage. *Biochem Biophys Res Commun*, **370**, 410-3.
- Sarkar, A., Das, J., Manna, P. & Sil, P.C. (2011) Nano-copper induces oxidative stress and apoptosis in kidney via both extrinsic and intrinsic pathways. *Toxicology*, **290**, 208-17.
- Scandinavian Formulas, I. (2011) Technical Mechanisms of Action, Pharmacokinetics, Safety and Clinical Use in Humans for Sodium Phenylbutyrate. In: (ed. I. Scandinavian Formulas), Sellersville, PA, USA.
- Schaeffer, C., Cattaneo, A., Trudu, M., Santambrogio, S., Bernascone, I., Giachino, D., Caridi, G., Campo, A., Murtas, C., Benoni, S., Izzi, C., De Marchi, M., Amoroso, A., Ghiggeri, G.M., Scolari, F., Bachi, A. & Rampoldi, L. (2012) Urinary secretion and extracellular aggregation of mutant uromodulin isoforms. *Kidney Int*, **81**, 769-78.
- Schaffer, P., Gombos, E., Meichelbeck, K., Kiss, A., Hart, P.S. & Bleyer, A.J. (2010) Childhood course of renal insufficiency in a family with a uromodulin gene mutation. *Pediatr Nephrol*, **25**, 1355-60.
- Schainuck, L.I., Striker, G.E., Cutler, R.E. & Benditt, E.P. (1970) Structural-functional correlations in renal disease. II. The correlations. *Hum Pathol*, **1**, 631-41.
- Schenk, E.A., Schwartz, R.H. & Lewis, R.A. (1971) Tamm-Horsfall mucoprotein. I. Localization in the kidney. *Lab Invest*, **25**, 92-5.
- Schmidt, R.F., Lang, F. & Heckmann, M. (2010) *Physiologie des Menschen: mit Pathophysiologie*. Springer Medizin Verlag, Heidelberg.
- Schrag, J.D., Procopio, D.O., Cygler, M., Thomas, D.Y. & Bergeron, J.J. (2003) Lectin control of protein folding and sorting in the secretory pathway. *Trends Biochem Sci*, **28**, 49-57.
- Schroder, M. & Kaufman, R.J. (2005) ER stress and the unfolded protein response. *Mutat Res*, **569**, 29-63.
- Scolari, F., Caridi, G., Rampoldi, L., Tardanico, R., Izzi, C., Pirulli, D., Amoroso, A., Casari, G. & Ghiggeri, G.M. (2004) Uromodulin storage diseases: clinical aspects and mechanisms. *Am J Kidney Dis*, **44**, 987-99.
- Scolari, F., Ghiggeri, G.M., Casari, G., Amoroso, A., Puzzer, D., Caridi, G.L., Valzorio, B., Tardanico, R., Vizzardì, V., Savoldi, S., Viola, B.F., Bossini, N., Prati, E., Gusmano, R.

- & Maiorca, R. (1998) Autosomal dominant medullary cystic disease: a disorder with variable clinical pictures and exclusion of linkage with the NPH1 locus. *Nephrol Dial Transplant*, **13**, 2536-46.
- Serafini-Cessi, F., Franceschi, C. & Sperti, S. (1979) Specific interaction of human Tamm-Horsfall glycoprotein with leucoagglutinin, a lectin from *Phaseolus vulgaris* (red kidney bean). *Biochem J*, **183**, 381-8.
- Serafini-Cessi, F., Malagolini, N. & Cavallone, D. (2003) Tamm-Horsfall glycoprotein: biology and clinical relevance. *Am J Kidney Dis*, **42**, 658-76.
- Sharon, N. (1987) Bacterial lectins, cell-cell recognition and infectious disease. *FEBS Lett*, **217**, 145-57.
- Sharp, C.K., Bergman, S.M., Stockwin, J.M., Robbin, M.L., Galliani, C. & Guay-Woodford, L.M. (1997) Dominantly transmitted glomerulocystic kidney disease: a distinct genetic entity. *J Am Soc Nephrol*, **8**, 77-84.
- Shore, G.C., Papa, F.R. & Oakes, S.A. (2011) Signaling cell death from the endoplasmic reticulum stress response. *Curr Opin Cell Biol*, **23**, 143-9.
- Sigma-Aldrich, C. (2011) 4-Hydroxy-TEMPO. In:
- Silbernagl, S. & Lang, F. (2005) Niere, Salz-Wasser-Haushalt. *Taschenatlas der Pathophysiologie*, pp. 92-131. Georg Thieme Verlag KG, Stuttgart.
- Smith, G.D., Robinson, C., Stewart, A.P., Edwards, E.L., Karet, H.I., Norden, A.G., Sandford, R.N. & Karet Frankl, F.E. (2011) Characterization of a recurrent in-frame UMOD indel mutation causing late-onset autosomal dominant end-stage renal failure. *Clin J Am Soc Nephrol*, **6**, 2766-74.
- Spira, A.I. & Carducci, M.A. (2003) Differentiation therapy. *Curr Opin Pharmacol*, **3**, 338-43.
- Stevenson, F.K., Cleave, A.J. & Kent, P.W. (1971) The effect of ions on the viscometric and ultracentrifugal behaviour of Tamm-Horsfall glycoprotein. *Biochim Biophys Acta*, **236**, 59-66.
- Takiue, Y., Hosoyamada, M., Yokoo, T., Kimura, M. & Shibasaki, T. (2008a) Progressive accumulation of intrinsic mouse uromodulin in the kidneys of transgenic mice harboring the mutant human uromodulin gene. *Biol Pharm Bull*, **31**, 405-11.
- Takiue, Y., Hosoyamada, M., Yokoo, T., Kimura, M., Ochiai, M., Kaneko, K., Ichida, K., Hosoya, T. & Shibasaki, T. (2008b) Production and characterization of transgenic mice harboring mutant human UMOD gene. *Nucleosides Nucleotides Nucleic Acids*, **27**, 596-600.
- Tamm, I. & Horsfall, F.L., Jr. (1950) Characterization and separation of an inhibitor of viral hemagglutination present in urine. *Proc Soc Exp Biol Med*, **74**, 106-8.

- Tamm, I. & Horsfall, F.L., Jr. (1952) A mucoprotein derived from human urine which reacts with influenza, mumps, and Newcastle disease viruses. *J Exp Med*, **95**, 71-97.
- Thomas, D.B., Davies, M., Peters, J.R. & Williams, J.D. (1993) Tamm Horsfall protein binds to a single class of carbohydrate specific receptors on human neutrophils. *Kidney Int*, **44**, 423-9.
- Travers, K.J., Patil, C.K., Wodicka, L., Lockhart, D.J., Weissman, J.S. & Walter, P. (2000) Functional and genomic analyses reveal an essential coordination between the unfolded protein response and ER-associated degradation. *Cell*, **101**, 249-58.
- Trombetta, E.S. & Parodi, A.J. (2003) Quality control and protein folding in the secretory pathway. *Annu Rev Cell Dev Biol*, **19**, 649-76.
- Ueda, A., Nagase, S., Yokoyama, H., Tada, M., Ohya, H., Kamada, H., Hirayama, A. & Koyama, A. (2002) Identification by an EPR technique of decreased mitochondrial reducing activity in puromycin aminonucleoside-induced nephrosis. *Free Radic Biol Med*, **33**, 1082-8.
- Ueda, A., Nagase, S., Yokoyama, H., Tada, M., Noda, H., Ohya, H., Kamada, H., Hirayama, A. & Koyama, A. (2003) Importance of renal mitochondria in the reduction of TEMPOL, a nitroxide radical. *Mol Cell Biochem*, **244**, 119-24.
- van Rooijen, J.J., Voskamp, A.F., Kamerling, J.P. & Vliegenthart, J.F. (1999) Glycosylation sites and site-specific glycosylation in human Tamm-Horsfall glycoprotein. *Glycobiology*, **9**, 21-30.
- Vaziri, N.D., Ding, Y. & Ni, Z. (2001) Compensatory up-regulation of nitric-oxide synthase isoforms in lead-induced hypertension; reversal by a superoxide dismutase-mimetic drug. *J Pharmacol Exp Ther*, **298**, 679-85.
- von Engelhardt, W. (2012) Niere. *Physiologie der Haustiere* (ed. by W. Von Engelhardt), pp. 292-320. Enke Verlag, Stuttgart.
- Vylet'al, P., Kublova, M., Kalbacova, M., Hodanova, K., Baresova, V., Stiburkova, B., Sikora, J., Hulkova, H., Zivny, J., Majewski, J., Simmonds, A., Fryns, J.P., Venkat-Raman, G., Elleder, M. & Kmoch, S. (2006) Alterations of uromodulin biology: a common denominator of the genetically heterogeneous FJHN/MCKD syndrome. *Kidney Int*, **70**, 1155-69.
- Vyletal, P., Bleyer, A.J. & Kmoch, S. (2010) Uromodulin biology and pathophysiology--an update. *Kidney Blood Press Res*, **33**, 456-75.
- Wang, D., Chen, Y., Chabrashvili, T., Aslam, S., Borrego Conde, L.J., Umans, J.G. & Wilcox, C.S. (2003) Role of oxidative stress in endothelial dysfunction and enhanced responses to angiotensin II of afferent arterioles from rabbits infused with angiotensin II. *J Am Soc Nephrol*, **14**, 2783-9.

- Wanke, R. (1996) *Charakterisierung der renalen Alterationen Wachstumshormon-transgener Mäuse: Ein Beitrag zur Morpho- und Pathogenese der progressiven Glomerulosklerose.*
- Wanke, R., Weis, S., Kluge, D., Kahnt, E., Schenck, E., Brem, G. & W., H. (1994) Morphometric evaluation of the pancreas of growth hormone-transgenic mice. *Acta Stereologica*,
- Wei, X., Xu, R., Yang, Z., Li, Z., Liao, Y., Johnson, R.J., Yu, X. & Chen, W. (2012) Novel uromodulin mutation in familial juvenile hyperuricemic nephropathy. *Am J Nephrol*, **36**, 114-20.
- Weibel, E.R. (1979) I. Practical methods for biological morphometry. . *Stereological methods*. Academic Press, London.
- Welch, W.J. & Brown, C.R. (1996) Influence of molecular and chemical chaperones on protein folding. *Cell Stress Chaperones*, **1**, 109-15.
- Welch, W.J., Mendonca, M., Aslam, S. & Wilcox, C.S. (2003) Roles of oxidative stress and AT1 receptors in renal hemodynamics and oxygenation in the postclipped 2K,1C kidney. *Hypertension*, **41**, 692-6.
- Welch, W.J., Mendonca, M., Blau, J., Karber, A., Dennehy, K., Patel, K., Lao, Y.S., Jose, P.A. & Wilcox, C.S. (2005) Antihypertensive response to prolonged tempol in the spontaneously hypertensive rat. *Kidney Int*, **68**, 179-87.
- Werner, J.M., Knott, V., Handford, P.A., Campbell, I.D. & Downing, A.K. (2000) Backbone dynamics of a cbEGF domain pair in the presence of calcium. *J Mol Biol*, **296**, 1065-78.
- Wiggins, R.C. (1987) Uromuroid (Tamm-Horsfall glycoprotein) forms different polymeric arrangements on a filter surface under different physicochemical conditions. *Clin Chim Acta*, **162**, 329-40.
- Wilcox, C.S. (2010) Effects of tempol and redox-cycling nitroxides in models of oxidative stress. *Pharmacol Ther*, **126**, 119-45.
- Wilcox, C.S. & Pearlman, A. (2008) Chemistry and antihypertensive effects of tempol and other nitroxides. *Pharmacol Rev*, **60**, 418-69.
- Williams, S.E., Reed, A.A., Galvanovskis, J., Antignac, C., Goodship, T., Karet, F.E., Kotanko, P., Lhotta, K., Moriniere, V., Williams, P., Wong, W., Rorsman, P. & Thakker, R.V. (2009) Uromodulin mutations causing familial juvenile hyperuricaemic nephropathy lead to protein maturation defects and retention in the endoplasmic reticulum. *Hum Mol Genet*, **18**, 2963-74.
- Wolf, M.T., Mucha, B.E., Attanasio, M., Zalewski, I., Karle, S.M., Neumann, H.P., Rahman, N., Bader, B., Baldamus, C.A., Otto, E., Witzgall, R., Fuchshuber, A. & Hildebrandt, F. (2003) Mutations of the Uromodulin gene in MCKD type 2 patients cluster in exon 4, which encodes three EGF-like domains. *Kidney Int*, **64**, 1580-7.

- Wolf, M.T., Beck, B.B., Zaucke, F., Kunze, A., Misselwitz, J., Ruley, J., Ronda, T., Fischer, A., Eifinger, F., Licht, C., Otto, E., Hoppe, B. & Hildebrandt, F. (2007) The Uromodulin C744G mutation causes MCKD2 and FJHN in children and adults and may be due to a possible founder effect. *Kidney Int*, **71**, 574-81.
- Wu, X.C. & Johns, E.J. (2004) Interactions between nitric oxide and superoxide on the neural regulation of proximal fluid reabsorption in hypertensive rats. *Exp Physiol*, **89**, 255-61.
- Wu, X.R., Sun, T.T. & Medina, J.J. (1996) In vitro binding of type 1-fimbriated Escherichia coli to uroplakins Ia and Ib: relation to urinary tract infections. *Proc Natl Acad Sci U S A*, **93**, 9630-5.
- Xu, H., Fink, G.D. & Galligan, J.J. (2002) Nitric oxide-independent effects of tempol on sympathetic nerve activity and blood pressure in DOCA-salt rats. *Am J Physiol Heart Circ Physiol*, **283**, H885-92.
- Xu, H., Fink, G.D. & Galligan, J.J. (2004) Tempol lowers blood pressure and sympathetic nerve activity but not vascular O₂- in DOCA-salt rats. *Hypertension*, **43**, 329-34.
- Yang, B. & Bankir, L. (2005) Urea and urine concentrating ability: new insights from studies in mice. *Am J Physiol Renal Physiol*, **288**, F881-96.
- Yang, H., Wu, C., Zhao, S. & Guo, J. (2004) Identification and characterization of D8C, a novel domain present in liver-specific LZP, uromodulin and glycoprotein 2, mutated in familial juvenile hyperuricaemic nephropathy. *FEBS Lett*, **578**, 236-8.
- Yokouchi, M., Hiramatsu, N., Hayakawa, K., Okamura, M., Du, S., Kasai, A., Takano, Y., Shitamura, A., Shimada, T., Yao, J. & Kitamura, M. (2008) Involvement of selective reactive oxygen species upstream of proapoptotic branches of unfolded protein response. *J Biol Chem*, **283**, 4252-60.
- Young, J.C., Agashe, V.R., Siegers, K. & Hartl, F.U. (2004) Pathways of chaperone-mediated protein folding in the cytosol. *Nat Rev Mol Cell Biol*, **5**, 781-91.
- Yu, C.L., Tsai, C.Y., Lin, W.M., Liao, T.S., Chen, H.L., Sun, K.H. & Chen, K.H. (1993) Tamm-Horsfall urinary glycoprotein enhances monokine release and augments lymphocyte proliferation. *Immunopharmacology*, **26**, 249-58.
- Yu, X., Thompson, M.M., Shi, D. & Tuchman, M. (2001) Quantification of benzoic, phenylacetic, and phenylbutyric acids from filter-paper blood spots by gas chromatography--mass spectrometry with stable isotope dilution. *Clin Chem*, **47**, 351-4.
- Zager, R.A., Cotran, R.S. & Hoyer, J.R. (1978) Pathologic localization of Tamm-Horsfall protein in interstitial deposits in renal disease. *Lab Invest*, **38**, 52-7.
- Zaucke, F., Boehnlein, J.M., Steffens, S., Polishchuk, R.S., Rampoldi, L., Fischer, A., Pasch, A., Boehm, C.W., Baasner, A., Attanasio, M., Hoppe, B., Hopfer, H., Beck, B.B., Sayer, J.A., Hildebrandt, F. & Wolf, M.T. (2010) Uromodulin is expressed in renal primary cilia

and UMOD mutations result in decreased ciliary uromodulin expression. *Hum Mol Genet*, **19**, 1985-97.

Zou, A.P., Li, N. & Cowley, A.W., Jr. (2001) Production and actions of superoxide in the renal medulla. *Hypertension*, **37**, 547-53.

8 Acknowledgements

First of all I would like to thank Prof. Dr. Eckhard Wolf for giving me the opportunity to work and learn at the Institute for Molecular Animal Breeding and Biotechnology over the past two years.

I am most indebted to my supervisor Prof. Dr. Rüdiger Wanke for his guidance through this study, for his clear and calm explanations and for encouraging my confidence at all times.

I would also like to express my gratitude to Prof. Dr. Bernhard Aigner for his interest in my work, for sharing valuable ideas and knowledge and for his precise proofreading of this dissertation.

I am particularly thankful to Dr. Elisabeth Kemter for seeing me through the past two years and for her tireless work and support in this project.

I wish to express my gratitude to Priv.-Doz. Dr. Nadja Herbach and Dr. Andreas Blutke for providing kind help and essential ideas concerning all things stereology. Thanks to Andi also for teaching me how to brew elderflower liqueur.

Thanks to Helga Hagemann and her team for excellent animal care, for helping to make the mouse experiment happen and for good times at the mouse facility.

I thank Martin Langenmayer who helped me in every way he could and who became a friend.

I am grateful to everyone at the Institute for Molecular Animal Breeding and Biotechnology and at the Institute for Veterinary Pathology for making my time there so memorable and for their kind help and support.

A huge thank you to my friends Pauline Fezert, Christina Braun and Lisa Streckl who walked with me every step of the way, shared unforgettable memories and never ceased to believe in me. I am so lucky to know you.

Thanks to Mai Le for being my little ally and for swimming with me. Keep going strong.

I thank Andrea Beck for good times and for entrusting me with her horse.

My biggest shout-out goes to Johanna Leitenbacher and to Anna Rettinger for being my closest friends over the past eight years and for living it up with me here in Munich. You are wonderful people and I will miss you so much.

Finally, I would like to thank my parents and siblings for their unconditional love and support in everything I choose to do.